

**Identification and validation of a novel autophagy
modulator that blocks autophagosome-lysosome fusion**

Dissertation
zur Erlangung des Doktorgrades
der Naturwissenschaften

vorgelegt beim Fachbereich Biochemie, Chemie und Pharmazie
der Johann Wolfgang Goethe-Universität
in Frankfurt am Main

von
Saba Ezazi Erdi
aus Tehran, Iran

Frankfurt (2022)
(D30)

vom Fachbereich Biochemie, Chemie und Pharmazie der
Johann Wolfgang Goethe - Universität als Dissertation angenommen.

Dekan: Prof. Dr. Clemens Glaubitz

Gutachter: Prof. Dr. Dieter Steinhilber

Prof. Dr. Carsten Claussen

Datum der Disputation: 26.07.2022

TABLE OF CONTENTS

ABBREVIATIONS	VII
FIGURE INDEX	X
TABLE INDEX	XI
1 INTRODUCTION	1
1.1 The history of autophagy.....	1
1.2 The autophagic machinery and regulation	2
1.2.1 Induction of autophagy	2
1.2.2 ULK1-ULK2 complex.....	3
1.2.3 PtdIns3K lipid kinase complex.....	4
1.2.4 Ubiquitin-like protein conjugation systems	5
1.2.5 Atg9 complex.....	5
1.3 Tools for autophagy-specific drug discovery	6
1.3.1 High content screening.....	6
1.3.2 Autophagy reporters	7
1.3.3 Autophagy substrates.....	10
1.3.4 Quantitative approach and electron microscopy	11
1.4 Pharmacological targeting of autophagy	12
1.4.1 Small-molecule inducers of autophagy	12
1.4.2 Small-molecule inhibitors of autophagy	14
1.4.3 Autophagy modulators in clinical use.....	17
1.5 Relevance of autophagy in cancer	19
1.5.1 Role in cancer	19
1.5.2 Current therapies.....	21
1.5.3 Cross-talk between ER stress and autophagy in cancer	21
2 RESEARCH AIMS	24
3 MATERIALS AND METHODS	25
3.1 Cell culture.....	25
3.1.1 Cultivation of cell lines	25
3.1.2 Lentiviral transfection.....	25
3.2 High-content screening for compounds that impair autophagic flux.....	26
3.2.1 Compounds and compound libraries	26
3.2.2 High-content screen and image analysis system	26
3.3 Secondary assays.....	28
3.3.1. Autophagic flux assay.....	28

3.3.3 Assessment of lysosomal function and measurement of lysosomal pH	29
3.3.4 Inhibition of intralysosomal proteolytic activity.....	30
3.4 Structure activity relationship map of C18	30
3.5 Determination of cytotoxicity	31
3.6 Caspase-3 and 7 activity.....	32
3.7 Determination of protein levels.....	32
3.7.1 Preparation of whole-cell lysates	32
3.7.2 Protein quantification	33
3.7.3 SDS-PAGE and Western blot	33
3.7.4 Stripping of PVDF membranes for phosphorylated protein detection.....	35
3.8 Gene expression analysis	35
3.8.1 RNA isolation and extraction	35
3.8.2 cDNA synthesis	35
3.8.3 Quantitative real-time polymerase chain reaction (qRT-PCR) assay.....	36
3.8.4 Quantification of qRT-PCR products.....	37
3.9 Transmission Electron Microscopy.....	38
3.10 Determination of intracellular calcium content.....	38
3.11 Statistical analysis.....	39
4 RESULTS.....	40
4.1 Identification of autophagy modulating drugs in HEK293T	40
4.1.1 Assay validation, selection of tool compounds and Z factor determination.....	40
4.1.2 Primary screen	43
4.1.3 Confirmation of hits.....	45
4.1.4 Summary of dose response studies.....	52
4.1.5 Western blot analysis of LC3B and p62	53
4.2 Secondary assays.....	56
4.2.1 Assay optimization.....	56
4.2.2 Additional dose-response studies	58
4.2.3 Protein expression.....	59
4.3 Cytotoxicity of and pro-apoptotic activity of C18.....	62
4.3.1 Effect of C18 on cell viability	62
4.3.2 Effect of C18 on pro-apoptotic caspases	64
4.4 Modulation of autophagic flux by C18	65
4.4.1 Starvation-induced autophagic flux.....	65
4.4.2 Inhibition of lysosome degradation	67
4.4.3 p62/SQSTM1 upregulation	70
4.4.3 Effect of C18 on autophagosome-lysosome fusion.....	72
4.4.4 Effect of C18 on lysosomal acidification.....	74

4.4.5 Effect of C18 on cathepsin B and cathepsin L	76
4.5 Hit expansion	79
4.5.1 Identification of C18 analogs	79
4.5.2 Characterization of biological activity of the C18 analogs	81
4.6 mTOR signalling and interaction with Rab7 GTPase.....	82
4.7 Endoplasmic reticulum stress and autophagy inhibition	84
4.7.1 Transmission electron microscopy analysis	84
4.7.2 Expression of ER stress-associated proteins.....	88
4.7.3 Direct measurement of intracellular calcium	89
5 DISCUSSION	91
5.1 Phenotypic screening leads to the identification of a novel autophagy inhibitor.....	91
5.2 C18 inhibits autophagic flux	93
5.3 Structure-activity relationship and lead optimisation.....	96
5.4 Regulation mechanisms and signalling pathways	97
5.4.1 Implication of cell death and apoptosis	97
5.4.2 mTOR-dependent autophagy inhibition	99
5.4.3 p62 regulation.....	102
5.5 Implication of ER stress and calcium signalling.....	103
5.6 Concluding remarks	107
6 SUMMARY	108
7 ZUSAMMENFASSUNG	113
8 REFERENCES	119
FUNDING	162
ACKNOWLEDGMENT	Ошибка! Закладка не определена.162
CURRICULUM VITAE.....	Ошибка! Закладка не определена.164

ABBREVIATIONS

4E-BP1	eukaryotic translation initiation factor 4E-binding protein1
AKT	protein kinase B
ALS	amyotrophic lateral sclerosis
AMBRA1	autophagy and beclin 1 regulator 1
AMPK	AMP-activated protein kinase
ANOVA	analysis of variance
ATF6	Activating transcription factor 6
ATG	autophagy-related
AV	autophagic vacuoles
BECN1	beclin1
BiP	immunoglobulin binding protein
BIS-TRIS	bis(2-hydroxyethyl)imino-tris(hydroxymethyl)methane
BSA	bovine serum albumin
Ca ²⁺	calcium
cDNA	complementary DNA
CHOP	C/EBP homologous protein
CMA	chaperone-mediated autophagy
C _t	cycle threshold
CTSB	cathepsin B
CTSL	cathepsin L
DMEM	Dulbecco's modified eagle medium
DMSO	dimethyl sulfoxide
DNA	deoxyribonucleic acid
EBSS	Earle's balanced salt solution
EDTA	ethylenediaminetetraacetic acid
EGFP	enhanced green fluorescent protein
EM	electron microscopy
ER	endoplasmic reticulum
FBS	fetal bovine serum
FDA	food and drug administration

GEMM	genetically engineered mouse models
HCC	hepatocellular carcinoma
HCS	high content screening
HDAC	histone deacetylase
HER2	human epidermal growth factor receptor 2
HIV	human immunodeficiency virus
HTS	high-throughput screening
IC ₅₀	half maximal inhibitory concentration
IRE1	inositol-requiring enzyme 1
KNIME	Konstanz information miner
LDS	lithium dodecyl sulfate
LTR	Lysotracker deep red
MACC	molecular access system
MAPK	mitogen-activated protein kinase
MEF	mouse embryonic fibroblast
MR	magic red
mRNA	messenger RNA
mTOR	mechanistic target of rapamycin
mTORC1	mechanistic target of rapamycin complex 1
mTORC2	mechanistic target of rapamycin complex 2
MTX	mitoxantrone
NCI	National Cancer Institute
NFE2L2	nuclear factor erythroid 2-like 2
NRF2	nuclear erythroid 2-related factor 2
PBMC	peripheral blood mononuclear cells
PBS	phosphate-buffered saline
PCR	polymerase chain reaction
PDAC	pancreatic ductal adenocarcinoma cells
PE	phosphatidylethanolamine
PERK	pancreatic ER kinase-like ER kinase
PFA	paraformaldehyde
PI3P	phosphatidylinositol 3-phosphate
PtdIns3K	class III phosphatidylinositol 3-kinase
PVDF	polyvinylidene fluoride

qPCR	quantitative PCR
RFP	red fluorescent protein
RIPA	radioimmunoprecipitation
RNA	ribonucleic acid
ROS	reactive oxygen species
RPLPO	ribosomal protein, large, P0
rpS6	ribosomal protein S6
RT	realtime
S6K	ribosomal protein S6 kinase
SAR	structure-activity relationship
SARS-CoV-2	severe acute respiratory syndrome coronavirus type 2
SEM	tandard error of the mean
SERCA	sarco/endoplasmic reticulum Ca ²⁺ ATPase
SNARE	Soluble N-ethylmaleimide-sensitive fusion attachment protein receptor
SPDEF	SAM pointed domain containing ETS transcription factor
Stx	syntaxin
TAE	tris-acetate
TBS	tris-buffered saline
TEM	Transmission electron microscopy
TFEB	transcription factor EB
Thr	threonine
TOR	target of Rapamycin
ULK1	Unc-51 like autophagy activating kinase 1
ULK2	Unc-51 like autophagy activating kinase 2
UPR	unfolded protein response
UPS	ubiquitin-proteasome system
XBP-1	X-box binding protein 1

FIGURE INDEX

Figure 1: The process of autophagy	4
Figure 2: KNIME workflow to assess molecular similarity to the hit compound	31
Figure 3: Assay optimization in TagRFP-mWassabi-LC3 tagged HEK293T	41
Figure 4: Representative images from the spot detection algorithm.....	42
Figure 5: Analysis of the primary screening results.	45
Figure 6: Summary of hit selection from the autophagy screens	52
Figure 7: Western blot analysis of LC3B and p62.....	55
Figure 8: Assay optimisation and validation to verify tool compounds.....	57
Figure 9: Structures, images and dose response curves for the active hits and the respective IC ₅₀ of each hit compound.	59
Figure 10: Western blot analysis of LC3 and p62	61
Figure 11: Cytotoxicity screen for C18 on immortalized cell lines.....	63
Figure 12: C18 induced caspase-3/7 apoptosis.....	65
Figure 13: Autophagic flux modulation by C18	67
Figure 14: C18 blockage of autophagic flux upon starvation-induced autophagy	69
Figure 15: C18 inhibition of autophagosome formation	71
Figure 16: C18-induced upregulation of p62 mRNA	72
Figure 17: C18 inhibition of autophagosome-lysosome fusion	74
Figure 18: Lysosomal pH measurement.....	76
Figure 19: C18 inhibition of cathepsins.....	77
Figure 20: Time-dependent suppression of lysosomal hydrolases.....	78
Figure 21: Structures, images and dose response curves for C18 analogs	81
Figure 22: C18 induced phosphorylation of 4E-BP1 and downregulation of Rab7 ...	83
Figure 23: Effect of C18 on cell morphology	87
Figure 24: Time- and dose-dependent expression of BiP and CHOP	89
Figure 25: Intracellular calcium mobilization by C18.....	90

TABLE INDEX

Table 1: High-throughput LC3-based autophagy screening assays	8
Table 2: High-throughput p62-based autophagy screening assays.....	10
Table 3: CQ and HCQ used for combinatorial treatment <i>in vivo</i> xenograft models...	21
Table 4: Primary antibodies	34
Table 5: Secondary antibodies	34
Table 6: Components of the cDNA synthesis master mix.....	36
Table 7: Components of the qPCR master mix	37
Table 8: List of the hits derived from primary screen	43
Table 9: List of confirmed hits and their chemical structures	46
Table 10: Table displaying compounds by hit class.....	53
Table 11: IC ₅₀ values from cytotoxicity assay.	64
Table 12: Structure–Activity Relationship (SAR) of C18 analogs.	79

1 INTRODUCTION

1.1 The history of autophagy

Autophagy is an evolutionarily conserved degradative pathway that takes place in all eukaryotic cells¹. The phenomena was described for the first time by deDuve and Wattiaux in 1966². Autophagy in both yeast and mammals can be divided into two main types, microautophagy and macroautophagy, which are subcategorised into selective or nonselective³. During macroautophagy, cargo is sequestered into a double-membrane vesicle, termed an autophagosome. Once matured, these autophagosomes fuse with an endosome and/or lysosome, forming an autolysosome. This step allows breakdown of cargo by lysosomal hydrolases and recycling of the resulting macromolecules back into the cytosol^{4, 5, 6}. In contrast, microautophagy involves the direct sequestration of cargo within the cytoplasm⁷. Mammalian cells carry out an additional type of autophagy, known as chaperone-mediated autophagy, which was identified in 1981⁸. Chaperone-mediated autophagy (CMA), as its name suggests, allows chaperone-dependent selection of unfolded and soluble cytosolic proteins that are then targeted to lysosomes and translocated across the lysosome membrane for degradation⁹. The focus of this study is macroautophagy in mammalian cells, hereafter referred to as autophagy.

Autophagy plays an important physiological role in human health. It degrades cytoplasmic material and eliminates cytotoxic protein aggregates, limits microbial proliferation and contributes to cell survival under stress conditions¹⁰. Nonselective autophagy is the bulk turnover of cytoplasm, whereas selective autophagy specifically targets damaged or unnecessary organelles, including mitochondria, peroxisomes, or invasive microbes¹¹. Each selective autophagy process involves specific components of the machinery, and accordingly is identified with a unique name - mitophagy for selective degradation of mitochondria by autophagy, pexophagy for peroxisomes, xenophagy for microbes and so on^{12, 13}.

Genetic screens in fungi and subsequent studies in yeast allowed the identification of genes encoding for autophagy-related (ATG) proteins and provided tremendous data regarding the protein-protein interactions^{14, 11}. So far,

more than 30 ATG genes have been identified in yeast with approximately half of these genes having mammalian homologs¹⁵. In the next part, ATG proteins of mammals involved in the core autophagic machinery will be reviewed.

1.2 The autophagic machinery and regulation

1.2.1 Induction of autophagy

In higher eukaryote cells, mechanistic target of rapamycin (mTOR), which is a serine/threonine kinase, regulates autophagy. This kinase is divided into two structurally and functionally different complexes termed mTOR complex 1 (mTORC1)^{16, 17, 18} and mTOR complex 2 (mTORC2)^{18, 19}. The primary role of mTORC1 is the control of cell growth, and the signal is modulated by intra- and extracellular nutrients, mainly amino acids and growth factor signalling, cellular energy (via AMP-activated protein kinase, AMPK) and oxygen levels²⁰. Activated mTORC1 promotes protein, lipid and nucleotide synthesis via the phosphorylation of its downstream effectors, including ribosomal protein S6 kinase1 (S6K1) and eukaryotic translation initiation factor 4E-binding protein1 (4E-BP1). Moreover, activation of mTORC1 inhibits catabolic processes via unc-51-like autophagy activating kinase 1 (ULK1), which leads to autophagy inhibition. Nutrient starvation causes mTORC1 inhibition, thereby activating autophagy. Oxidative stress can also activate autophagy via mTORC1 or by endoplasmic reticulum (ER) stress^{21, 22}. There is considerably less evidence on the role of mTORC2 in the regulation of autophagy, compared to mTORC1, because traditionally it was considered as rapamycin-insensitive. However, recent studies show that rapamycin can also suppress mTORC2^{23, 24}.

The stages of autophagy are as following: induction, nucleation of the phagophore, expansion of the phagophore, completion of the autophagosome, fusion with the endosomes/lysosomes, and the final steps of degradation and recycling of the breakdown products²⁵. The initial step in the formation of the phagophore is the recruitment of autophagic proteins in the cell^{26, 27}. The phagophore then elongates and is sealed around the cargo to form a double-membrane vesicle. This is the final step of autophagosome biogenesis. Autophagosome maturation involves removal and recycling of the ATG proteins from the surface in a process requiring phosphatidylinositol 3-phosphate (PI3P) turnover and members of the Atg8/LC3-specific Atg4 protease family. Once

matured, an autophagosome will fuse with a lysosome to form an autolysosome. The autolysosome will then degrade the cargo and recycle the breakdown products back into the cytoplasm²⁸. At a molecular level, activation of AMPK and/or inhibition of mTOR kinases cause a series of events that lead to the production of the phagophore^{29, 30}.

1.2.2 ULK1-ULK2 complex

Activation of the ULK1-ULK2 kinase complex downstream of AMPK and mTOR signalling is the first step in autophagosome maturation³⁰. As stated in the name, the complex includes ULK1 and ULK2, which are mammalian homologs of yeast Atg1³¹. It also includes Atg13 (a homolog of yeast Atg13)³², RB1CC1/FIP200 (a homolog of yeast Atg17)³³ and C12orf44/Atg101 (absent in yeast)³⁴. ULK1/2 interact with Atg13, which directly binds to RB1CC1, resulting in increased ULK1/2 kinase activity^{34, 35}. In addition, Atg101 is important for the stability and basal phosphorylation of Atg13 and ULK1³⁴. The ULK1/2 complex is nutrient independent and it is formed even in nutrient-rich conditions³³. In this case, mTORC1 phosphorylates and inhibits ULK1/2 and ATG13, which impairs the interaction between ULK1 and AMPK³⁶. Under starved conditions in the cell, mTOR is released from the complex, resulting in ULK1/2 activation. The complex will then be phosphorylated and presumably activating Atg13 and RB1CC1 (**Figure 1A**). AMBRA1 (autophagy and beclin 1 regulator 1) and BECN1 (beclin1), which promote PtdIns3K (class III phosphatidylinositol 3-kinase) lipid kinase complex, are also phosphorylated by ULK1^{37, 38}.

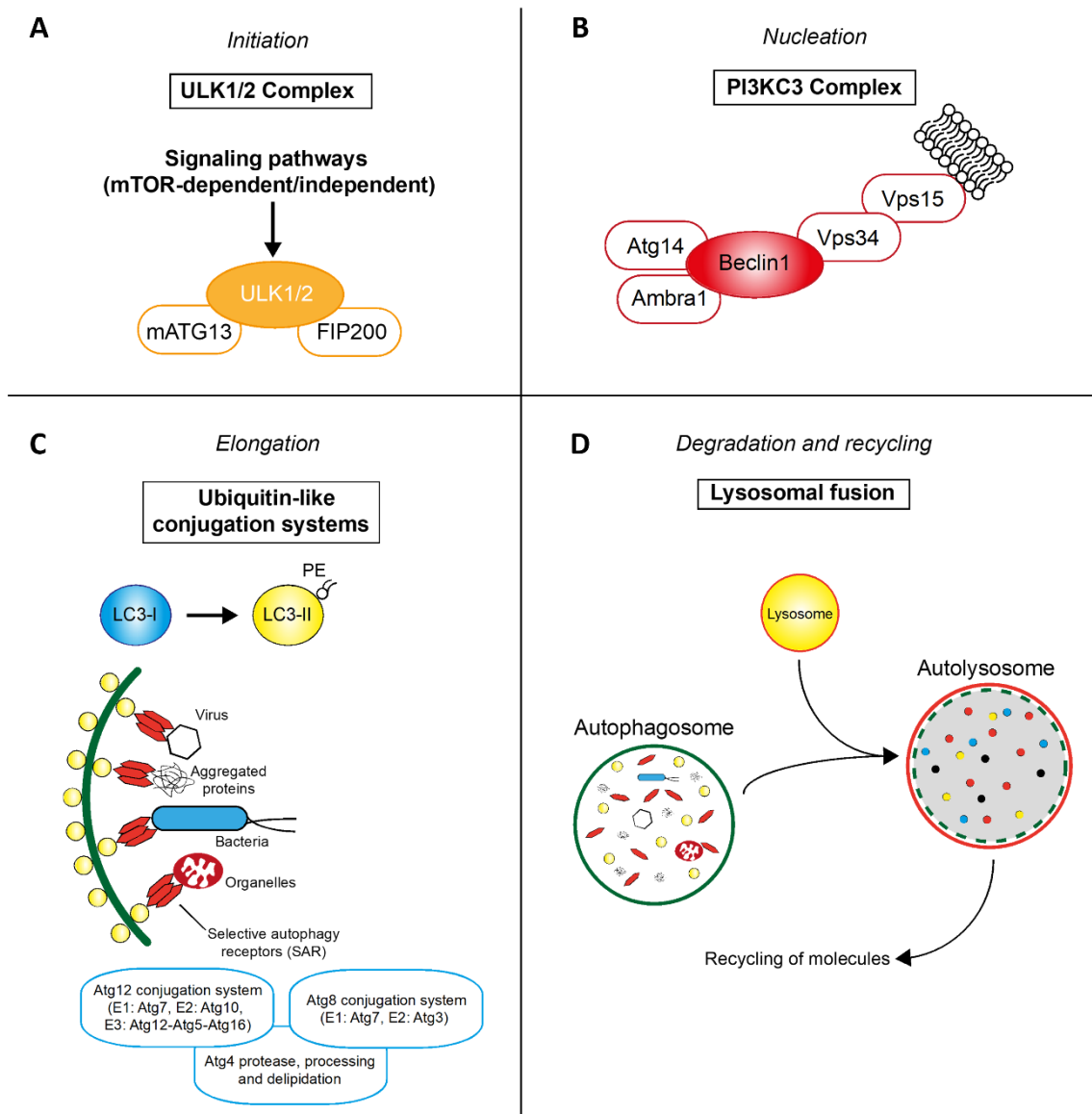


Figure 1: The process of autophagy. Stages include: **(A)** Initiation, **(B)** nucleation, **(C)** elongation and **(D)** degradation. Modulation at certain points of the process by activators (green) and inhibitors of autophagy (red) are shown. Figure adapted from Kocak et al.¹⁵

1.2.3 PtdIns3K lipid kinase complex

As mentioned above, the ULK1-ULK2 complex is responsible for the activation of PtdIns3K lipid kinase complex¹¹. There are primarily two PtdIns3K complexes responsible for the generation of PtdIns3P-rich membranes, which act as platforms for autophagosome formation^{39, 40, 41}. PtdIns3K complexes are conserved in both yeast and mammals, consisting of a core composed of Vps34/PIK3C3, Vps15/PIK3R4 and Vps30/BECN1 (**Figure 1B**). BECN1 is a

key regulatory protein that facilitates PtdIns3P synthesis carried out by PIK3C3 and PIK3R4. In nutrient rich conditions, BCL2 binds to BECN1 to inhibit autophagy. In contrast, during autophagy-inducing conditions, BECN1 is released from BCL2 and can interact with other proteins to suppress or stimulate autophagosome formation^{42, 43}. Furthermore, PtdIns3P facilitates the recruitment of phospholipid-binding ATG proteins, such as WIPIs (WD repeat domain, phosphoinositide interacting) including WIPI1, WIPI2, WIPI3 and WIPI4^{44, 45}.

1.2.4 Ubiquitin-like protein conjugation systems

Research mammals have identified two ubiquitin-like proteins, Atg12 and Atg8/LC3, and their respective conjugation systems^{46, 47}. Atg12 is conjugated to ATG5 in a reaction that requires Atg7 (E1-like enzyme) and Atg10 (E2-like enzymes, respectively). Atg12-Atg5 conjugate further interacts with Atg16L to form the Atg16L complex (Atg12-Atg5-Atg16L)⁴⁸. There are several homologs of yeast Atg8 in mammalian cells, including LC3, GATE16, GABARAP and ATG8L⁴⁹. Among them, microtubule-associated protein 1 light chain 3 (LC3) has been best characterized and considered as an autophagosome marker⁵⁰. Initially, LC3 is synthesized as proLC3, but is cleaved at its C-terminal by Atg4 to generate the cytosolic LC3-I with an exposed C-terminal glycine. LC3-I is conjugated to phosphatidylethanolamine (PE) by Atg7 and Atg3 to form membrane-bound form LC3-II⁵¹. LC3/GABARAP play additional roles such as activating ULK1-ULK2 complex^{52, 53} and cargo recognition targeted for lysosomal degradation⁵⁴. LC3 also interacts with autophagy substrates, such as SQSTM1/p62, NBR1, OPTN, CALCOCO2/NDP52 and TAX1BP1⁵⁴ to mediate autophagosome formation and eventually autophagic degradation (**Figure 1C-D**). It is of note that these ubiquitination-like systems are closely connected and essential for autophagy. Therefore, mutation of any member of the conjugates leads to defects in autophagosome formation⁵⁵.

1.2.5 Atg9 complex

Atg9 has a conserved role in directing membrane transport from various sources to the phagophore^{56, 57}. Atg9 and Atg16L are interconnected as they fuse in the process of autophagosome formation⁵⁸. Atg9 activity is dependent on ULK1, PIK3C3/VPS34 kinases and WIPI2 (a homolog of yeast Atg18)^{59, 48}.

There are two Atg9 orthologues in mammals, Atg9A and Atg9B. Under nutrient-rich conditions, both of them are located in the trans-Golgi network and late endosomes. However, Atg9B is expressed only in the placenta and pituitary gland, whereas Atg9A is expressed ubiquitously and is not obviously incorporated into the autophagosomes^{56, 59}.

1.3 Tools for autophagy-specific drug discovery

1.3.1 High content screening

A powerful tool available to analyse biological systems is fluorescence microscopy. Development of a wide spectrum of biological probes and fluorophores in fluorescent microscopy have provided unique insights into cellular events⁶⁰. Nonetheless, these systems are labour-intensive and time-consuming, and often incompatible with higher throughput screening (HTS). High content screening (HCS) bridges the gap between depth and throughput of biological experiments by combining fluorescence microscopy and HTS⁶¹. In recent years, high content approaches have become popular among scientists and widely used to for the assessment of autophagy in a large number of samples, which has led to discovery of many autophagy inducers or inhibitors⁶². HCS can identify biologically active compounds, as well as their mechanisms of action, thereby increasing the chemical diversity of possible drug leads⁶¹. An analysis of FDA-approved drugs between the years 1999 and 2008 by Swinney and Anthony⁶³ confirmed that phenotypic screening lead to discovery of more first-in-class drugs, compared to target-based screening during that period.

A key question after HCS campaigns becomes how to best prioritize and mine data, and select hits for further evaluation. Such decisions are usually supposed by medicinal chemists who evaluate structure-activity relationship (SAR) information that might be contained in screening data. SAR information allows one to estimate the chemical optimization potential of hits and can be used to predict biological activity from molecular structure⁶⁴. Compounds with similar structure have similar function⁶⁵, and SAR can be used to group compounds with chemically similar structures to predict target and/or pathways involved⁶⁶.

1.3.2 Autophagy reporters

After the Japanese cell biologist Yoshinori Ohsumi won the Nobel Prize for his discoveries into the mechanisms of autophagy in 2016⁶⁷, an increasing number of interest was attracted to the field. Thus, many screening programs followed with the goal to identify autophagy modulators.

The protein reporter that is widely used for this purpose is MAP1LC3 or short LC3. Cells can be transfected with a number of fluorescent-tagged reporters of LC3, such as GFP-LC3⁴⁶, mRFP-GFP-LC3⁶⁸ and GFP-LC3-RFP-LC3ΔG⁶⁹ to measure cytosolic LC3-II. These methods, Advantages and disadvantages, as well as additional assays are listed in **Table 1**.

The two most widely used reporters are GFP-LC3 and dual tandem reporters, such as mRFP-GFP-Lc3. GFP-LC3, also called GFP-Atg8, is used to evaluate autophagy induction by quantifying the GFP positive puncta per cell as an indication of the autophagosome number. A decrease in GFP-LC3 fluorescence is a good indicator of LC3 degradation by lysosomes⁷⁰. In some cases, autophagosomes accumulate because of a block in fusion with lysosomes, deficit in degradation process or inability of the lysosomes to keep up with the increased autophagosome biogenesis^{71, 72,73}. To confirm that compounds are also affecting the flux, they must be studied in presence or absence of lysosomal degradation inhibitors^{74, 75}. The presence of lysosomal inhibitors should increase the number of GFP-LC3-positive structures, whereas the absence of an effect on the total number of GFP-LC3 puncta indicates a defect in autophagic flux⁷⁶. The major limitation of this technique, as mentioned above, is the inability to differentiate between autophagosomes and autolysosomes without presence of a lysosomal inhibitor. Additionally, a reduction in the intensity of the GFP may indicate either reduced flux or efficient turnover⁷⁷. Thus, thorough evaluation by secondary assays is needed to distinguish between these possibilities^{74, 78}.

The tandem fluorescent-tagged-mRFP-GFP-LC3 method is based on a dual reporter that overcomes the limitations of the GFP-LC3 reporter method by distinguishing between autophagosomes and autolysosomes without the need to use a lysosomal inhibitor. When mRFP-GFP-LC3 is overexpressed in a cell

line, the autophagosomes emit both mRFP and GFP signals, while the autolysosomes emit only mRFP signal because GFP signal is quenched due to acidic pH⁶⁸. This allows in the image-based analysis to quantify the number of autophagosomes (colocalization of mRFP and GFP positive puncta) and autolysosomes (only mRFP positive). In general, an early stage autophagy activator will increase autophagosomes and autolysosomes, an early stage autophagy inhibitor will decrease both these compartments, whereas a late stage autophagy blocker will increase autophagosomes and decrease autolysosomes⁶². This method can be utilized either as primary screen or as a secondary assay to GFP-LC3 screen. There also some alternative fluorescent proteins that can be used. These include replacing mRFP with mCherry that has better photostability⁷⁹ or with mTagRFP which is brighter and has better photostability than both mRFP and mCherry. GFP can also be replaced with mWasabi that is more acid sensitive than GFP and has higher signal⁸⁰. Another important factor to consider is that GFP is sensitive to pH, therefore is very important to choose appropriate fixing solutions to keep the pH unchanged when fixing to avoid losing the acidic environment in the autolysosomes⁸¹.

Measuring the clearance of autophagic substrates (e.g. p62/SQSTM1 clearance) along with other secondary assays following the primary screen should be used to reduce chances of artifacts⁶². In addition to the above, due to close relationship between autophagic flux with the onset of apoptosis⁸², it is recommended to monitor cell death parameters alongside autophagy over time as some compounds could induce autophagy due to their toxic effect on the cells.

Table 1: High-throughput LC3-based autophagy screening assays, and their advantages and disadvantages

Screening platform	Advantages	Disadvantages	Reference
GFP-LC3	(1) Simple readout (2) Easy detection	(1) Unable to distinguish between autophagy inducers or inhibitors (2) No detection of autophagic flux	46, 83, 74, 78
mRFP/mcherry-	(1) Measures	(1) Proper acidification of	68, 74, 78

EGFP/GFP-LC3	<p>autophagic flux</p> <p>(2) Can distinguish between autophagy inducers or inhibitors</p>	<p>the lysosomes required</p>
GFP-LC3-RFP-LC3ΔG	<p>(1) Measures autophagic flux</p> <p>(2) Can distinguish between autophagy inducers or inhibitors</p>	<p>(1) Low time resolution, therefore not ideal for investigating the distinct stages of autophagy such as autophagosome formation and maturation ^{69, 77}</p> <p>(2) Homologous recombination could occur, resulting in non-degradable GFP-LC3ΔG</p> <p>(3) Analysis in different cell lines requires comparable expression levels of the reporter</p>
Renilla Luciferase-LC3	<p>(1) Straightforward assay</p> <p>(2) Real-time measurements</p> <p>(3) Measures autophagic flux</p> <p>(4) Alternative to immunoblotting</p>	<p>(1) Used to complement primary assays such as GFP-LC3 ^{84, 85}</p> <p>(2) Multiple time points have to be tested</p>
LC3 TR-FRET	<p>(1) Straightforward assay</p> <p>(2) Label-free quantification</p> <p>(3) Does not rely on overexpression of LC3</p>	<p>(1) No detection of autophagic flux ⁸⁶</p> <p>(2) Results for unknown compounds should be interpreted carefully when cytotoxicity is evident</p> <p>(3) Multiple doses and time points have to be tested</p>

(4) Used in combination with p62 TR-FRET to assess autophagic flux

1.3.3 Autophagy substrates

The next approach to study autophagy is based on autophagy substrates. As briefly mentioned earlier, a classical substrate for autophagy is p62/SQSTM1. This protein is an autophagy receptor for various ubiquitinated cargoes. An induction of autophagy increases the clearance of SQSTM1/p62 while inhibition of autophagy causes its accumulation^{87, 88}. For screening purposes, one would ideally require a stable inducible cell line where the transgene product is temporally expressed before the treatment with compounds, such as GFP-p62⁸⁷. Alternatively a luciferase-tagged p62 (p62-fLuc)^{89, 90} could be utilized for high-throughput (**Table 2**). Although p62 is a specific autophagy substrate in most mammalian cell lines measuring its autophagic degradation or accumulation can be problematic as in some cell lines where levels of p62 might not reflect autophagic activity. In certain cases, there is no change in the overall amount of p62 despite strong levels of autophagy induction⁹¹ or under nutrient-starvation condition⁹². Moreover, a reduction in the protein can also indicate cleavage of the protein and, hence, blockage of autophagy⁹³, hence results should be interpreted carefully.

Table 2: High-throughput p62-based autophagy screening assays, and their advantages and disadvantages.

Screening platform	Advantages	Disadvantages	Reference
GFP-p62	(1) Measures clearance of autophagic cargo as a marker for overall autophagic flux	(1) Measured in isolation does not reflect autophagic activity (2) Overexpression over long time periods can cause aggregates (3) Inactivation of certain genes may cause accumulation of GFP-	^{87, 88, 94}

		p62 aggregates
p62-fLuc	(1) Straightforward assay	(1) Measured in isolation ^{89, 90}
	(2) Real-time measurements	does not reflect autophagic activity
	(3) Measures clearance of autophagic cargo as a marker for overall autophagic flux	(2) Transcriptional changes could affect readout
p62 TR-FRET	(1) Straightforward assay	(1) Results for unknown ⁸⁶
	(2) Label-free quantification	compounds should be interpreted carefully
	(3) Measures clearance of autophagic cargo as a marker for overall autophagic flux	when cytotoxicity is evident
	(4) Does not rely on overexpression of p62	(2) Multiple doses and time points have to be tested

1.3.4 Quantitative approach and electron microscopy

Once compounds have been identified, there are additional assays with lower throughput that can be used, aiming at the independent validation of the modulatory effect of compounds. The conversion from endogenous LC3-I to LC3-II, as well as from GFP-LC3-I to GFP-LC3-II can be detected by immunoblotting using antibodies against LC3 and GFP, respectively. Increased LC3-II correlates with increased number of autophagosomes. The ratio of LC3-II to LC3-I is often used to determine autophagic rate. However, simple comparison of LC3-I and LC3-II may not be appropriate as LC3-II is degraded in autophagy, hence making interpretation of the results of LC3 ratio problematic. Additionally, the amount of LC3-II alone is not enough to indicate the flux, which is more accurately measured in presence and absence of a lysosomal protease inhibitor such as Bafilomycin A1⁹⁵. Furthermore, due to tissue and cell variability, the amount of LC3-II alone is not always sufficient to assess autophagy and it should be combined with results of p62 degradation^{95, 75}.

Lastly, a traditional yet powerful and sensitive tool used for years in autophagy research is electron microscopy (EM), which has provided clear evidence of different forms of autophagy, based on the type of cargo inside the

autophagosomes⁹⁶. These include mitophagy⁹⁷, lipophagy⁹⁸ and pexophagy⁹⁹. In EM, the changes in autophagic flux can be monitored according to the numbers of early-stage autophagosomes and late-stage autophagic vacuoles^{100, 101, 102}. EM can also differentiate between normal and abnormal morphological features, such as incomplete fusion of the autophagosome and lysosome depending on the condition of the cell¹⁰³.

1.4 Pharmacological targeting of autophagy

1.4.1 Small-molecule inducers of autophagy

The ability to study various aspects of autophagy by observing the effects of small molecules and gene manipulation using physiologically relevant models is of great importance, not only in understanding autophagy but also in producing effective drugs that can be taken into clinical trials. So far, a number of autophagy modulators have been discovered using independent studies and screening approaches, with many of them proven beneficial in *in vivo* models^{104, 105, 106}. These compounds can inhibit or induce autophagy either via the classical mTOR pathway, or independent of this. However, there are still many questions to be answered about how autophagy affects cellular function. Some of the important studies in disease context are described below.

Rapamycin, also known as sirolimus, is a natural product discovered in 1972 as an anti-bacterial, anti-fungi and immunosuppressant¹⁰⁷. Due to its immunosuppressive effect, rapamycin was used in the National Cancer Institute (NCI) Developmental Therapeutics Program for an anti-tumor screen in 60 tumor cell lines. The results indicated that rapamycin inhibited tumor growth in a number of these cell lines including mammary, colon 26, B16 43 melanocarcinoma, and EM ependymoblastoma¹⁰⁸. Based on these test results, NCI advanced rapamycin as a priority drug¹⁰⁹. Other studies followed up shortly and confirmed its inhibitory effect on tumor growth by binding to its target protein, collectively decided to call target of rapamycin (TOR)¹¹⁰. Rapamycin, described as an allosteric inhibitor of mTORC1, forms a complex with FKBP-12 and binds to the FRB domain of mTOR, leading to an acute inhibition of mTORC1^{111, 112}. However, prolonged suppression of mTORC1 also leads to disruption of a negative feedback loop and hyperphosphorylation of AKT through activation of PI3K¹¹³. Proof of rapamycin's anti-tumor effect via the

mTOR pathway¹¹⁴, together with its poor aqueous solubility and immunosuppressive properties, led to the development of rapamycin analogs as chemotherapeutic agents¹¹⁵. There are several rapamycin analogs (so called rapalogs) that are currently used in preclinical and clinical trials with higher solubility and potency than rapamycin. These include: tacrolimus (FK-506), temsirolimus (CCI779), everolimus (RAD001), and deforolimus (AP23573)¹¹⁶. The initial rapalogs do not fully inhibit mTORC1 and mTORC2^{117, 118}, thus second generation mTOR inhibitors were designed to act as ATP-competitive agents to directly bind to both complexes mTORC1 and mTORC2, called pan-mTOR inhibitors. Within this category, torin 1¹¹⁷ and torin 2¹¹⁹, have very low half-maximal inhibitory concentrations (IC₅₀) and elicit stronger autophagy induction^{117, 119, 120}. Other pan-mTOR competitive inhibitors include PP242^{121, 122}, PP30¹²¹, Ku-0063794^{123, 124}, AZD8055¹²⁵, AZD2014¹²⁶ and WYE-354¹²⁷. Although very potent, compounds such as torin1 and torin2 are more toxic than rapamycin itself^{128, 129}. Moreover, He et al.¹³⁰ describe rapalogs as generally less toxic compared to pan-mTOR inhibitors.

In addition to the above, there are also dual inhibitors of mTOR and PI3K pathways, especially important for cancer chemotherapy¹³¹. PI-103¹³², NVP-BGT226^{133, 134}, NVP-BEZ235¹³⁵, PF-04691502¹³⁶, PKI-587¹³⁷ and GDC-0980¹³⁸ are examples of autophagy inducers with therapeutic potential in various types of cancer. The mTOR-PI3K inhibitors are more promising than the rapalogs, but they are limited by lack of specificity, as inhibition of both mTOR and PI3K pathways will also affect other key cellular pathways, such as protein synthesis, apoptosis and immune cell activation and differentiation¹³⁹. AKT inhibition also holds important regulatory role for autophagy activation. Many synthetic and natural AKT inhibitors are derived from screening programs. Of note are AZD5363¹⁴⁰, GSK690693¹⁴¹, GDC0032¹⁴², GDC0068¹⁴³ and MK-2206¹⁴⁴ that stimulate autophagic response. Moreover, studies indicate a synergistic role for AKT inhibitors and lysosomal inhibitors in tumour inhibition^{140, 145}. Furthermore, direct and indirect modulators of AMPK have been associated with autophagy induction. Potent AMPK activators include A-769,662¹⁴⁶, GSK621¹⁴⁷, PT1¹⁴⁸, Compound C/dorsomorphin¹⁴⁹, and AICAR^{150, 151}. Also, resveratrol, a natural

polyphenol and caloric restriction mimetic, activates autophagy via AMPK-dependent inhibition of mTOR^{152, 153}.

It is a fact that mTOR controls vital cellular functions like cell growth and translation and its inhibition can have great therapeutic potential, however it can also lead to undesirable side-effects unrelated to autophagy induction⁶². To prevent this, many mTOR-independent autophagy inducers have been identified so far, such as trehalose¹⁵⁴, small-molecule enhancers of rapamycin (SMERs)¹⁵⁵, inositol monophosphate inhibitors (lithium, carbamazepine, valproic acid, L-690330)¹⁵⁶, nitric oxide synthase inhibitors (L-NAME)¹⁵⁷, L-type Ca²⁺ channel blockers (amiodarone, verapamil, loperamide, nimodipine and nitrendipine), imidazoline-1 receptor (I1R) agonists (clonidine and rilmenidine), calpain inhibitors (calpastatin and calpeptin), G_{sα} inhibitor (NF449), ATP-sensitive K⁺ channel agonist (minoxidil)^{158, 159}, indatraline and chlorpromazine¹⁶⁰. A combinatorial approach in enhancing autophagy with rapamycin and mTOR-independent autophagy inducers such as lithium, trehalose and SMERs is promising due to their additive effect¹⁶¹. Rapalogs, such as temsirolimus and everolimus, can also be used in combination therapies. These strategies improve drug efficacy by inhibiting multiple targets including those activated by removal of feedback loops or those involved in parallel pathways. Moreover, they may delay the emergence of drug resistance¹⁶².

1.4.2 Small-molecule inhibitors of autophagy

Different compounds are described in the literature as potential autophagy inhibitors. However, most of them have poor selectivity, which limits their application¹⁶³. This part will cover current autophagy inhibitors that target class III PI3-Kinase and lysosomal function.

Inhibition of the mTOR-PI3K-AKT signalling pathway with compounds that target PIK3C3 lipid kinase has the potential to inhibit autophagy¹⁵. Examples of pan-PI3K inhibitors include 3-methyladenine (3-MA)¹⁶⁴, wortmannin¹⁶⁵ and LY294002¹⁶⁶. 3-MA was discovered via the screening of a large number of purines and related substances (unpublished data), using isolated hepatocytes from starved rats, and showed remarkable selectivity in being able to inhibit

endogenous protein degradation without affecting protein synthesis¹⁶⁴. Despite wide usage, 3-MA is a difficult compound to work with because it is potent only at high millimolar concentrations and has low solubility at room temperature. To overcome this problem, three 3-MA derivatives have been generated through a screen using compounds derived from chemical modifications of 3-MA. This approach revealed improved solubility and potency in inhibiting autophagy¹⁶⁷. Furthermore, there are other concerns regarding the use of 3-MA, including promotion of glycogen breakdown and induction of cell death by apoptosis, both which occur independent of its autophagic effect on the PI3K pathway^{168, 169, 170}. The second drug, wortmannin, was initially discovered as a mold metabolite with anti-inflammatory activities¹⁷¹. Wortmannin is a potent PI3K inhibitor with an IC₅₀ of 10-50 nM for PI3K classes I, II and III^{172, 173}. LY294002, on the other hand, is a synthetic inhibitor of PI3K and has limited potency (IC₅₀ at the micromolar level). Both wortmannin and LY294002 have shown antiproteolytic effect, accompanied by inhibition of autophagic sequestration¹⁷⁴. Although the three inhibitors described above inhibit autophagy, they mostly have limited potency (except for wortmannin) and cause off-target effects on various lipid and protein kinases¹⁶³, as well as being linked to adverse effects in patients (e.g. respiratory infections, urinary tract infections, gastrointestinal pain, thrombocytopenia and dyslipidemia)¹⁷⁵. In addition, their pharmacological properties such as solubility, stability, ADME and pharmacokinetic (PK) parameters are not fully characterized. All these factors point out to the fact that one needs to be cautious when interpreting preclinical and clinical data regarding these inhibitors and their role in autophagy. For therapeutic exploitation of autophagy, novel pan-PI3K inhibitors have also been identified. PT210 and GSK-2126458 are such examples but their effect on autophagy is yet to be explored^{176, 177}.

Another group of widely used autophagy inhibitors are lysosomal lumen alkalizers, which act by neutralizing the acidic pH in the lumen of lysosomes, hence affecting lysosomal function. This results in the inhibition of various lysosomal hydrolases that require low pH for their activity¹⁷⁸. Bafilomycin A1 (BafA1) and chloroquine (CQ) are commonly used lysosomal lumen alkalizers that inhibit autophagy by targeting the lysosomes¹⁷⁹. BafA1 was one of the first

macrolide antibiotics isolated from *Streptomyces gresius*, and has been proven to be a potent inhibitor of the vacuolar H⁺ATPase, which regulates lysosomal pH^{180, 181, 182}. BafA1 at low nanomolar concentrations inhibits autophagic flux by preventing the acidification of endosomes and lysosomes¹⁷⁹. Furthermore, studies show that BafA1 inhibits viral replication of Influenza A and B¹⁸³ and is effective against cancer, both alone or in combination with other drugs^{184, 185}. Overall, BafA1 is a promising drug candidate for cancer treatment but the substantial toxicity and structural complexity of make it a difficult candidate for therapy¹⁸⁶.

Similarly, CQ is now widely used as an inhibitor of autophagy in both cell culture and *in vivo*⁷⁸. It was first synthesized in 1934 by Hans Andersag and his colleagues at Bayer Laboratories and introduced in 1945 as an anti-malarial medicine¹⁸⁷. Later on was found that CQ is a lysosomotropic weak base and when diffuses into the lysosome it becomes protonated, thus changing the lysosomal pH and preventing autophagic degradation in the lysosome¹⁸⁸. There also CQ derivatives, such as hydroxychloroquine (HCQ) and Lys01. HCQ is known to accumulate in the lysosomes, resulting in deacidification, reduced lysosomal function, and inhibition of autophagic flux¹⁸⁹. Short-term CQ/HCQ treatment is usually safe, but some adverse effects such as retinopathy and cardiotoxicity have been reported with increased duration of exposure or high dosages¹⁹⁰. Moreover, autophagy independent effects which cause toxicity have also been reported with these drugs¹⁵. Lys01 overcomes the toxicity issues of CQ and HCQ treatment. Lys01 is a dimeric form of CQ with 10-fold higher potency in cellular assays compared to HCQ. Moreover, a water-soluble salt of Lys01, Lys05, acts potently and deacidifies lysosomes *in vitro* and *in vivo*¹⁹¹. Other compounds with CQ-like activities have also been identified, including monensin¹⁹² and lucanthone¹⁹³. Moreover, ROC-325, a novel compound with structural similarities with both HCQ and lucanthone, significantly inhibits autophagy and exhibits therapeutic benefits against a broad range of tumor types¹⁹⁴. The quinolizidine alkaloid matrine¹⁹⁵, the antibiotic azithromycin¹⁹⁶, and lysosomal protease inhibitors E64d, pepstatin A, and leupeptin are other examples of lysosome-targeting autophagy inhibitors¹⁹⁷.

While above mentioned are the most widely used autophagy inhibitors, recent efforts have focused on identifying more selective small molecule compounds that can target autophagy. For example, SBI-0206965 is a ULK1-ULK2 complex inhibitor that blocks autophagy by enhancing mTOR activation and provides protection against acute axonal degeneration *in vitro* and *in vivo*¹⁹⁸. Furthermore, Dyczynski et al.¹⁹⁹ describe a small molecule inhibitor of the class III phosphatidylinositol 3-kinase Vps34, SB02024, that inhibits autophagy *in vitro* and *in vivo*, and improves sensitivity of breast cancer cells to sunitinib.

Another novel approach is ATG4 and ATG7 inhibition. NSC185058²⁰⁰, UAMC-2526²⁰¹, Tioconazole²⁰², LV-320²⁰³ and S130²⁰⁴ are examples of ATG4 inhibitors that exhibited antitumor activity both in *in vitro* and *in vivo* models. On the other hand, pyrazolopyrimidine sulfamates are selective ATG7 inhibitors with remarkable modulation of some autophagic markers (e.g. LC3B and SQSTM1) in *in vitro* and *in vivo* models¹⁴⁸ but the lack of an effect on ATG12–ATG5 complex and some inhibitory effect toward other E1 enzymes limits their use in clinical settings.

1.4.3 Autophagy modulators in clinical use

Currently the most popular autophagy drugs in the clinic, and the only two which have made it so far, are CQ and its derivative HCQ. HCQ is usually preferred because it is less toxic than CQ at peak concentrations^{205, 206}. With this information, various clinical trials for cancer patients have been carried out. The initial phase I/II clinical studies with CQ/HCQ including pharmacokinetic and pharmacodynamics assays have been conducted to evaluate the safety and the success in suppression of autophagy in tissues or cancer, either alone or in combinatory therapies. These studies demonstrated that FDA-approved doses for CQ/HCQ inhibit autophagy and are well tolerated in most patients. A phase I/II clinical trial using HCQ for newly diagnosed glioblastoma patients indicated that HCQ combination with radiation therapy and temozolomide inhibited autophagy, marked by increased autophagic vacuoles (AVs) and LC3-II in peripheral blood mononuclear cells (PBMC)²⁰⁷. Similarly, studies using combination therapy for pancreatic cancer were undertaken. Targeting RAS signalling pathways in pancreatic tumours results in marked activation of autophagic flux, making pancreatic ductal adenocarcinoma cells (PDACs) more

sensitive to autophagy inhibitors²⁰⁸. On contrary, a phase II clinical trial using HCQ reported negligible therapeutic efficacy in patients with previously treated metastatic pancreatic adenocarcinoma, even though preclinical data in mice showed tumour regression²⁰⁹. Despite these results, simultaneous inhibition of autophagy with enzymes of the RAS pathway is still an appropriate approach. A combinatorial approach using HCQ and RAS pathway inhibitor, trametinib, on one patient suffering from KRAS-mutated PDAC who had exhausted all other available treatments was able to demonstrate striking disease response²¹⁰. Additionally, evidence indicates that histone deacetylase inhibitors can induce autophagy. To investigate this further, a phase I clinical trial was carried out using a combination therapy with HCQ and histone deacetylase (HDAC) inhibitor (vorinostat). The results of this study indicate that HCQ may increase the efficacy of HDAC inhibitors in patients with advanced solid tumors²¹¹. Lastly, combination of an mTOR inhibitor (e.g. temsirolimus) and autophagy inhibitor (HCQ) is a promising approach to prevent disease progression in solid tumors and melanoma. This strategy proved to be safe, with significant antitumor activity²¹².

Overall, there are more than 70 trials combining HCQ and CQ with chemotherapy and radiotherapy. These clinical trials involved combination therapy with either temozolomide, bortezomib, temsirolimus, vorinostat or doxorubicin for patients suffering from various types of cancer (e.g. melanoma, colorectal cancer, myeloma and renal cell carcinoma). Results showed that HCQ had significant antitumor activity in patients^{205, 213, 212, 211}. Although HCQ/CQ addition to the chemotherapy treatment is relatively safe, the improvements in cancer progression are still modest, possibly due to lack of specificity to the autophagy machinery¹⁵. Moreover, high doses of HCQ were shown to be toxic, thus limiting efficacy²⁰⁷. In addition, in March 2020, FDA issued an emergency authorization for the use of CQ/HCQ as experimental treatments for SARS-CoV-2. However this was revoked in July 2020 due to the lack of benefits and serious side effects²¹⁴.

While autophagy inhibitors are widely used for cancer therapy, autophagy inducing agents have shown considerable potential for the prevention or treatment of infectious diseases, neurodegenerative disorders, aging, and

metabolic diseases¹⁰⁶. Studies suggest the activation of autophagy with rapamycin and a BECN1-derived peptide can limit the virulence of some viruses such as the human immunodeficiency virus (HIV), West Nile virus, chikungunya virus, and more recently for severe acute respiratory syndrome coronavirus type 2 (SARS-CoV-2)^{215, 216, 217, 214}.

In neurodegeneration, stimulating autophagic activity in neurons with small molecules might have protective role¹⁵. Several phase II clinical trials are planned to study the clinical effects of rapamycin on amyotrophic lateral sclerosis (ALS) (NCT03359538) and Alzheimer's disease (NCT04629495) patients. Other autophagy inducers currently under clinical investigation for ALS are colchicine (NCT03693781) and tamoxifen (NCT02166944)¹⁵. In addition, mTOR-independent autophagy inducers such as rilmenidine, spermidine and lithium have also been used in clinical settings but their efficacy remains elusive^{15, 218, 219}.

1.5 Relevance of autophagy in cancer

1.5.1 Role in cancer

Even though genetic inactivation of autophagy in human cancers is rare, the role of autophagy has been studied and identified in preclinical models, using genetically engineered mouse models (GEMMs). The recurring theme from autophagy inhibition in GEMMs is that autophagy involved in elimination of oxidative stress, activation of DNA damage response mechanism, inflammation and regulation of mTOR and Nrf2 signalling²²⁰. These events are known to cause genomic instability and sustained oncogenic signalling that impute autophagy inhibition with promoting tumour formation. However, once the tumour established, cancer cells use autophagy to evade apoptosis and cope with cancer-associated stress conditions²²¹. So far, resolution of these enigmas surrounding autophagy function has proved challenging.

Among mammalian ATG proteins, Beclin1, ATG5, ATG7, ATG12, ATG16L1 and LC3B are the most studied with respect to certain aspects of immunity²²². As mentioned, a frequent ATG gene that is absent in human cancer is BECN1. Loss of BECN1 occurs in many cancers such as breast, prostate and ovarian cancers²²⁰. Studies show that BECN1 heterozygous mice are prone to develop

spontaneous carcinomas of liver, lung and mammary hyperplasia late in life²²³. Moreover, mice without either one of the core autophagy proteins, Atg5 or Atg7, were born alive but died after the first day of delivery due to neuronal dysfunction^{224, 225}. Interestingly, neuronal transgenic Atg5 expression rescued them from neonatal death²²⁶. Additionally, chronic p62 elevation in hepatocellular carcinoma (HCC) tumours has been proposed to contribute tumour growth by enhancing the Nrf2 signalling, which is a major defence mechanism against oxidative stress and can activate oncogenic signalling pathways^{227, 228}. These studies support that autophagy might play a tumour suppressive role and limit tumour formation. Nevertheless, the exact mechanism of how autophagy inhibition lead to tumour formation is largely unknown. Even though loss of ATG genes seen in preclinical models has not been verified in human cancer, autophagy inhibition might come into play by different mechanisms. On the other hand, once tumour is established, autophagy induction promotes tumour cell survival²²¹.

The impact of autophagy inhibition on the efficacy of anti-tumour therapies has been mostly studied in immune compromised mice to avoid tumour rejection. However, these studies might demonstrate different outcomes when the immune system is intact. For example, inhibition of autophagy by the depletion of Atg5 or Atg7 in CT26- and MCA205-driven tumours affected their response to chemotherapy (Mitoxantrone, MTX) differently respective of the presence of immune system²²⁹. In immunocompetent mice, systemic MTX treatment limited the growth of autophagy-competent tumours, however proliferation of autophagy-deficient tumours were not affected. Surprisingly, in immune deficient mice, anti-tumour activity of MTX were lost irrespective of their autophagic competence. These results reveal that MTX exerts its anti-tumour activity by stimulating immune surveillance of cancer cells in the presence of active autophagy. In addition, inhibition of autophagy using CQ decreases anti-tumour activity of curcumin against human epidermal growth factor receptor 2 (HER2) overexpressing breast cancer in immune-competent mice, while increases it in immune-deficient mice²³⁰. These findings demonstrate the interplay between the host immunity and cancer autophagy, and caution is advised when deciding what treatment is necessary.

1.5.2 Current therapies

Targeting autophagy as adjuvant therapy in addition to cancer therapy regimes is highly sought after. It is obvious from the preclinical studies that autophagy inhibition is a potential therapeutic strategy in cancer, but it is unknown which tumours will be most vulnerable²²³. In this regard, plenty of completed or on-going clinical trials were reported, mostly in combination with other targeted therapies, to evaluate the potential of CQ/HCQ as an adjuvant therapy in cancer treatment. Thus, an autophagy inhibitor with any combinations listed (**Table 3**) could be beneficial for patients in targeted cancer therapy.

Table 3: CQ and HCQ used for combinatorial treatment *in vivo* xenograft models.

Model	Treatment	Reference
Human HT29- or HCT8-driven colon cancer xenograft	CQ+ Vorinostat	²³¹
TRAMP mouse model of prostate cancer	CQ+ Sulforaphane	²³²
Patient- derived pancreatic ductal adenocarcinoma tumour tissues	CQ+ Gemcitabine	²³³
U87MG-driven glioma xenograft	CQ+ Temozolomide	²³⁴
MDA-MB-231-driven breast cancer xenograft	CQ+ Cyclophosphamide	²³⁵
HCC-827-driven non-small cell lung cancer xenograft	CQ+ MK2206 + Gefitinib	²³⁴
Myc/p53ER ^{IAM} lymphomic xenograft	CQ+ Cyclophosphamide	²³⁶
UACC903-driven melanoma xenograft	HCQ+ Temsirolimus	²³⁷
SGC7901-driven human gastric cancer xenograft	CQ+ Cisplatin	²³⁸
H358- or H460-driven non-small cell lung cancer xenograft	HCQ+ Erlotinib	²³⁹
Huh7 hepatocarcinoma xenograft	CQ+ Oxaliplatin	²⁴⁰

1.5.3 Cross-talk between ER stress and autophagy in cancer

Oncogenic mutations cause changes in the cellular metabolism, which ultimately lead to tumorigenesis. In order for cancer cells to sustain their

uncontrolled growth, they demand high protein levels²⁴¹, which are sustained by the nucleolus and the endoplasmic reticulum^{242, 243, 244}. Since autophagy has an important role in ER homeostasis, modulation of autophagy seems to be promising in anticancer therapy. The ER is a large specialized organelle responsible for many roles in the cell including calcium storage, protein synthesis and lipid metabolism. Under certain conditions the ER function can be altered, such as nutrient starvation, hypoxia, acidosis, drug toxicity and irradiation. They cause accumulation of the misfolded proteins in the ER and, subsequently, lead to ER stress development²⁴⁵. ER homeostasis is mainly regulated by two processes: the unfolded protein response (UPR) and autophagy²⁴⁶. UPR senses unfolded and misfolded proteins in the ER lumen and transmits the signal to the cell nucleus, where it initiates a transcriptional program tailored to reinstate homeostasis²⁴⁷. Selective autophagic degradation in the ER is termed ER-phagy. ER-phagy is subcategorised in three different types: macro-ERphagy, micro-ERphagy and an ER-derived vesicular pathway²⁴⁶. In macro-ERphagy, autophagosomes sequester ER fragments and fuse with lysosomes to enable their degradation²⁴⁸. In micro-ER-phagy, lysosomal membranes invaginate or engulf portions of the ER into the lysosomal lumen²⁴⁹. Finally, vesicular delivery is a novel mechanism for lysosomal degradation of ER, in which small vesicles containing misfolded proteins split off from the ER and directly fuse with lysosomes for degradation²⁵⁰. ER-phagy constantly occurs at a low level to maintain ER homeostasis and can be increased, if needed, to restore cellular conditions²⁵¹. To do this, the autophagic machinery employs ubiquitins and other selective autophagy receptors. Ubiquitin attach to the cargo, and are recognized by autophagy receptors which in turn link the cargo to the autophagic membrane. Alternatively, cargo selection can also be facilitated by autophagy receptors that are directly part of the targeted organelle and become activated when autophagic degradation is triggered. The latter mechanism is predominant in ER-phagy²⁵².

As mentioned above, any disturbances in the ER lumen will activate sensors that initiate a cascade of events downstream of UPR to restore ER homeostasis. The key UPR sensors are: pancreatic ER kinase-like ER kinase

(PERK), inositol-requiring enzyme 1 (IRE1)/X-box binding protein 1 (XBP-1), and activating transcription factor 6 (ATF6). Under normal functioning ER, these transmembrane proteins (PERK, IRE1, and ATF6) are bound to the chaperone BiP/GRP78 in the ER lumen²⁵³. Under stress conditions, BiP binds to the UPR sensors and thereby renders their activation²⁵⁴. In events of chronic or acute ER stress, the adaptive UPR can be overwhelmed. This will trigger terminal UPR, leading to apoptosis²⁵⁵. Several studies have reported that induction of GADD153, also known as CHOP, correlates with the onset of apoptosis^{256, 254, 257}. CHOP is a stress-inducible transcription factor that is robustly expressed in response to ER stress²⁵⁸. ER-mediated apoptosis caused by CHOP pathway is relevant to many diseases that cause ER stress^{259, 260} and is becoming a highly researched topic by investigators in the field. Moreover, CHOP has been identified as a direct regulator of several autophagy genes²². CHOP modulates the induction of autophagosomes during ER stress by inhibiting LC3-II protein levels and GFP-LC3B dots in human colon cancer²⁶¹. Furthermore, UPR-activated CHOP acts as a guardian against hepatitis C virus by causing autolysosome maturation via an LC3B-II-dependent mechanism²⁶². The effect of CHOP is also context dependent. At the onset of amino acid starvation, CHOP can upregulate the expression of autophagy-related genes while in the later stages of starvation it inhibits autophagy and gradually triggers the onset of apoptosis²⁶³. The multifunctional role of CHOP makes it an important marker to take into consideration for autophagy studies.

Lastly, calcium (Ca^{2+}) has been implicated in autophagic signalling pathways²⁶⁴. Calcium is a major intracellular messenger that regulates gene transcription, proliferation, cell motility, cell signalling, neuronal regulation, autophagy and apoptosis²⁶⁵ and it is largely stored in the ER²⁶⁶. ER-stress leads to Ca^{2+} release from the ER into the cytosol, which, in turn, can activate UPR and numerous kinases and proteases involved in autophagy^{267, 268, 269}. Perturbations in Ca^{2+} homeostasis have major impacts on autophagy by participating in ER stress²⁶⁹. Given this observation, monitoring Ca^{2+} opens a possible way to control autophagy for therapeutic purposes.

2 RESEARCH AIMS

Therapeutic exploitation of autophagy with small-molecules is in high demand due to the lack of potent compounds that would selectively modulate various stages of the autophagic machinery. In the case of cancer, autophagy has been shown to play a dual role, both as tumor suppressor and tumor promoter. Inhibiting autophagy is currently being developed as a new treatment strategy for various types of cancer. The most widely used autophagy inhibitors in clinical trials include chloroquine (CQ) and its derivative hydroxychloroquine (HCQ), either alone or in combination with other cancer drugs or radiation. The results of these clinical trials indicate some improvements in cancer patients but high micromolar concentrations of CQ and HCQ are required to inhibit autophagy which cause toxic effects and thereby limiting their clinical use. Consequently, the search for more potent autophagy inhibitors continues.

The aim of the present study was to validate hits derived from a previously established high content screening campaign and conduct secondary assays with the goal to select and characterize the most potent autophagy inhibitor.

During this study, compound 18 (C18) was identified as a novel late stage autophagy inhibitor that blocks autophagic flux by impairing autophagosome-lysosome fusion, hence reducing lysosome acidity and the occurrence of

autophagy within cells. In addition, a close link between C18-induced autophagy inhibition and ER stress was found, which encourages further studies into the compound due to therapeutic benefits that this combination brings in cancer therapy.

3 MATERIALS AND METHODS

3.1 Cell culture

3.1.1 Cultivation of cell lines

U2OS cells (CLS GmbH, #300364, Eppenheim, Germany) were cultured in DMEM (#DMEM-HXRXA), supplemented with 10% (v/v) FBS (#FBS-12A), 100 U/ml of penicillin and 100 µg/ml of streptomycin (PS-B) and 1mM L-Glutamine (GLN-B) from Capricorn Scientific GmbH, Ebsdorfergrund, Germany. The human HEK293T cell line (#CRL-3216™) were purchased from ATCC, Wesel, Germany, and cultured in the same condition as U2OS cells. All cell lines were maintained at 37°C in a humidified 95% air and 5% CO₂ atmosphere. For subculture, cells were washed in PBS (#PBS-1A) and passaged two to three times a week by using trypsin-EDTA buffer (#try-1B) From Capricorn Scientific GmbH, Ebsdorfergrund, Germany. For visualization of cell morphology EVOS FL microscope was used (Invitrogen, Carlsbad, CA, USA).

3.1.2 Lentiviral transfection

U2OS cells with doxycycline-inducible expression of mCherry-EGFP-LC3B cells were kindly provided by Prof. Dr. Anne Simonsen, University of Oslo, Norway. N-terminal double-tagged (mCherry-EGFP) LC3B was cloned into the pLVX-Tight-Puro vector (Takara Bio USA, Mountain View, CA, USA) to generate the pLVX-Tight-Puro-mCherry-EGFP-LC3B construct. Plasmids were transfected into U2OS cells to produce lentivirus from the pLVX-Tet-On-Advance (Takara

Bio USA) regulator vector and the pLVX-Tight-Puro-mCherry-EGFP-LC3B response vector. U2OS-mCherry-EGFP-LC3B cells were selected in 50 µg/ml G418 (Carl Roth GmbH, #CP11.3, Karlsruhe, Germany) and 2µg/mL puromycin (Sigma-Aldrich, #P8833, Steinheim, Germany). Selection antibiotics were removed prior to experiment and cells were incubated with 0.5 µg/ml doxycycline (Sigma-Aldrich, #D3072, Steinheim, Germany) overnight prior to confocal microscopy to induce expression of the mCherry-EGFP-LC3 tag. Human embryonic kidney 293T cells (HEK293T) stably expressing TagRFP-mWassabi-LC3 were kindly provided by Prof. Dr. Lucie Carrier, University Medical Center Hamburg-Eppendorf, Germany. They were established as described previously⁸⁰. Cell culture conditions were as explained above. All cell lines received were tested negative for mycoplasma contamination (MycoAlert™ Mycoplasma Detection Kit, Lonza, Cologne, Germany).

3.2 High-content screening for compounds that impair autophagic flux

3.2.1 Compounds and compound libraries

BafA1 (#BVT-0252) was purchased from AdipoGen LifeSciences (Hamburg, Germany) and dissolved in DMSO to make a stock solution of 100 µM. Torin1 (#Cay10997), torin2 (#Cay14185), rapamycin (#Cay13346), ABT-737 (#Cay11501) and leupeptin (#Cay14026) were purchased from Cayman Chemicals (Hamburg, Germany). CQ (#S6999), trifluoperazine dihydrochloride (#SKF5019), pepstatin (#S7381) and doxorubicin (#S1208) from Selleck Chemicals (Munich, Germany), and MG-132 from Enzo Life Sciences (#BML-PI102, Lörrach, Germany). All compounds were diluted in DMSO to make a stock solution of 10 mM. 3-methyladenine (Selleck Chemicals, #S2767, Munich, Germany) was diluted directly in cell culture media to a final volume of 5 mM before use. Compounds used in high-throughput screen were from ChemBioNet library and FDA approved drug library V2, available in-house in DMSO solution at a concentration of 10 mM.

3.2.2 High-content screen and image analysis system

Assay optimization was carried out to find the best tool compounds. For the assay, PerkinElmer CellCarrier 384-well plates (PerkinElmer, #6007550, Waltham, MA, USA) were coated with poly-D-lysine (Sigma-Aldrich, #P7280, Steinheim, Germany) prior to cell seeding. This was achieved according to the

manufacturer's instructions. TagRFP-mWassabi-LC3B tagged HEK293T cells were seeded at 400,000 cells per ml and incubated at 37°C in a humidified 95% air and 5% CO₂ atmosphere overnight. The next day, cells were treated with compounds for 4 hours (h) and imaged using Operetta high content imaging analysis system (PerkinElmer, Waltham, MA, USA) to quantify the number of fluorescent autophagic puncta, which are either positive for both TagRFP and mWassabi positive (representing autophagosomes) or TagRFP positive and mWassabi negative (representing autolysosomes). 11 replicates of each condition per plate were used. The ratio of TagRFP positive puncta to TagRFP and mWassabi positive puncta was used to analyse data. The Z factor was calculated²⁷⁰ to determine the most effective compounds to be used for high-throughput screening.

For high throughput screening, a total of 4153 compounds from the ChemBioNet collection and 499 compounds from the Enzo FDA-approved drug library were screened at Fraunhofer IME ScreeningPort in Hamburg. The screen was carried out by an undergraduate student, Rashmi Tandon, who identified compounds for their autophagy modulating activity. Compounds in triplicate were added to plates at a final concentration of 10 µM using the Echo 550 Liquid Handler (Labcyte, San Jose, CA, USA) and incubated for 4 h. DMSO (negative control, 0.1%), BafA1 (inhibitor, 100 nM), torin1 (inducer, 1 µM) and 3-MA (inducer, 5 mM) were added on every plate for reference. Eight replicates of each control compound has been included on each plate. After 4 h incubation time, cells were washed in PBS using the ELx405™ Washer (BioTek Instruments, Winooski, Vermont, United States) and then fixed with 4% paraformaldehyde (PFA) solution (Sigma-Aldrich, #158127, Steinheim, Germany) for 20 min (min) at room temperature. After fixation, they were washed three times with PBS, and stained with 1 µg/ml Hoechst 33258 (Invitrogen Life Technologies, #H3569, Carlsbad, CA, USA) for 15 min. Cells were then imaged on Operetta using a 20x objective to quantify the number of TagRFP and mWassabi positive and TagRFP positive and mWassabi negative puncta. Data was analysed in Columbus Image Data Storage and Automated Analysis System from PerkinElmer. The fluorescent images of eight fields per well in the three fluorescent probe channels were acquired in each confocal

scan. All results were then exported from Columbus and data was visualised in Activity Base 8.0 (IDBS). All plates were visually inspected for patterns and wells with abnormal high and abnormal low number of nuclei were invalidated. Data was normalised to DMSO to remove plate-to-plate variability. Compounds that can upregulate the number of autophagic puncta to be equal or more than 3-fold above the mean of the negative control in the same plate were identified as positive compounds for autophagy inducers or inhibitors. After hit selection, hit confirmation was carried out for the positive compounds. Compounds were tested in triplicates at 10 μ M. 11-point dose response curves were generated for the hit confirmation compounds. IC₅₀ values were calculated from the curves using GraphPad Prism 9 software.

3.3 Secondary assays

3.3.1. Autophagic flux assay

U2OS-mCherry-EGFP-LC3B cells were seeded in PerkinElmer CellCarrier 384-well plates at a density of 200,000 cells per ml in complete media containing 0.5 μ g/ml doxycycline overnight. Cells were allowed to settle overnight at 37°C in a humidified 95% air and 5% CO₂ atmosphere to reach 70-80% confluency and then were treated with compounds as followed: DMSO (vehicle, 0.1%), BafA1 (negative control, 100 nM), torin2 (positive control, 250 nM) or desired concentrations of positive compounds from the screen. Lowest active concentration of reference compounds, BafA1 and torin2, were optimised beforehand. For starvation experiment, cells were washed three times with EBSS media (Invitrogen Life Technologies, #24010, Carlsbad, CA, USA) before incubation with EBSS media containing compounds. Serum starvation was carried out at the same time with compound treatment for 4 h. All compounds were added with Echo liquid handler. Cells were then fixed in 4% paraformaldehyde as described above and stained with Hoechst 33258 for 15 min. To detect the colocalization of EGFP-LC3 puncta with p62, after fixation, cells were permeabilized with 0.1% Triton X-100 (Carl Roth, #3051, Karlsruhe, Germany) in PBS for 15 min at room temperature, washed three times with PBS, then blocked in blocking buffer containing 3% BSA (Carl Roth, #8076.4, Karlsruhe, Germany) and 0.1% Tween20 (Carl Roth, #9127.1, Karlsruhe, Germany) in PBS for 30 min at room temperature. After blocking, cells were

incubated with anti-p62 primary antibody (Progen, #GP62-C, Heidelberg, Germany) in blocking buffer overnight at 4°C. The next day, cells were then washed three times with PBS, incubated in AlexaFluor 647 anti-guinea pig secondary antibody (Invitrogen Life Technologies, #A-21450, Carlsbad, CA, USA) in blocking buffer for 2h at room temperature. Cells were then washed with PBS again and stained with Hoechst 33258 for 15 min. Imaging was done on Operetta using a 20X objective. The number of puncta/cell was determined using Columbus (PerkinElmer). The analysis script used was an optimised version of the analysis used for the HCS. The intensity of mCherry⁺ (red) and mCherry⁺EGFP⁺ (yellow) puncta in DMSO-treated cells was taken as a threshold and population of puncta above the threshold were calculated. At least three replicates per condition have been monitored and eight images per well were analysed.

3.3.3 Assessment of lysosomal function and measurement of lysosomal pH

To assess lysosomal function, the autophagosome - lysosome fusion was evaluated using the LysoTracker® Deep Red dye (Invitrogen Life Technologies, #L12492, Carlsbad, CA, USA). U2OS-mCherry-EGFP-LC3 cells were seeded as described above. DMSO, BafA1 (100 nM), torin2 (250 nM) and desired concentrations of compound 18 (C18) were added for 4 h. Following incubation time, cells were washed twice in PBS and incubated with lysosomal-specific probe LysoTracker dye at a concentration of 50 nM for 30 min at 37°C. Cells were washed two times with PBS and incubated in complete media for imaging. The excitation wavelength was from 615 to 645 nm and the emission wavelength was from 655 to 760 nm. Imaging was done on Perkin Elmer Operetta high content confocal microscope, using a 20x objective. The number of puncta/cell was determined using Columbus (PerkinElmer). The number of positive cells for EGFP and LysoTracker was determined using Columbus (PerkinElmer). Three replicates per condition have been monitored and eight images per well were analysed.

Measurement of lysosomal pH in U2OS cells was performed using a ratiometric lysosomal pH indicator dye called LysoSensor® Yellow/Blue DND-160 (Invitrogen Life Technologies, #L7545, Carlsbad, CA, USA). Following 4 h compound treatment, cells were washed twice in PBS and incubated with

LysoSensor Yellow/Blue at a concentration of 2 μM for 5 min prior to measurement using Operetta confocal microscopy. Excitation wavelength was from 355 to 385 nm, and emission wavelengths were collected from 430 to 500 nm for the blue emission and 500 to 550 nm for the yellow emission. Images were analyzed in Columbus software. Blue fluorescence is an indicator of basic conditions and yellow fluorescence of acidic conditions. The intensity of the fluorescence signals are quantified and the ratio of yellow to blue fluorescence intensity is used as a representation of lysosomal pH.

3.3.4 Inhibition of intralysosomal proteolytic activity

Magic Red Cathepsin B (#937) and Magic Red Cathepsin L (#941) assay kits were purchased from Immunohistochemistry technologies, Bloomington, MN, USA. Cathepsin B (CTSB) and Cathepsin L (CTSL) activities in living cells were determined in accordance to manufacturer's instructions. U2OS cells were seeded in CellCarrier 384-well plates at a density of 200,000 cells per ml in complete media and allowed to settle overnight at 37° in a humidified 95% air and 5% CO₂ atmosphere to reach 80% confluency. The next day, cells were treated with 3 μM , 1 μM and 0.3 μM C18 for 4 h. After incubation time, CTSB and CTSL dye diluted in complete media were prepared. Cells were washed in PBS and fresh media containing the dyes was added to the cells. Cells were incubated with the dye for 30 min at 37°C. After incubation time, cells were washed twice in PBS, one minute each, and stained with fluorescence of living cells were obtained on Operetta using a 20x objective. Samples were read at 510-560 nm excitation and 570-620 nm emission for cathepsin activity. The number of fluorescent puncta were determined using Columbus software. Three replicates per condition have been monitored and eight images per well were analysed.

3.4 Structure activity relationship map of C18

To further define the biological activity of C18, SAR analysis was performed. After identification of C18 from the screen, a similarity assessment was performed to verify whether the program can find a more potent compound with chemical similarity to C18. In order to expand the candidate list, a MACCS fingerprint²⁷¹ similarity run was performed against ENAMINE HTS collection, available in-house. This collection of 200,000 commercial compounds spans

different subgroups like kinase, G-protein coupled receptors, protease inhibitors or binders together with a 50K diversity subset of Enamine HTS collection. Taking advantage from a KNIME workflow ad hoc prepared, MACCS fingerprints for each molecule have been calculated and the Tanimoto similarities towards C18 was performed. In general, Tanimoto similarity measure is frequently applied to fingerprint features based on their two-dimensional (2D) structures²⁷². Tanimoto metrics calculate the fraction of shared bits between chemical fingerprints in the range of 0 to 1 (in this case using classical MACCS fingerprints). Tanimoto similarity score equals 1 implies almost identity (beside chirality in enantiomers or in diastereoisomers). Tanimoto similarity score above 0.7 have been used to generate a list of candidates which have been subsequently purchased from MolPort (Riga, Latvia) and tested. The workflow for similarity check is described in **Figure 2**.

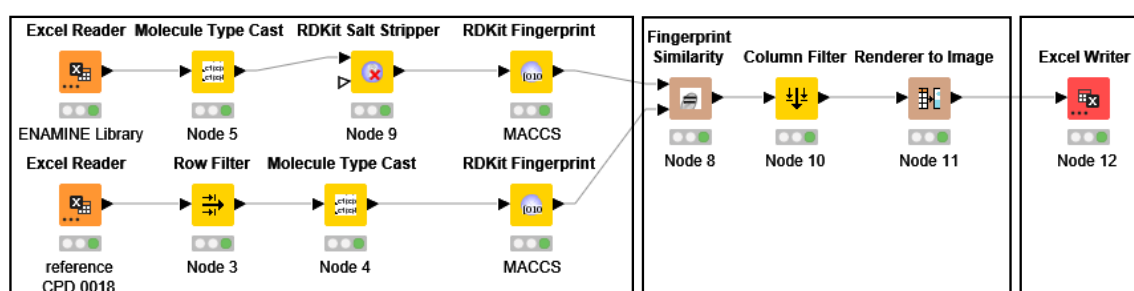


Figure 2: KNIME workflow to assess molecular similarity to the hit compound. In the first part, the workflow takes a reference molecule (here CPD 0018), and searches for similar molecules in the ENAMINE database. The similarity search is based on the MACCS fingerprints. The second part is the chemical calculations. In the third part, the molecules comparison and calculated predictions are exported as an Excel file.

3.5 Determination of cytotoxicity

Cell viability assay was performed using the RealTime-Glo™ MT Cell Viability Assay (Promega, #G9711, Madison, WI, USA), according to the manufacturer's instructions. U2OS cells, bone osteosarcoma epithelial cells, and HEK293, a human embryonic kidney cells were plated at 100,000 cells per ml in a microplate with 384 wells (Greiner Bio-One, #781080, Frickenhausen, Germany) and following overnight attachment, were incubated with fresh pre-warmed media at 37°C containing 1 x RT-Glo buffer (MT Cell Viability Substrate and NanoLuc® Enzyme). After 1 h incubation with RealTime-Glo reagent, luminescence signal was recorded on Fluent 780 (Tecan, Maennedorf,

Switzerland). This readout represent the background signal. Once background signal was obtained, cells were exposed to compounds using Echo liquid handler. Plate was incubated in the Cytomat 10 automated incubator (Thermofisher Scientific, Carlsbad, CA, USA) and luminescence signal was recorded on Fluent 780 for up to 72 h. Mean IC₅₀ values were calculated from the cell toxicity data obtained using GraphPad Prism for the immortalized cell lines.

3.6 Caspase-3 and 7 activity

Apoptosis measurements in U2OS cells were performed on the JuLI™ Stage Real-Time Cell History Recorder (Nanoentek, Seoul, Korea) with a DEVD substrate (IncuCyte Caspase-3/7 Red Reagent for Apoptosis, #4704, Essen BioScience, Ann Arbor, MI, USA). Cells were seeded at 100,000 per ml in PerkinElmer CellCarrier 384-well plates. The next day, C18 in complete media containing 0.7 μM apoptosis dye were added on in the wells containing cells in triplicates. DMSO (0.1%) was used as negative control. Four images per well were taken. The rate of kinetic activation of caspase-3/7 was monitored using a 20x objective inside a cell culture incubator (37°C, 5% CO₂) in order to ensure stable conditions for long-term measurements. Fluorescent images were taken every 2 h for 46 h and caspase-3/7 activity was quantified using the integrated software. JuLI™ STAT software was used to calculate the mean of red objects per well as a measure of apoptosis. Excitation wavelength was 630 nm and emission wavelength was 650 nm.

3.7 Determination of protein levels

3.7.1 Preparation of whole-cell lysates

U2OS cells and HEK293T cells were seeded in a 6-well plate (Greiner Bio-One, #657160, Frickenhausen, Germany) at 500,000 cells/well and allowed to settle overnight until they reached 80% confluency. DMSO, EBSS, BafA1 (100 nM) and concentrations of C18 in normal condition (DMEM media) or starved condition (EBSS media), and in presence or absence of BafA1, were added to the cells. All treatments were carried out for 4 h, unless stated otherwise. After treatment, cells were washed with PBS, collected, and lysed in chilled RIPA buffer (Thermofisher Scientific, #89901, Carlsbad, CA, USA) supplemented with cComplete™ Protease Inhibitor Cocktail (Roche, #CO-RO, Basel, Switzerland)

and phoSTOP (Roche, #PHOSS-RO, Basel, Switzerland) for 10 min on ice, and then centrifuged at 14,000 g for 10 min at 4°C to collect the supernatant fraction.

3.7.2 Protein quantification

The concentration of protein in samples was calculated using Pierce™ BCA Protein Assay Kit (ThermoFisher Scientific, #23225 Carlsbad, CA, USA), according to the manufacturer's instructions. BSA standards were prepared in lysis buffer, with concentrations between 20-2000 µg/ml. Protein concentration was detected using the microplate procedure. The absorbance at 560 nm was measured on Envision plate reader (Perkin Elmer, Waltham, MA, USA). A BSA standard curve was plotted in GraphPad prism to determine the equation of the line, which is used to calculate the protein concentration of each unknown sample.

3.7.3 SDS-PAGE and Western blot

Whole-cell lysates were diluted to a final concentration of 20 µg/µl in a volume of 40 µl containing 1x LDS sample buffer (#B0007) and 1 x sample reducing agent (#B0004) from Invitrogen Life Technologies (Carlsbad, CA, USA). Samples were denatured at 95°C for 5 min. Samples were then loaded in pre-casted NativePAGE™ 4 to 16% BIS-TRIS gels (Invitrogen, #BN1002BOX, Carlsbad, CA, USA) and separated at 200V for 45 min at room temperature in 1x Bolt™ MOPS SDS running buffer (Invitrogen, #B0001, Carlsbad, CA, USA). Two lanes of each gel was loaded with 10 µl PageRuler™ Plus Prestained Protein Ladder (ThermoFisher Scientific, #26619, Carlsbad, CA, USA) for determination of the protein size. Before start, 0.5 ml Bolt™ Antioxidant (Invitrogen, #BT0005, Carlsbad, CA, USA) was added in the middle of the chamber to maintain reducing conditions and to prevent re-oxidation of sensitive amino acids. After separation, the proteins were blotted onto a PVDF membrane (Invitrogen, #LC2007, Carlsbad, CA, USA) at 30V for 1 h on ice in 1x Bolt™ Transfer Buffer (Invitrogen, #BT0006, Carlsbad, CA, USA) containing 10% ethanol and 0.5 ml Bolt™ Antioxidant per 500 ml buffer. Membranes were blocked for 1 h at room temperature with agitation in 5% milk in TBS (Alfa Aesar, #J60764, Haverhill, MA, USA) containing 0.1% Tween (Carl Roth, #9127.1, Karlsruhe, Germany) for p62 detection and 5% BSA in TBS-Tween

0.1% for all other proteins. Primary and secondary antibodies were diluted in blocking buffer according to **Table 4** and **Table 5**. Primary antibody incubation was performed overnight at 4°C. Afterwards, membranes were washed three times for 5 min in TBS-Tween 0.1% and incubated with secondary antibodies for 1 h at room temperature, protected from light. After washing three times for 5 min in TBS-Tween 0.1% bands were detected using WesternSure® PREMIUM Chemiluminescent Substrate (Li-Cor Biosciences, #926-95000, Bad Homburg, Germany). Densitometry analysis was performed using ImageJ 1.53e (NIH, USA). The intensity of bands were quantified and proteins were normalized to the loading control, β -actin. The ratio of indicated protein to β -Actin indicates overall protein expression.

Table 4: Primary antibodies

Primary Antibody	Dilution	Manufacturer, catalog # and RRID
Mouse anti-LC3	1:1000	Cell Signalling Technology, #83506S, AB_2800018
Guinea pig anti-p62	1:1000	Progen, #GP62-C, AB_2687531
Rabbit anti-Rab7	1:1000	Cell Signalling Technology, #9367S, AB_1904103
Rabbit anti-4E-BP1	1:1000	Cell Signalling Technology, #9644S, AB_2097841
Rabbit anti-phospho-4E-BP1	1:1000	Cell Signalling Technology, #2855S, AB_560835
Rabbit anti-CHOP	1:1000	Cell Signalling Technology, #5554S, AB_10694399
Rabbit anti-BiP	1:1000	Cell Signalling Technology, #3177S, AB_2119845
Rabbit anti- β -Actin	1:1000	Cell Signalling Technology, #4970S, AB_2223172

Table 5: Secondary antibodies

Secondary Antibody	Dilution	Manufacturer, catalog # and RRID
Goat anti-rabbit IgG, HRP-conjugated	1:5000	LI-COR® Biosciences, #P/N 926-80011, AB_2721264
Goat anti-mouse IgG, HRP-conjugated	1:5000	LI-COR® Biosciences, #P/N 926-80010, AB_2721263
Anti-guinea pig IgG, HRP-conjugated	1:5000	Invitrogen Life Technologies, #A18769, AB_2535546

3.7.4 Striping of PVDF membranes for phosphorylated protein detection

To incubate PVDF membranes several times with different primary antibodies, they were stripped using Restore™ Western Blot Stripping Buffer from ThermoFisher Scientific (Carlsbad, CA, USA). Previously blocked, probed and detected membrane with chemiluminescent is washed three times in TBS-Tween 0.1% to remove the chemiluminescent substrates. Membrane is then incubated in the stripping buffer with agitation for 15 min at room temperature to detach bound antibodies. The blot is removed and washed three times in TBS-Tween 0.1%, and tested to confirm that all antibodies have been removed. Next, the blot is blocked and incubated with appropriate primary and secondary antibodies as described in section 6.3. Each membrane was stripped up to four times.

3.8 Gene expression analysis

3.8.1 RNA isolation and extraction

Total RNA was isolated using RNeasy Plus Mini Kit (Qiagen, #74134, Hilden, Germany). U2OS cells were treated for 4 h with DMSO, EBSS, BafA1 (100 nM) and C18 in normal or starved condition, and in presence or absence of BafA1. After incubation, cells were washed with 500 μ L PBS and homogenized in RLT plus buffer containing 500 μ M β -mercaptoethanol (ThermoFisher Scientific, #11528926, Carlsbad, CA, USA). Cells were harvested using a scraper (Corning, #3010, NY, USA). Before proceeding with RNA extraction, total lysates were subjected to a second homogenization using QIAshredder (Qiagen, #79656, Hilden, Germany) for complete disruption of the RNA. Concentration and purity of the extracted RNA samples were assessed using NanoDrop-1000 from Peqlab (Erlangen, Germany). The amount of RNA (in ng/ μ L) was recorded, as well as the A260/A280 and A260/A230 ratios.

3.8.2 cDNA synthesis

After determination of the RNA concentration, RNA was reversed transcribed into cDNA using the RevertAid H Minus First Strand cDNA Synthesis Kit from ThermoFisher Scientific (#K1632, Carlsbad, CA, USA) according to manufacturer's instructions. For cDNA synthesis, RNA samples were diluted with RNase-free water to a concentration of 70 ng/ μ L in a total volume of 11 μ L, so that equal amount of total RNA were used for reverse transcription for all

samples. In case of a low RNA yield, the sample was used undiluted. The RNA was mixed with 1 μ l of the hexamer primer and heated at 65°C for 5 min in the PCR thermocycler FlexCycler2 from Analytic Jena (Jena, Germany). In the meantime, the reverse transcription mastermix was prepared on ice according to **Table 6**. After incubation, 8 μ l of mastermix was added to all samples and incubated for 5 min at 25°C, 60 min at 42°C and 5 min at 70°C using the PCR thermocycler to complete cDNA synthesis.

Table 6: Components of the cDNA synthesis master mix

MasterMix	Volume (μl) 1X
Reaction buffer (5X)	4
RiboLock RNase Inhibitor (20 U/ μ l)	1
10 nM dNTP Mix	2
RevertAid H Minus M-MuLV Reverse Transcriptase (200 U/ μ L)	1
Total	8

3.8.3 Quantitative real-time polymerase chain reaction (qRT-PCR) assay

Relative quantification of mRNA expression was assessed by real-time PCR using the TaqMan® Assay. For each primer a master mix was prepared as described in **Table 7**. cDNA samples were diluted based on the RNA amounts used during their cDNA synthesis. The final assay concentration of cDNA was between 30-40 ng/ μ l. The assay was carried out in the 96 well format using the PCR plates from Sarstedt (#72.1979.202, Nümbrecht, Germany). 8 μ l of the mastermix were transferred to the wells of a precooled plate, followed by addition of 2 μ l cDNA or RNA-free water (for the no template control). Afterwards, the PCR plate was centrifuged for 15 seconds at 4000 g, than sealed with an adhesive PCR film (Peqlab, #82-0558, Erlangen, Germany) to prevent volume loss during the qPCR. A compression pad was put on top of the PCR plate for additional thermal seal. The qPCR was performed with the 7900HT Fast Real Time PCR System from Applied Biosystems (California, USA) and using the linked software Sequence Detection System (SDS) version 2.4. The thermocycling condition consisted of denaturation for 2 min at 50°C

and 10 min at 95°C, followed by amplification for 40 cycles at 95°C for 15 seconds each, and annealing-extension at 60°C for 1 min. Every sample, including the negative control, was tested in triplicate. RPLP0 (ribosomal protein, large, P0) was used as a housekeeping gene. The resulting CT (cycle threshold) values for target gene samples were normalized against the corresponding RPLP0 CT values. The double delta Ct method, also known as $\Delta\Delta\text{Ct}$ method, was calculated according to Livak and Schmittgen²⁷³. In order to get the fold change expression of a gene, two to the power of negative $\Delta\Delta\text{Ct}$ was calculated.

Table 7: Components of the qPCR master mix

MasterMix	Volume (µl) 1X
20X TaqMan Gene 1 Expression Assay	0.5
2X TaqMan Gene Expression MasterMix	5
RNase-free water	2.5
Total	8

3.8.4 Quantification of qRT-PCR products

To confirm that the fragments created by RT-qPCR are of the correct size gel electrophoresis was performed. In this work, 2% agarose gel (ThermoFisher Scientific, #16500-500, Carlsbad, CA, USA) was prepared. The agarose was mixed with ROTIPHORESE ® TAE buffer (Carl Roth, #CL86.1, Karlsruhe, Germany) and boiled using a microwave until solution is clear and all particles are dissolved. Then, 5 µl/100 ml Roti® Gel Stain (Carl Roth, #3865.1, Karlsruhe, Germany) intercalating dye was added to the agarose gel for visualization of the DNA bands under UV light. The gel was poured into a previously prepared gel tray with a 20-well comb in place and allowed to be solidified. Once the gel hardened, the tray together with the solid gel was placed in the electrophoresis chamber PerfectBlue™ Horizontal Maxi Gel System from VWR (Pennsylvania, USA) and fully covered with 1x TAE Buffer prepared previously. The triplicates of each sample were pooled together from section 8.3. DNA samples were mixed with 1x TriTrack DNA Loading Dye

(ThermoFisher Scientific, #R1161, Carlsbad, CA, USA). GeneRuler DNA Ladder Mix (ThermoFisher Scientific, #SM0332, Carlsbad, CA, USA) was also prepared according to the manufacturer's instructions in RNA-free water to estimate the DNA size. Prepared samples including the DNA ladders were loaded into the pre-cast wells of the gel and electrophoresis was conducted at 120 to 180 V for about 1.5 h using the Biometra P25 from Analytik Jena (Jena, Germany). Afterwards the PCR products were visualized under UV light using the GEL iX20 Imager (Intas Science Imaging, Göttingen, Germany) at 310 nm.

3.9 Transmission Electron Microscopy

U2OS cells were seeded onto T25 flasks and allowed to grow until reached 80% confluency. Cells were then treated with 3 μ M C18 in normal or starved condition, in presence or absence of BafA1 for 4 h at 37°C. After designated incubation time, cells were directly subjected to fixation without any washing steps. First, cells were fixed in 2x fixation buffer (4% freshly prepared PFA, 5% glutaraldehyde, in 0.1 M sodium cacodylate pH 7.4) for 20 min at room temperature. After 20 min, cells were further fixed in 1x fixation buffer (2% freshly prepared PFA, 2.5% glutaraldehyde, in 0.1 M sodium cacodylate pH 7.4) for 2 h at room temperature. The next steps, dehydration and embedding with Epon resin were achieved as previously described²⁷⁴. 70 nm thin sections were cut using a Leica EM UC7 ultra microtome (Leica Microsystems, Wetzlar, Germany) and stained with uranyl acetate and lead citrate. Cell sections were analyzed using an 80 kV transmission electron microscope Talos 200Fi (FEI, Eindhoven, Netherlands). The analysis of the samples was performed by Dr. Muriel Mari at University Medical Center Groningen (UMCG) in The Netherlands.

3.10 Determination of intracellular calcium content

Changes in free cytosolic Ca^{2+} were investigated using the fluorescent Ca^{2+} binding dye, Fluo-4, during the application of compounds in U2OS cells. Cells were plated at 225,000 cells per ml in a 384-well plate (Corning, #3764, NY, USA) and incubated overnight. Cells should be at approximately 90% confluency overnight, which is the optimum density for this assay. Next, cells were incubated with 2.5 mmol/L Fluo-4 Direct calcium reagent (Fluo-4 Direct Calcium Assay Starter Pack, #F10471, ThermoFisher Scientific, Carlsbad, CA,

USA) and incubated for 1 h at 37°C. After 1 h, Fluo-4 dye was removed and C18 in complete media was added to the cells. The relative fluorescence was measured on Envision microplate reader every 60 seconds for 15 min, using excitation at 494 nm and emission at 516 nm. Thapsigargin (Absource Diagnostics, #S7895, Munich, Germany) was used as a positive control. Furthermore, to better understand the effect of C18 on ER Ca²⁺ stores, the effect of C18 in presence of thapsigargin was studied. Cells were pre-incubated with 1 µM thapsigargin for 5 min prior to addition of various concentrations of C18. The relative fluorescence was measured immediately after addition of C18 every 60 seconds for 15 min.

3.11 Statistical analysis

To evaluate the quality of the assays, a screening window coefficient, known as Z factor, is defined according to the method proposed by Zhang and colleagues²⁷⁰. Z factor is defined as the equation below. Generally a Z factor > 0.2 is suitable for cell-based assays²⁷⁵.

$$Z\ factor = 1 - \frac{3\ SD\ of\ sample + 3\ SD\ of\ control}{|mean\ of\ sample - mean\ of\ control|}$$

For dose-dependent studies, the curves were fitted in GraphPad Prism 9 Software and the IC₅₀ was computed using the nonlinear regression option.

All experiments were conducted at least three times, unless stated otherwise. At least two repeats per condition were used in each experiment. The data were pooled for determination of the mean ± standard error of the mean (SEM). All data were analysed by GraphPad using analysis of variance (ANOVA) to determine the statistical significance (p value). One-way ANOVA was performed when analyzing non-grouped data. Grouped data was analyzed using two-way ANOVA, and when significant multiple comparisons were performed with the Dunnett's or Sidak's test. A p value < 0.05 was considered to be significant (*p < 0.05, **p < 0.01, ***p < 0.001 and ****p < 0.0001).

4 RESULTS

4.1 Identification of autophagy modulating drugs in HEK293T

4.1.1 Assay validation, selection of tool compounds and Z factor determination

Prior to screening, assay optimization was carried out to find the best tool compounds. The activity of various FDA-approved compounds that modulate autophagy was tested in HEK293T cells with stable expression of TagRFP-mWassabi-LC3. TagRFP-mWassabi-LC3B tagged HEK293T cells were treated with compounds for 4 h to modulate autophagy and then processed for confocal microscopy analysis. The number of TagRFP⁺mWassabi⁺-LC3B (autophagosomes) and TagRFP⁺mWassabi⁻-LC3B (autolysosomes) per cell were quantified (**Figure 4A**). Next, the autophagic flux was estimated using the ratio of TagRFP⁺ (red) to TagRFP⁺ mWassabi⁺ (yellow) puncta, normalised to the ratio of the negative control (DMSO). **Figure 4B** indicates the most potent autophagy modulators tested in this assay. BafA1 at a concentration of 100 nM significantly decreased the ratio of red puncta to yellow puncta ($p < 0.0001$), which correlates with reduced number of autolysosome. The assay window to identify autophagy inhibitors is very good (3-5), with a Z factor of 0.4²⁷⁶. Normalisation did not reduce the assay window or Z factor. Regarding inducers, the mTOR inhibitor torin1 and the BH3 mimetic ABT-737 were selected. Both torin1 and ABT-737 were able to significantly increase the ratio of red to yellow puncta ($p < 0.0001$ and $p = 0.0078$ respectively). The effect of ABT-737 was not statistically significant when data was normalized to the negative control (DMSO). The assay window to identify autophagy inducers is relatively low (1.16 for torin1 and 1.6 for ABT-737) but it is representative of activators. However, it could be difficult to identify hits that induce autophagy. Longer incubation time (6 h) was also tested but increasing time increased variability between replicates (data not shown).

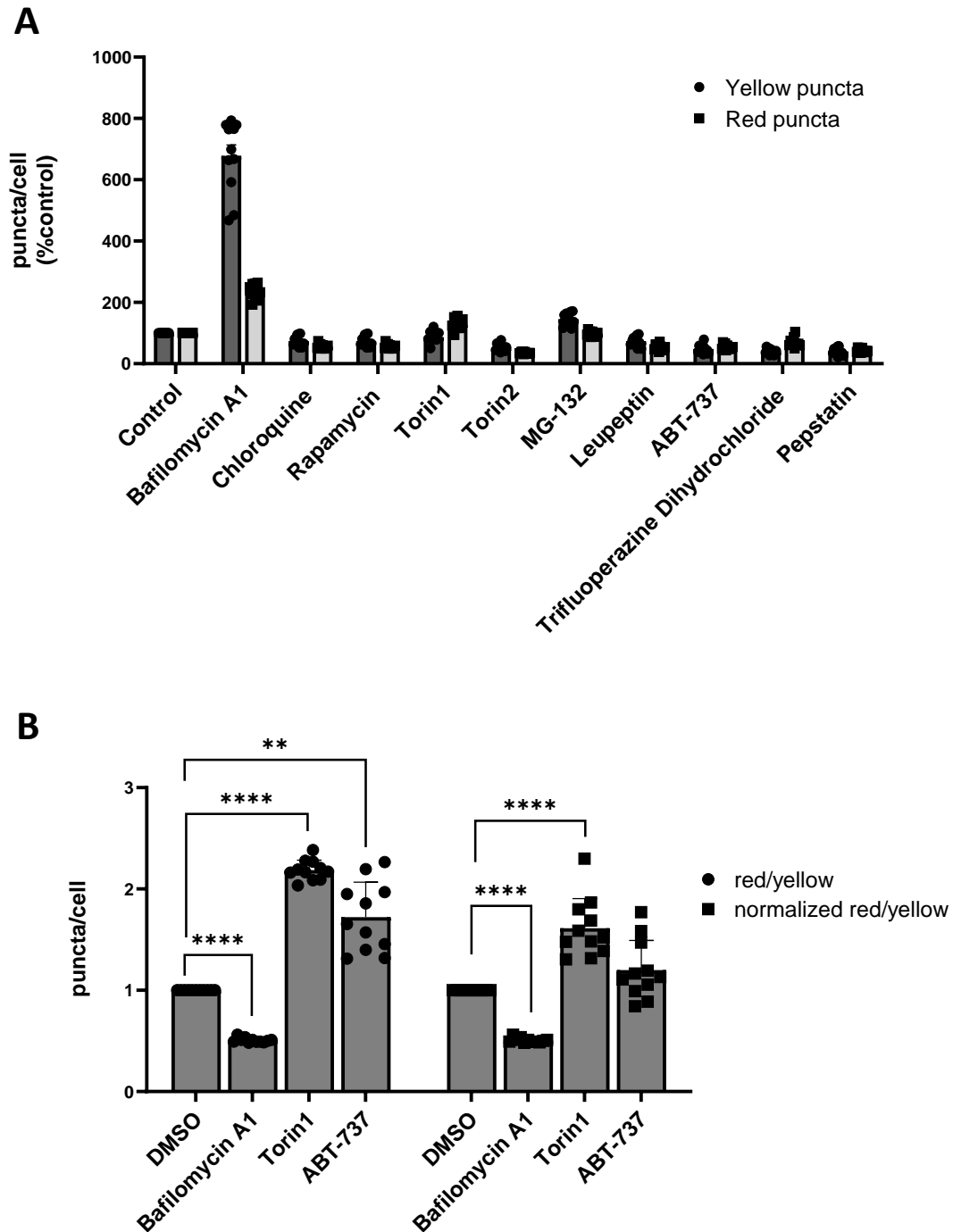


Figure 3: Assay optimization in TagRFP-mWassabi-LC3 tagged HEK293T. (A) High content analysis of stably transfected HEK293T cells after 4 h treatment with BafA1 (100 nM), CQ (10 μ M), rapamycin (10 μ M), torin1 (10 μ M), torin2 (10 μ M), MG-132 (5 μ M), leupeptin (10 μ M), ABT-737 (10 μ M), trifluoperazine dihydrochloride (10 μ M) and pepstatin (10 μ M). Yellow puncta represents TagRFP⁺ mWassabi⁺ puncta and red puncta represents TagRFP⁺ puncta. The ratio red/yellow shows autophagic flux. **(B)** Indicates tool compounds selected for the high-throughput screening. Individual values are indicated. Only puncta $\geq 0.3 \mu$ m in size were counted. Data are presented as mean \pm SEM of at least three independent biological replicates. At least 8 technical replicates per condition were quantified.

As part of the assay optimisation, two spot detection algorithms either having excluded or not excluded the nucleus have been conducted. The respective ratios (red/yellow puncta) hardly change between the two options. Therefore, the spot detection was ran across the entire cell and the number yellow puncta and red puncta per cell were quantified (**Figure 4**). Absolute numbers of puncta may vary, hence the red/yellow ratios were normalized to DMSO. Overall, tool compounds show very good correlation with regard to day-to-day, plate-to-plate and batch-to-batch variability. The assay in its current configuration is fit for screening.

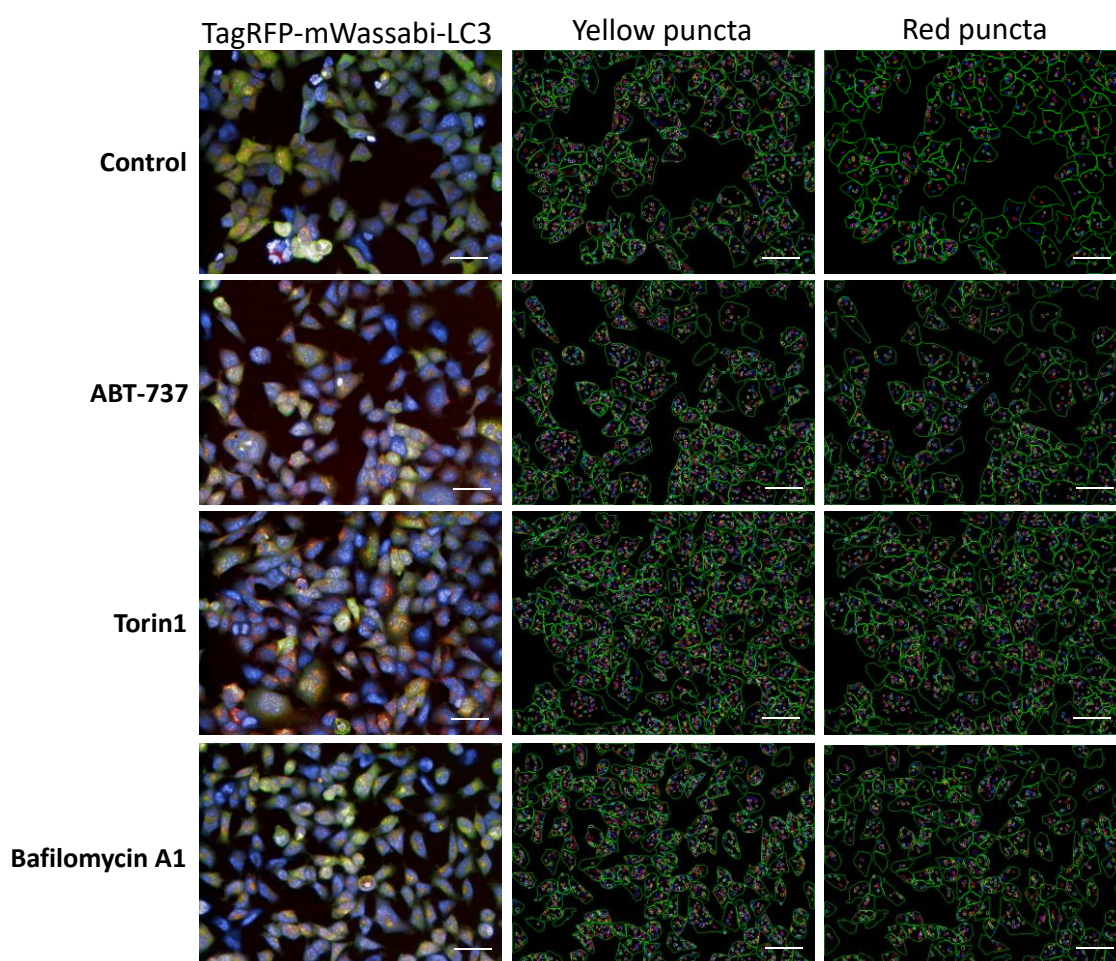


Figure 4: Representative images from the spot detection algorithm. Raw images of the tool compounds (left panel) with boundary of cells in which yellow puncta (middle panel) and red puncta (right panel) were quantified. Bar 50 μM . Only puncta $\geq 0.3 \mu\text{M}$ in size were counted. Data are presented as mean \pm SEM of at least three independent biological replicates. At least 8 technical replicates per condition were quantified.

4.1.2 Primary screen

In total, 48 compounds showed superior autophagy modulation and have been selected for hit confirmation. From these hits, 38 compounds were from the ChemBioNet library and 10 compounds from the FDA-approved library (**Table 8**). Hits were classified as high priority, if active 3-fold above the mean of the negative control in the same plate, and low priority if they were borderline of hit criterion. From ChemBioNet library, 25 low priority hits and 13 high priority hits have been identified. From high priority hits, 10 were belonging to the same hit series. From low priority hits, 7 hits showed late inhibition similar to BafA1. Intriguingly, from 10 hits identified from ENZO library, 4 hits were described previously as autophagy modulators (ENZ_0000713, ENZ_0000735, ENZ_0000104 and ENZ_0000737). Published data indicates that ENZ_000713, known as reserpine, inhibits autophagic flux²⁷⁷). On the other hand, ENZ_0000104 and ENZ_0000737, known as idarubicin and tadalafil, have been shown to increase autophagic flux^{278, 279, 280}. Regarding ENZ_0000735, known as sunitinib, controversial effects have been seen^{281, 282, 283, 284, 285}, which suggests a possible biphasic effect²⁸⁶. In line with these findings, the screen also identified sirolimus (rapamycin), a known autophagy inducer¹⁰⁹, as one of the active compounds which, altogether, confirm that assay is reliable for detection of autophagy modulators. There were some plate-to-plate variability (**Figure 5A**), however normalizing the ratio to DMSO improved this (**Figure 5B**). When variance was still high, hit selection was done manually on a plate basis to better distinguish between compound and plate effect. Torin1 performed well in ENZO library assay plates but did not increase number of red puncta in some of the plates containing ChemBioNet compounds.

Table 8: List of the hits derived from primary screen.

31809_ChemDiv_8015-2378	31509_ChemDiv_5018-0023	25911_ChemDiv_1606-0410
31939_ChemDiv_8017-6948	31511_ChemDiv_5018-0024	25927_ChemDiv_8005-5567
31955_ChemDiv_5408-3403	31481_ChemDiv_5018-0012	25755_ChemDiv_8014-1098
31738_ChemDiv_5424-0241	31513_ChemDiv_5018-0025	25916_ChemDiv_K088-0682
31946_ChemDiv_5554-1215	31483_ChemDiv_5018-0013	25919_ChemDiv_2036-0570

30839_ChemDiv_4568-7276	31515_ChemDiv_7165-0130	25680_ChemDiv_C367-0082
30890_ChemDiv_C720-0070	31517_ChemDiv_7165-0812	ENZ_0000001
31010_ChemDiv_5966-0051	31487_ChemDiv_5018-0018	ENZ_0000007
31042_ChemDiv_4729-1361	26609_ChemDiv_D055-0186	ENZ_0000087
31106_ChemDiv_8017-7353	26425_ChemDiv_8014-1404	ENZ_0000009
31234_ChemDiv_4826-0011	26602_ChemDiv_1439-0276	ENZ_0000010
30973_ChemDiv_4478-7598	26604_ChemDiv_2422-1298	ENZ_0000104
30975_ChemDiv_6231-0134	26397_ChemDiv_6145-0677	ENZ_0000141
31505_ChemDiv_5018-0020	25969_ChemDiv_3448-3303	ENZ_0000713
31537_ChemDiv_5018-0066	25634_ChemDiv_8012-5632	ENZ_0000735
31507_ChemDiv_5018-0021	25638_ChemDiv_C301-6223	ENZ_0000737

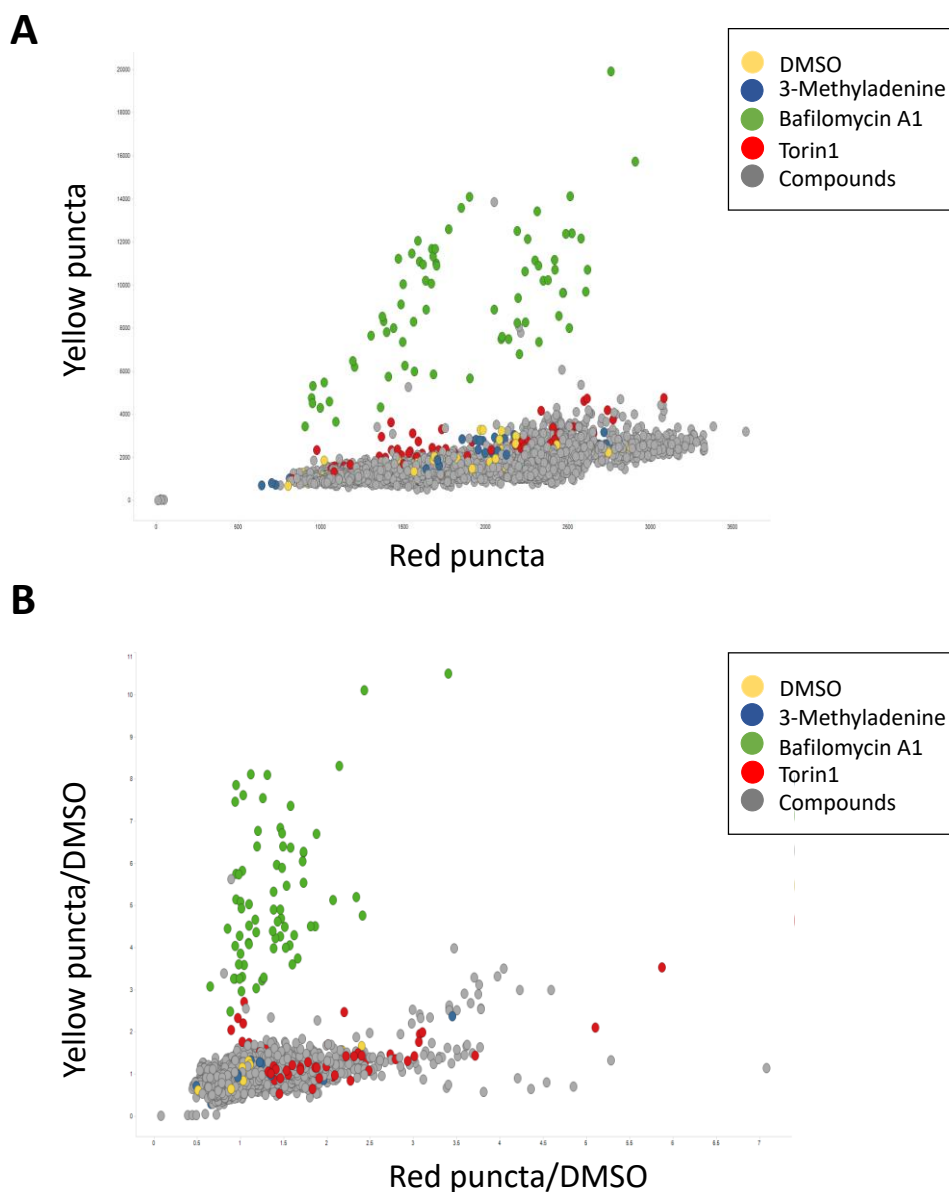


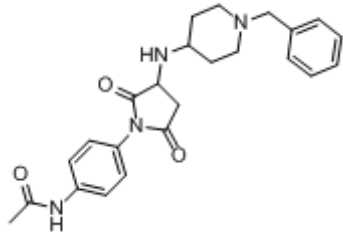
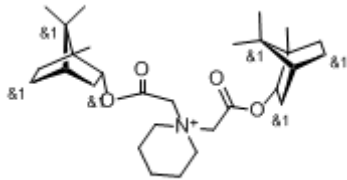
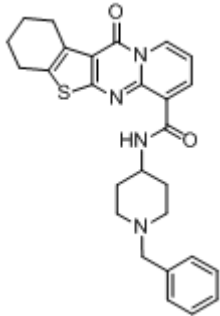
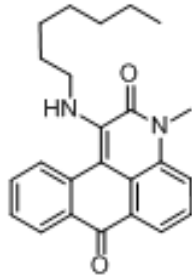
Figure 5: Analysis of the primary screening results. Data is plotted as **(A)** yellow puncta per cell over red puncta per cell and **(B)** yellow puncta over red puncta, both normalized to control (DMSO). Hits are indicated in grey. Data are represented as mean of three replicates from two independent experiments.

4.1.3 Confirmation of hits

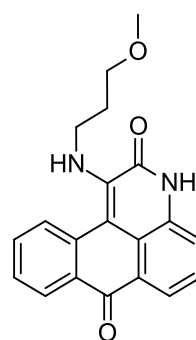
During hit confirmation, a total of 25 compounds were classified as hits (**Table 9**). A compound was selected as hit if the mean of yellow puncta and/or red puncta was 3-fold above the mean of the yellow puncta and/or red puncta of negative control (DMSO) in the same plate. The confirmation rate was of approximately 51%, of which 9 were of the category yellow/DMSO (inhibitors)

and 22 were of the category red/DMSO (inducers), including the 10 high priority hits identified in the primary screen. An overall of 6 compounds fall into both categories yellow/DMSO and red/DMSO. Torin1 was ineffective at this stage and decreased number of yellow and number of red puncta for unknown reason (**Figure 6**). Otherwise a good data quality was achieved with $Z' > 0.7$ (based on increase in number of yellow spots in BafA1-treated cells compared to DMSO-treated cells).

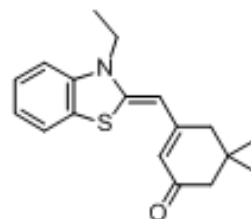
Table 9: List of confirmed hits and their chemical structures

Compound ID	Hit class	Structure
31042_ChemDiv_4729-1361	yellow/DMSO	
31946_ChemDiv_5554-1215	yellow/DMSO	
25680_ChemDiv_C367-0082	red/DMSO	
26397_ChemDiv_6145-0677	red/DMSO	

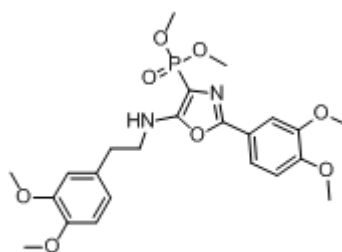
26425_ChemDiv_8014-1404 red/DMSO



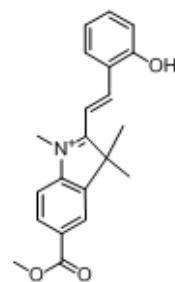
26604_ChemDiv_2422-1298 red/DMSO



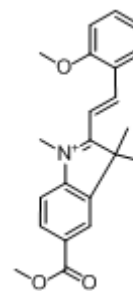
26609_ChemDiv_D055-0186 red/DMSO



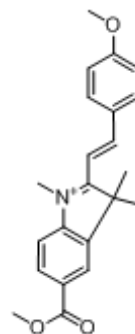
31481_ChemDiv_5018-0012 red/DMSO



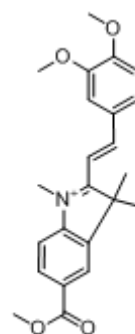
31487_ChemDiv_5018-0018 red/DMSO



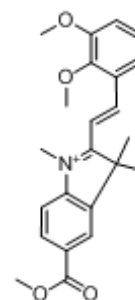
31505_ChemDiv_5018-0020 red/DMSO



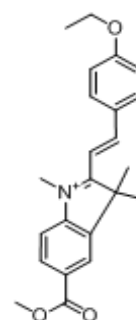
31507_ChemDiv_5018-0021 red/DMSO



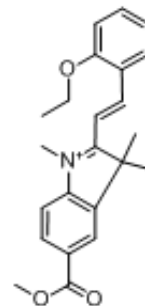
31509_ChemDiv_5018-0023 red/DMSO



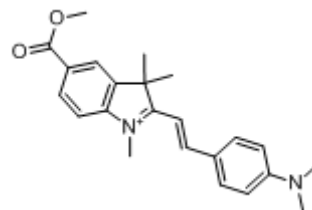
31511_ChemDiv_5018-0024 red/DMSO



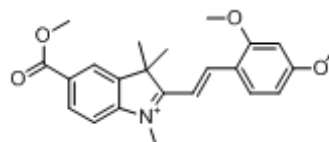
31513_ChemDiv_5018-0025 red/DMSO



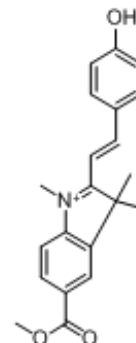
31515_ChemDiv_7165-0130 red/DMSO



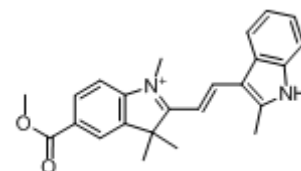
31517_ChemDiv_7165-0812 red/DMSO



31483_ChemDiv_5018-0013 yellow/DMSO; red/DMSO

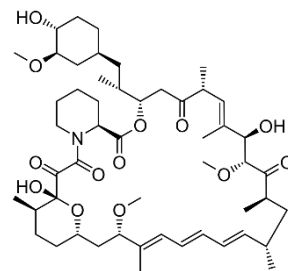


31537_ChemDiv_5018-0066 yellow/DMSO; red/DMSO



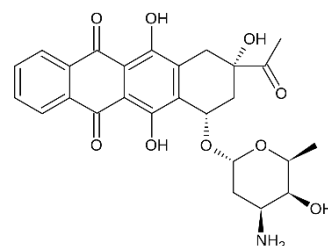
ENZ_000007

yellow/DMSO; red/DMSO



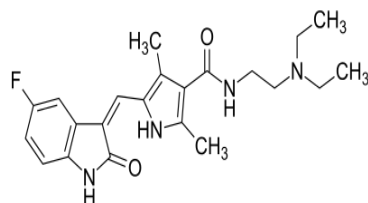
ENZ_0000104

yellow/DMSO; red/DMSO



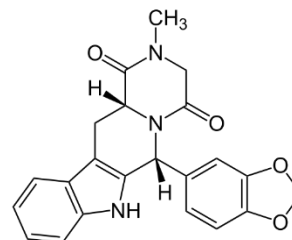
ENZ_0000735

yellow/DMSO; red/DMSO



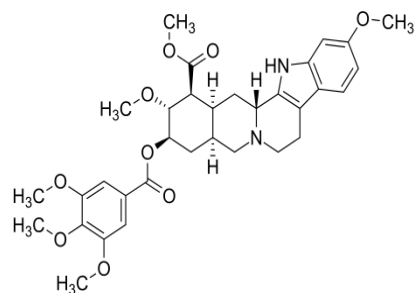
ENZ_0000737

yellow/DMSO; red/DMSO



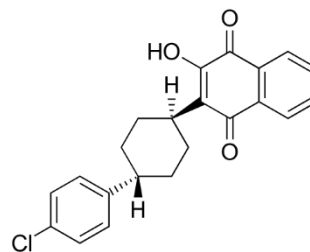
ENZ_0000713

yellow/DMSO



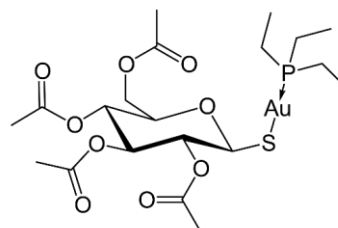
ENZ_000087

red/DMSO



ENZ_000141

red/DMSO



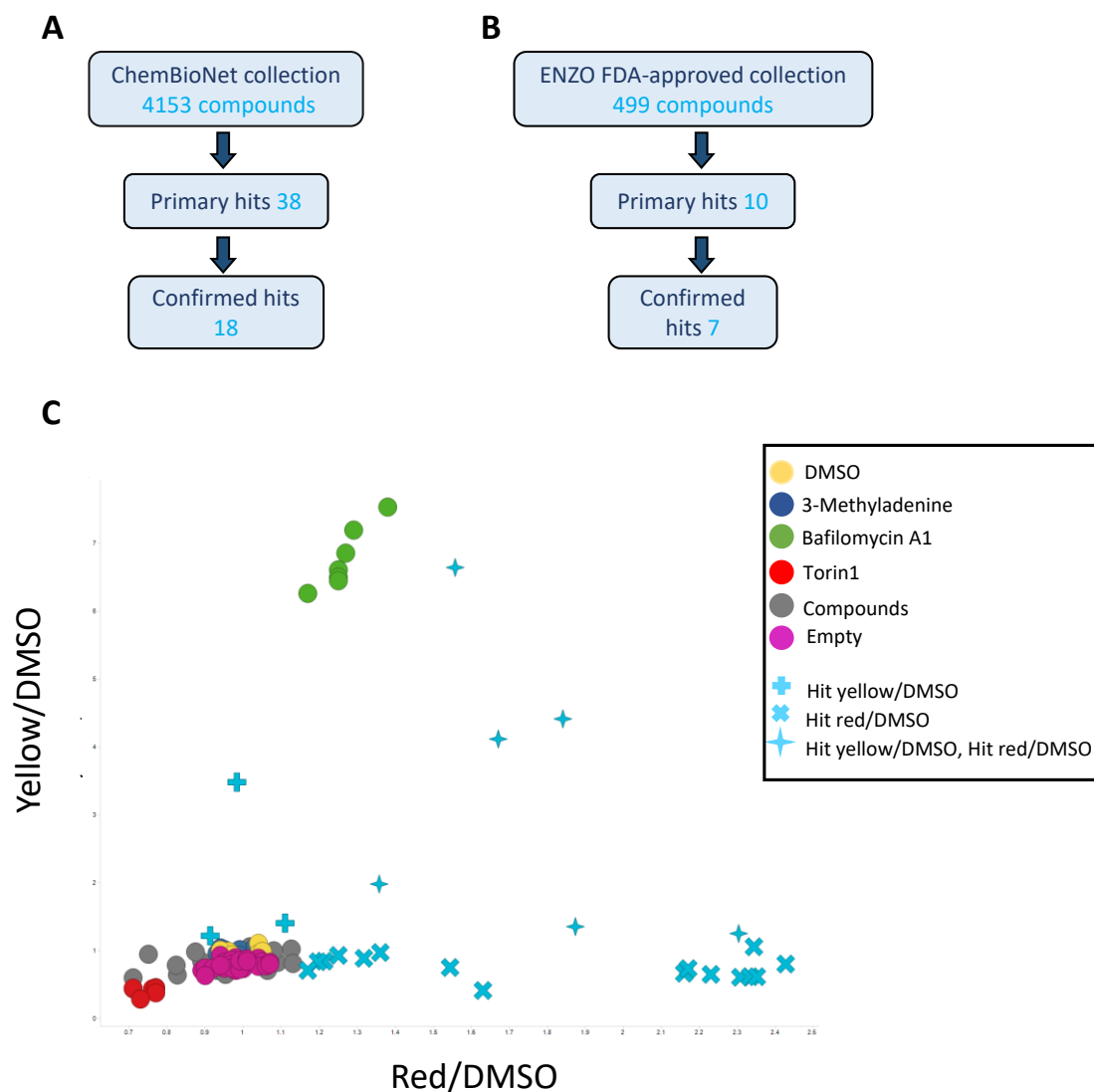


Figure 6: Summary of hit selection from the autophagy screens. (A) ChemBioNet library screen and **(B)** Enzo FDA-approved library. **(C)** Graphical representation of confirmed hits to increase or inhibit autophagy. Number of puncta was normalised to control (DMSO). Data are represented as mean of three replicates from two independent experiments.

4.1.4 Summary of dose response studies

Having confirmed the hits, the next step was to show dose-dependent activity. For this purpose, 11-point dose response curves for 25 confirmed hits were generated. 6 out of 25 compounds were profiled correctly, confirming findings from the primary screen. 2 compounds confirmed, previously as hit in red/DMSO category, increased in yellow/DMSO and 4 compounds from the FDA-approved library, previously fallen in both categories, were profiled as hit in

yellow/DMSO category. In total, 12 compounds were classified as active in a dose-dependent manner (**Table 10**).

Table 10: Table displaying compounds by hit class.

Compound ID	Hit class	Confirmed (Yes/No)
31042_ChemDiv_4729-1361	yellow/DMSO	Yes
31946_ChemDiv_5554-1215	yellow/DMSO	Yes
26397_ChemDiv_6145-0677	red/DMSO	yellow/DMSO
26604_ChemDiv_2422-1298	red/DMSO	yellow/DMSO
31487_ChemDiv_5018-0018	red/DMSO	Yes
31505_ChemDiv_5018-0020	red/DMSO	Yes
31511_ChemDiv_5018-0024	red/DMSO	Yes
31517_ChemDiv_7165-0812	red/DMSO	Yes
ENZ_0000104	yellow/DMSO; red/DMSO	yellow/DMSO
ENZ_0000735	yellow/DMSO; red/DMSO	yellow/DMSO
ENZ_0000737	yellow/DMSO; red/DMSO	yellow/DMSO
ENZ_0000713	yellow/DMSO	yellow/DMSO

4.1.5 Western blot analysis of LC3B and p62

The analysis of lipidated LC3-II is the go-to method to indirectly measure changes in autophagy²⁸⁷. The lipidated form of LC3, referred to as LC3-II, has a molecular weight of 14-16 kDa on SDS-PAGE gels while non-lipidated LC3-I has a molecular weight of 16-18 kDa⁴⁶. This difference in migration is detected by western blot and in order to determine autophagosome formation. To elucidate whether the compounds caused changes in autophagy, the amount of lipidated LC3-II upon compound treatment in HEK293T cells was detected and quantified. Cells were treated with 10 μ M compounds from **Table 10** and lysates were collected. The relative protein levels of LC3-II are shown in **Figure 7**. The amount of LC3-II to the loading control, β -actin, is used for comparisons. Results show increased LC3-II with 4 compounds from the screen, including ENZ_0000713, ENZ_0000735, ENZ_0000104 and 31487_ChemDiv_5018-0018. ENZ_0000713 and ENZ_0000735 significantly increased LC3-II more than 5-fold compared to DMSO ($p < 0.0001$). Similarly, ENZ_0000104 and 31487_ChemDiv_5018-0018 also caused a significant increase by 2.5-fold ($p = 0.0448$) and 2-fold respectively ($p = 0.0161$). The effects were similar to BafA1,

which caused on average a marked increase of 5.38 in LC3-II ($p < 0.0001$). The starvation media (EBSS), an inducer of autophagy, slightly decreased LC3-II levels.

A second approach widely used to detect autophagic flux is measuring p62/SQSTM1 degradation²⁸⁸. An induction of autophagy increases the degradation of SQSTM1/p62 while inhibition of autophagy causes its accumulation. Hence, p62 levels can be used as an index of autophagic degradative capacity. **Figure 7** shows that 100 nM BafA1 significantly increased the expression of p62 protein by 2- to 5-fold compared to the control (DMSO). ENZ_0000713, ENZ_0000735 and ChemDiv_5018-0018 also followed the same trend as BafA1 and significantly increased the p62 protein levels. ENZ_0000713, ENZ_0000735 and ChemDiv_5018-0018 significantly increased p62 protein expression by 2-fold compared to DMSO ($p = 0.0063$, $p = 0.0038$ and $p = 0.003$). EBSS did not increase p62 protein expression. Overall, this data suggests that p62 can be used as a reliable marker to study autophagic flux, in particular to measure autophagy inhibitors. Moreover, data confirms previous findings that ENZ_0000713 and ENZ_0000735 inhibit autophagy. Since that information is already in the public domain and the aim is to identify a novel compound, it was decided to prioritise the hit from the ChemBionet library ChemDiv_5018-0018, referred to as compound 18 (C18).

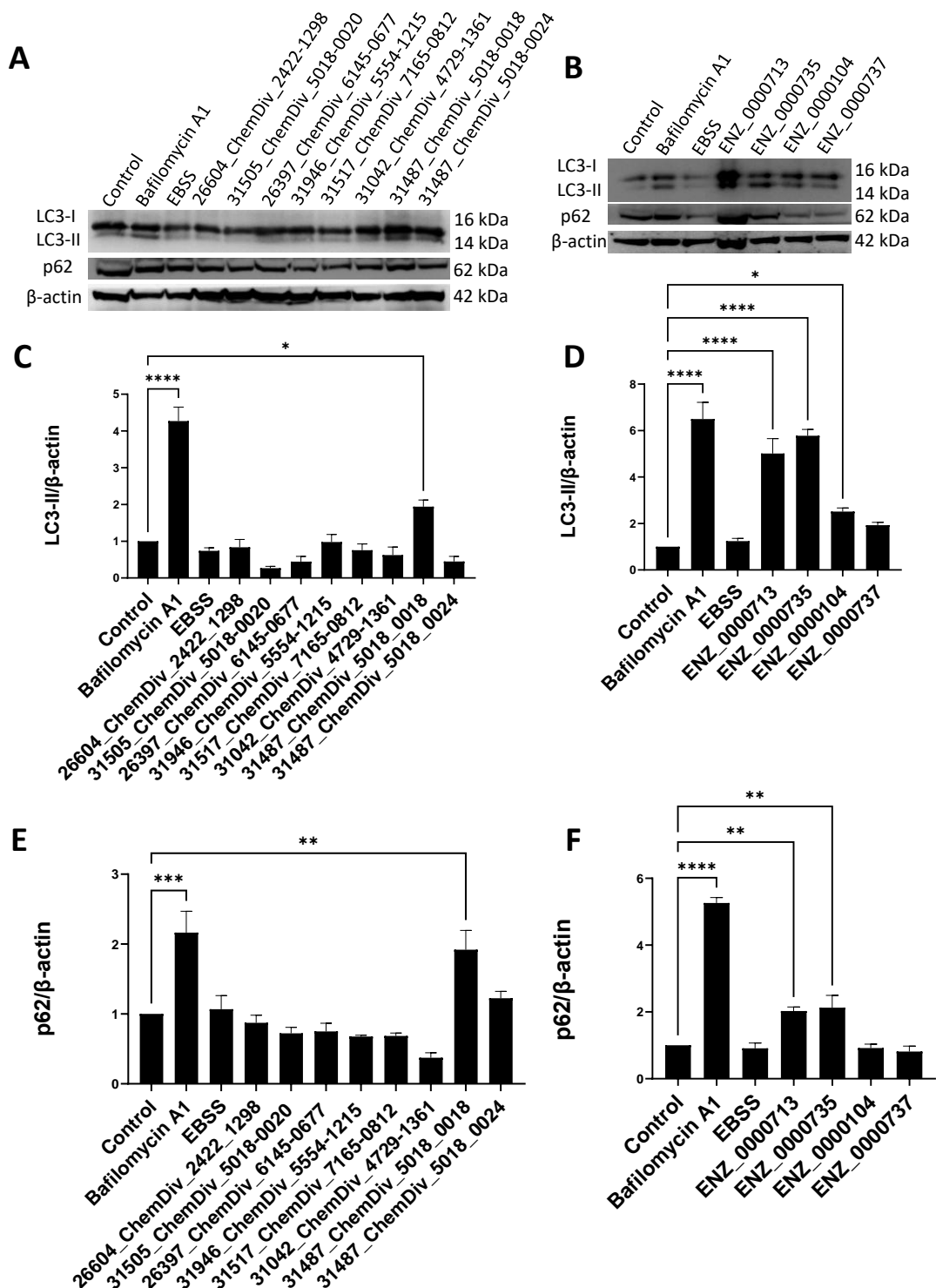


Figure 7: Western blot analysis of LC3B and p62. HEK293T cells were treated with 10 μ M hit compounds for 4 h. Representative blots for hits from **(A)** ChemBioNet library and **(B)** Enzo FDA-approved drug library. DMSO (0.1%) was used as a negative control. BafA1 (100 nM) was used as a positive control for autophagy inhibition and EBSS for autophagy induction. β -actin was applied as a loading control. The protein expression levels of **(C-D)** LC3B and **(E-F)** p62 were calculated. Data was normalised to the loading control (β -actin). Data are presented as mean \pm SEM of at least three independent biological replicates.

4.2 Secondary assays

4.2.1 Assay optimization

The aim of the assay optimization at this step was to check whether the effect seen previously with compounds in HEK293T cells is present in a comparable system and can be quantified accordingly. For this purposes, mCherry-EGFP-LC3B tagged U2OS cells were used. The assay used previously for high throughput screening was optimised accordingly. These cells contain a tet-on system for doxycycline-inducible gene expression²⁸⁹, thereby incubated overnight with doxycycline to induce the expression of mCherry-EGFP-LC3B. The next day, cells were incubated with BafA1 and torin2 to check the expression of the tandem probe and the ability to reliably quantify autophagic flux using these cells. Torin2 (250 nM) and BafA1 (100 nM) were selected based on concentrations found in literature to activate or inhibit autophagy. BafA1 (100 nM) increased the accumulation of autophagosomes, marked by colocalization of mCherry and EGFP positive puncta (referred to as yellow puncta) but decreased autolysosomes indicated by increase in mCherry (red puncta). On the other hand, torin2 increased both autophagosomes and lysosomes, marked by accumulation of yellow puncta and red puncta (**Figure 8A**).

Next, the number of puncta per cell (**Figure 8B-C**) was quantified following treatment of cells with fixed concentration of BafA1 and torin2. BafA1 at 100 nM caused over 3-fold increase in number of yellow puncta per cell, and causing an 8-fold decrease in number of red puncta per cell compared to control. The effect was statistically significant ($p < 0.0001$). The assay window to identify autophagy inhibitors is very good (3-4), with a good Z factor of 0.36. On the other hand, torin2 markedly increased both number of yellow puncta ($p < 0.0001$) and red puncta ($p < 0.0001$) by 1.5-fold and 1.8-fold respectively. Torin2 effect can be variable and subjected to plate to plate and batch to batch variance. Hence, making it more difficult to identify autophagy inducers. This was expected and also shown previously to be the case in the screening campaign. In addition, dose-dependent efficacy was assessed. As **Figure 8D** shows, BafA1 was very potent ($IC_{50} = 7.5$ nM) and the effect was dose dependent. BafA1 completely inhibited formation of autolysosomes, suggested

by dose dependent increased in number of yellow puncta. Similarly, torin2 also increased the accumulation of autophagosomes, but only slightly increased accumulation of autolysosomes at high concentrations (**Figure 8E**).

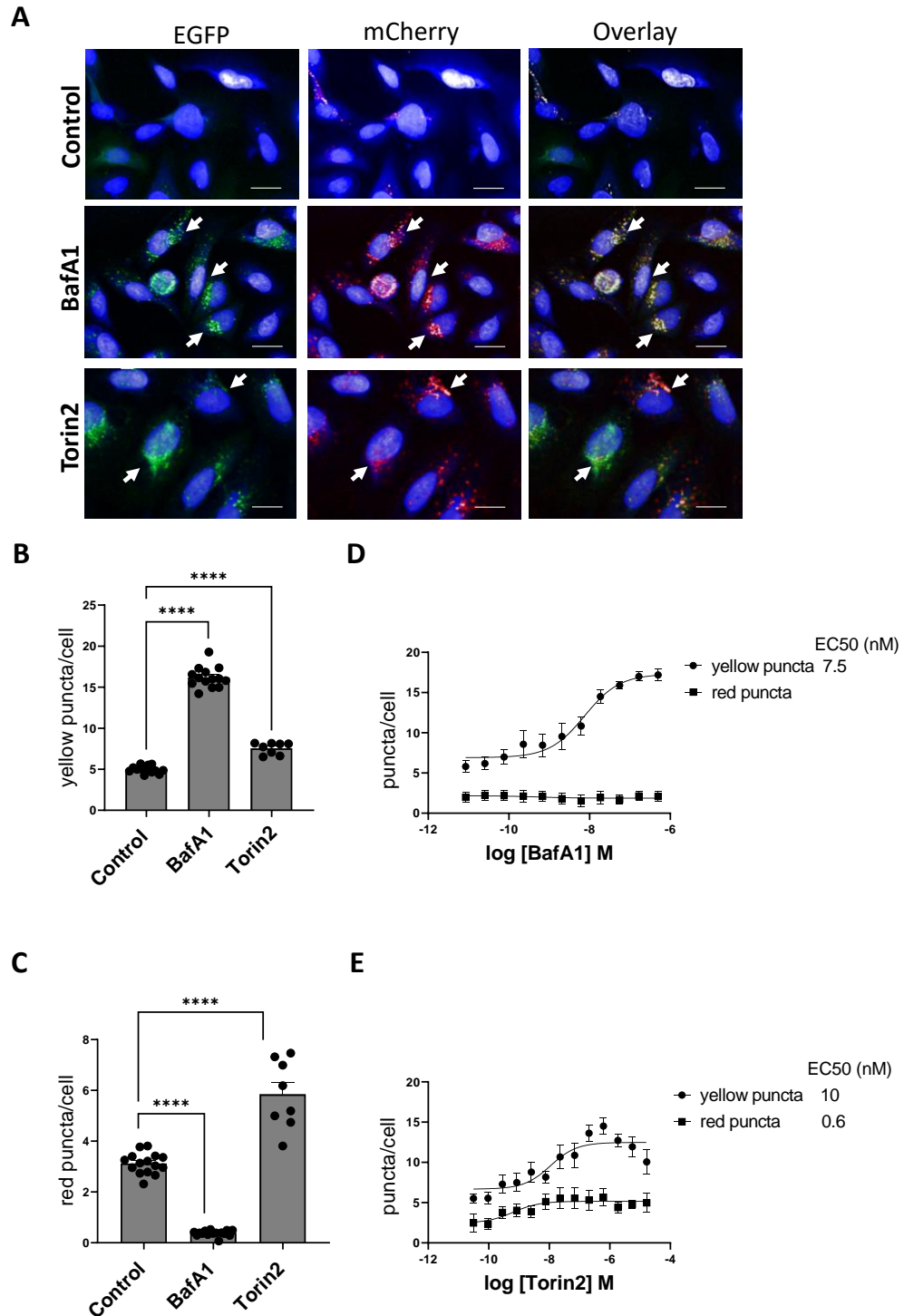


Figure 8: Assay optimisation and validation to verify tool compounds. (A) Representative confocal microscopy images of mCherry-EGFP-LC3 tagged U2Os cells treated for 4 h with BafA1 (100 nM) and torin2 (250 nM). Arrows indicate colocalized mCherry (representing

autolysosomes) and EGFP (representing neutral autophagosomes). Arrowheads indicate obvious examples of colocalized EGFP and mCherry. Scale bar 50 μm . **(B)** Quantification of LC3⁺ puncta with following treatment with BafA1 (100 nM) and **(C)** torin2 (250 nM) for 4 h. Yellow puncta per cell represents colocalization of mCherry⁺ and EGFP⁺ puncta while red puncta represents only mCherry⁺ puncta. Only puncta $\geq 0.3 \mu\text{m}$ in size were counted. Individual values are indicated. **(D, E)** Dose response curves for BafA1 and torin2 following 4 h treatment. Nonlinear regression of the dose-response curves was used to determine the IC₅₀ values. Data are presented as mean \pm SEM of at least three independent biological replicates. At least 8 technical replicates per condition were quantified.

4.2.2 Additional dose-response studies

As described previously, 12 small molecule compounds were identified from the screen, 4 of which were from the FDA-approved drug library. Therefore, dose response studies of the hits, characterized above, were conducted. The goal was to confirm the activity and determine IC₅₀ values for each compound. **Figure 9** shows the hit compounds that were successfully modulating autophagy in a dose dependent manner. A total of 4 out of 12 compounds were active in dose response studies. ENZ_0000713 and ENZ_0000735, also known as reserpine and sunitinib were confirmed positive and increased number of yellow puncta, suggesting autophagy inhibition. The IC₅₀ for autophagy inhibition was 0.7 μM for reserpine and 0.9 μM for idarubicin. ENZ_0000104, known as idarubicin, increased both number of yellow puncta and red puncta, with a lower potency than the autophagy inhibitors from the same library. Idarubicin has an IC₅₀ of approximately 4 μM . All effects were dose dependent. From ChemBioNet library, ChemDiv_5018-0018 was active and showed increase in number of yellow puncta (IC₅₀ = 1.9 μM) and a slight increase in number of red puncta (IC₅₀ = 5.9 μM). Since previous findings indicated autophagy inhibition, the modest increase in red puncta could mean that there is still some autophagy activation that C18 failed to block.

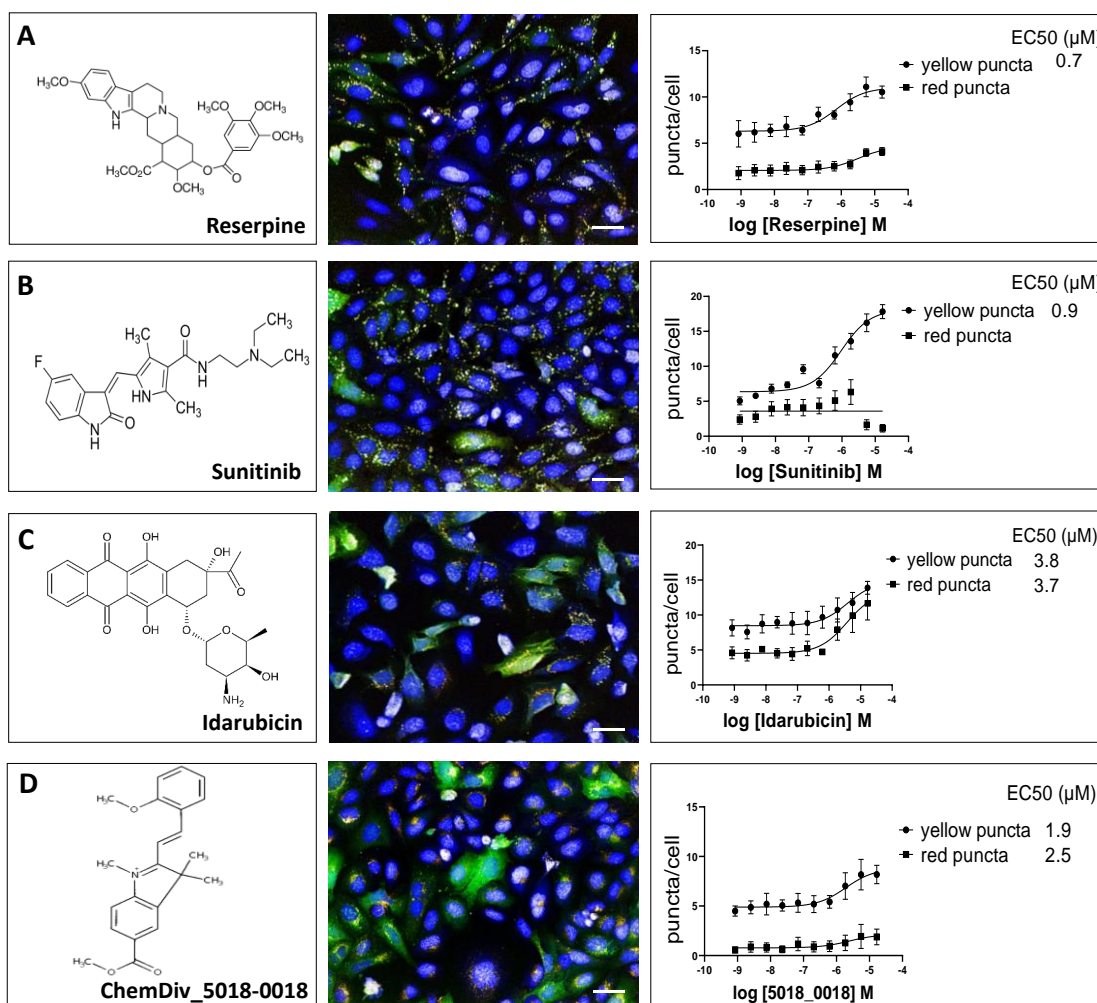


Figure 9: Structures, images and dose response curves for the active hits and the respective IC_{50} of each hit compound. (A-C) Represent hits from the Enzo FDA-approved drug library. (D) Represents a hit from ChemBioNet library. **(A-D)** First column, chemical structures and names of each compound. Second column are representative images of each hit compound at the most efficacious concentration showing Hoechst (blue), EGFP (green) and mCherry (red). Bar 50 μM . Third column represents the dose response curves used for computing the IC_{50} for each hit compound. Nonlinear regression of the dose-response curves was used to determine the IC_{50} values. The yellow puncta represents colocalization of mCherry⁺ and EGFP⁺ puncta while red puncta represents only mCherry⁺ puncta. Only puncta $\geq 0.3 \mu\text{m}$ in size were counted. Data are presented as mean \pm SEM of at least three independent biological replicates. At least 8 technical replicates per condition were quantified.

4.2.3 Protein expression

U2OS cells were treated with control (DMSO, 0.1%), BafA1 (100 nM), EBSS (starvation media) and C18 at various concentrations for 4 h. After collecting the lysates, they were subjected to Western blot analysis of LC3 and p62. The

relative protein levels of LC3-II and p62 are shown in **Figure 10**. Significant increase of LC3-II protein expressions were observed, consistent with previous findings. Treatment with 5 μ M C18 caused a marked increase of over 8-fold in LC3-II compared to the control ($p < 0.0001$). A concentration of 3 μ M C18 also caused an approximately 4-fold increase in LC3-II accumulation ($p = 0.04$) (**Figure 10C**). Interestingly, p62 followed the same trend and significantly accumulated in a dose-dependent manner, with a 3-fold increase induced by 5 μ M C18 ($p = 0.0019$) and 3 μ M C18 ($p = 0.0028$) (**Figure 10D**). Furthermore, C18 (3 μ M) was selected and the time-dependent changes in autophagic activity were investigated. The elevation of LC3 and p62 levels were only slightly increasing with short incubation times, however 4 h treatment significantly increased LC3-II accumulation ($p = 0.0053$) and prevented p62 degradation ($p = 0.0120$), thus inhibiting autophagy (**Figure 10E-F**).

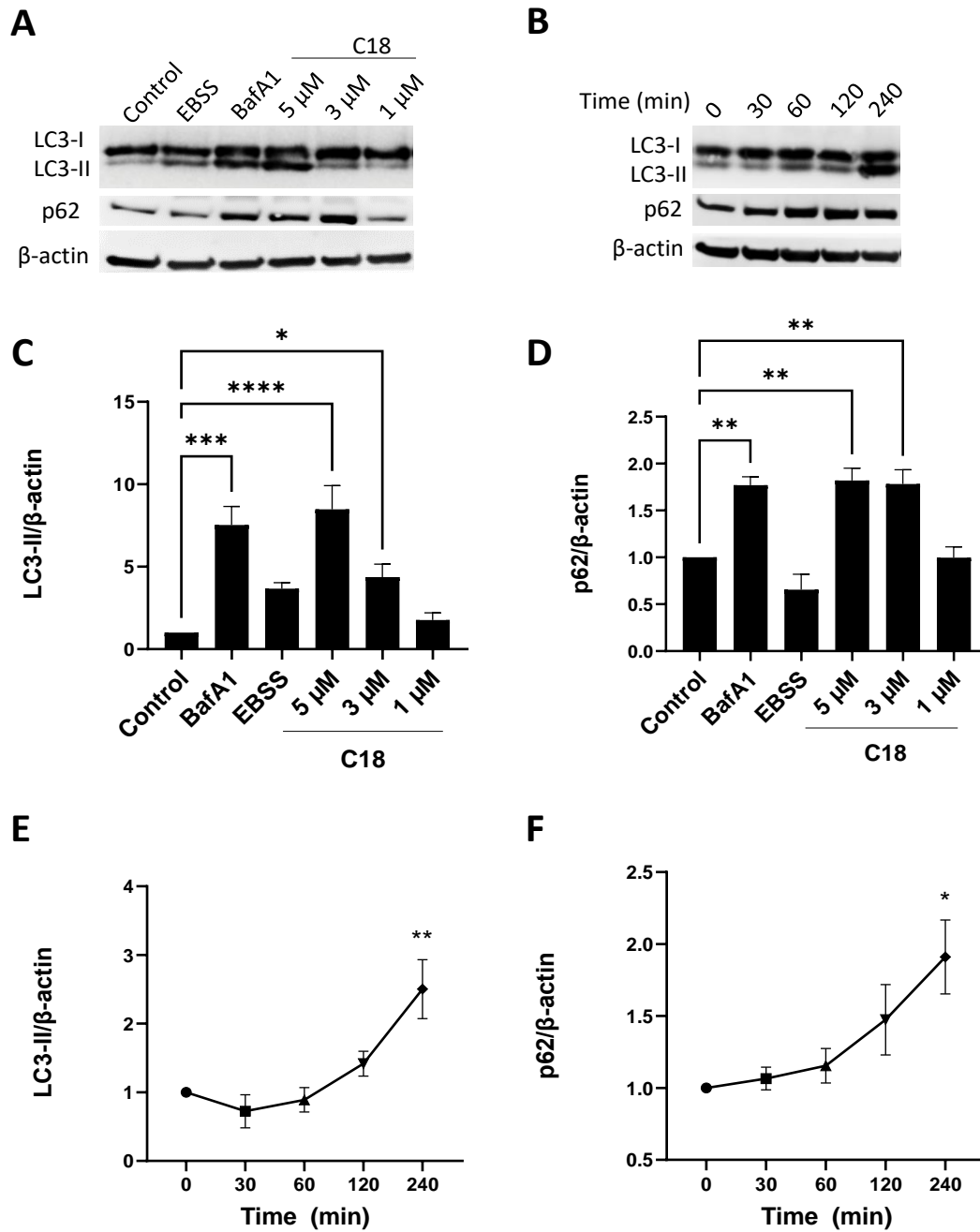


Figure 10: Western blot analysis of LC3 and p62. U2OS cells were treated with **(A)** increasing concentration of C18 and **(B)** increasing incubation times. β -actin served as loading control. **(C-F)** Densitometry data analysis for all tested conditions was performed. Blots shown are representative. Data are presented as mean \pm SEM of at least three independent biological replicates normalized to the loading control.

4.3 Cytotoxicity of and pro-apoptotic activity of C18

4.3.1 Effect of C18 on cell viability

C18 is a novel compound with unknown mechanism of action, thus possible cytotoxic effects may exist. C18 induced cytotoxicity was investigated by incubating C18 at various time points in two cell lines, U2OS cells, human bone osteosarcoma epithelial cells, and HEK293, a human embryonic kidney cells, using a real-time assay technology. The Promega RealTime-Glo™ MT Cell Viability Assay is nonlytic, homogeneous assay that provides informative cytotoxicity kinetics data by measuring luminescence signal produced by the viable cells. The number of viable cells is proportional to the amount of luminescent signal, which is directly proportional to the amount of NanoLuc® substrate used in the NanoLuc® luciferase reaction. The NanoLuc® substrate is only produced in live cells where the cell-permeant prosubstrate is reduced. Therefore, as the number of metabolically active cells decreases, the glo signal decreases proportionally. In addition to the timing of the drug effect, a detailed interrogation of the various drug doses was performed and the IC₅₀ values were determined. Changes in cell viability induced by C18 at 11 concentrations after 0 (right after the chemical administration), 2, 4, 8, 24, and 72 h of exposure were measured. Extensive cytotoxicity studies revealed concentration-dependent cytotoxicity and similar sub-micromolar IC₅₀ values in both cell lines after long incubation times (24 h and 72 h). At short incubation times (up to 4 h) HEK293 has slightly better tolerance to C18 compared to U2OS cells (**Figure 11A-B**). Nonetheless, overall tolerance to C18 was good, allowing a decent window to detect autophagic activity. **Table 11** shows the IC₅₀ values following treatment with C18. At 4 h after treatment (same as incubation time in autophagy assays) the IC₅₀ values for U2OS and HEK293 cells were 20 μM and 31 μM respectively. Considering that efficacy was seen at concentration of 5 μM and below, the active concentration is 4-fold and 5-fold respectively lower than the IC₅₀ in U2OS cells and HEK293 cells.

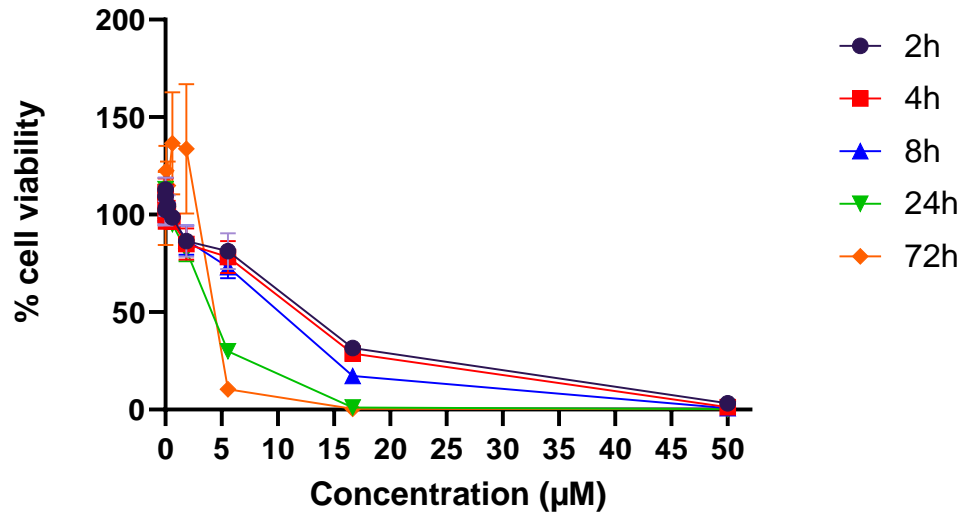
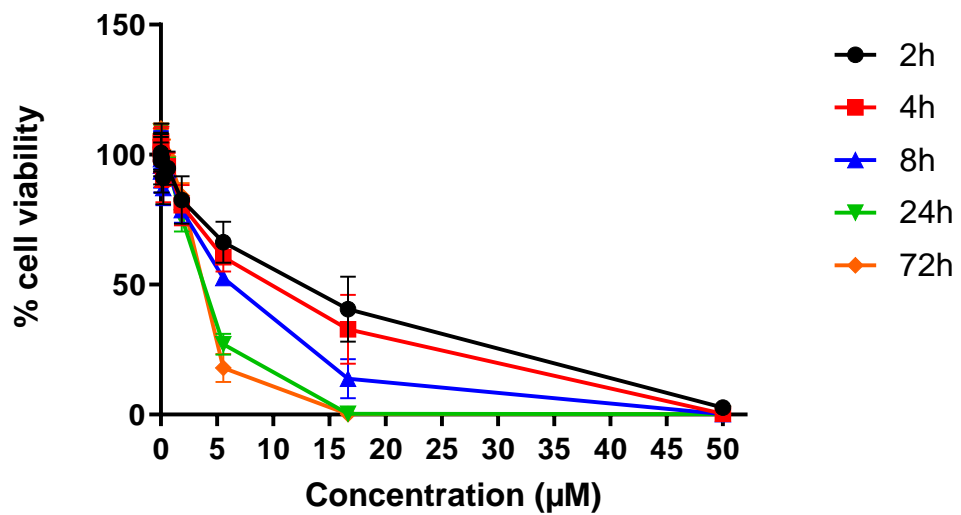
A**B**

Figure 11: Cytotoxicity screen for C18 on immortalized cell lines following 2, 4, 8, 24 and 72 h treatment. Concentration dependent cytotoxic activity of C18 in **(A)** human bone osteosarcoma U2OS cells and **(B)** human embryonic kidney HEK293 cells. Data are presented as % cell viability and represent mean \pm SEM (average of 3 biological replicates with $n = 2$).

Table 11: IC₅₀ values from cytotoxicity assay. U2OS and HEK293 cell lines were analysed following 2, 4, 8, 24 and 72 h treatment with C18. Nonlinear regression of the dose-response curves was used to determine the IC₅₀ values. Data represents mean ± SEM (average of 3 biological replicates with n = 2).

	U2OS	HEK293
Time (h)	IC ₅₀ (µM)	IC ₅₀ (µM)
2	25	42
4	20	31
8	13	6
24	4	4
72	3	3

4.3.2 Effect of C18 on pro-apoptotic caspases

To examine whether cell apoptosis was involved in C18-induced cell death the role of caspases, in particular caspase-3 and caspase-7, was investigated using U2OS cells. IncuCyte® caspase-3/7 red dye is a cell-permeable, non-toxic dye conjugated to the caspase-3/7 recognition and cleavage sequence DEVD. It is non-fluorescent until is activated by caspase-3/7 apoptosis activity. Once cleaved, the dye is capable of emitting red fluorescence upon DNA binding, thus identifying the dead and dying cells by live cell imaging. Results indicate that the red fluorescent U2OS cells start to increase in number shortly after the addition of C18, with as low as 2 h post-treatment. The activation of apoptosis was both dose- and time-dependent. The highest number of fluorescent red cells was reached using 5 µM C18 at approximately 14 h post-treatment, after which it reaches a plateau phase (**Figure 12**). Lower concentrations of compound caused a more modest increase in apoptosis. These results thus demonstrate that C18 triggers apoptosis.

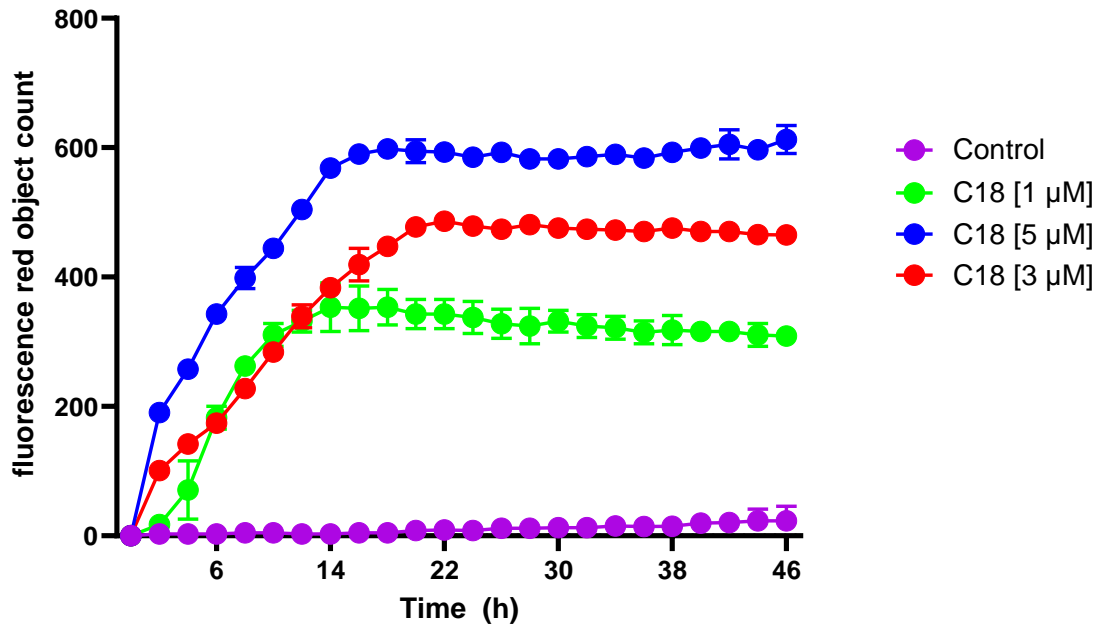


Figure 12: C18 induced caspase-3/7 apoptosis. Figure represents the time course of activation of caspase-3/7 in U2OS cells in the presence of increasing concentrations of C18. Apoptosis has been quantified as the number of red fluorescent caspase-3 and caspase-7 active objects for each time point. Data are presented as mean \pm SD of three biological replicates. At least 8 technical replicates per condition were quantified.

4.4 Modulation of autophagic flux by C18

4.4.1 Starvation-induced autophagic flux

Yellow puncta accumulation upon C18 treatment suggests that fusion of autophagosomes with lysosomes might be blocked. To determine whether C18 prevented autophagosomes from reaching lysosomes, the previously established tandem tagged mCherry-EGFP-LC3 probe was used. U2OS cells expressing mCherry-EGFP-LC3B tag were cultured overnight in medium containing doxycycline and treated them with C18 for 4 h on the next day. This incubation time was shown to be enough to induce or inhibit autophagy. This probe can dissect whether an autophagosome has fused with a lysosome, based on the distinct chemical properties of EGFP and mCherry fluorophores. Under non-lysosomal and near-neutral pH conditions, both EGFP and mCherry fluoresce. However, the low pH in the lumen of the lysosome quenches the EGFP signal but not the mCherry signal. In addition, cells were nutrient starved to induce autophagy and to compare results to the fed condition. Results show

that BafA1 causes the accumulation of mCherry⁺EGFP⁺ puncta in normal conditions. Here, it was shown that starving BafA1 treated cells enhanced the accumulation of mCherry⁺EGFP⁺ puncta, suggesting further accumulation of autophagosomes and inhibition of autophagy (**Figure 13A**). If C18 can block basal autophagic flux and thus cause LC3-II accumulation, then it is possible that it might also block the flux of induced autophagy. Indeed, when cells were subjected to starvation in combination with C18, U2OS cells exhibited a more pronounced accumulation of mCherry⁺EGFP⁺ puncta compared with EBSS incubation alone or C18-treatment alone under normal conditions, suggesting a blocked autophagic flux. The number of autophagosomes (yellow puncta) and autolysosomes (red puncta) per cell were quantified to assess whether the changes were significant. The results are presented in **Figure 13B-C** by comparing the number of yellow puncta and red puncta per cell under normal conditions (fed) with those in nutrient-starved condition. BafA1 causes a significant increase of 3.6-fold in yellow puncta compared to DMSO under fed conditions ($p < 0.0001$) and 2-fold increase in yellow puncta under starvation condition ($p < 0.0001$). C18 also significantly increases yellow puncta by 2.5-fold under nutrient rich conditions ($p = 0.0008$) and 1.5-fold in starved condition ($p = 0.0144$). Both BafA1 and C18 were able to significantly decrease the number of autolysosomes (red puncta) under fed condition ($p < 0.0001$). The effect was equally significant in starved cells ($p < 0.0001$). This reinforced the possibility that C18 does not induce autophagy, but blocks autophagic flux.

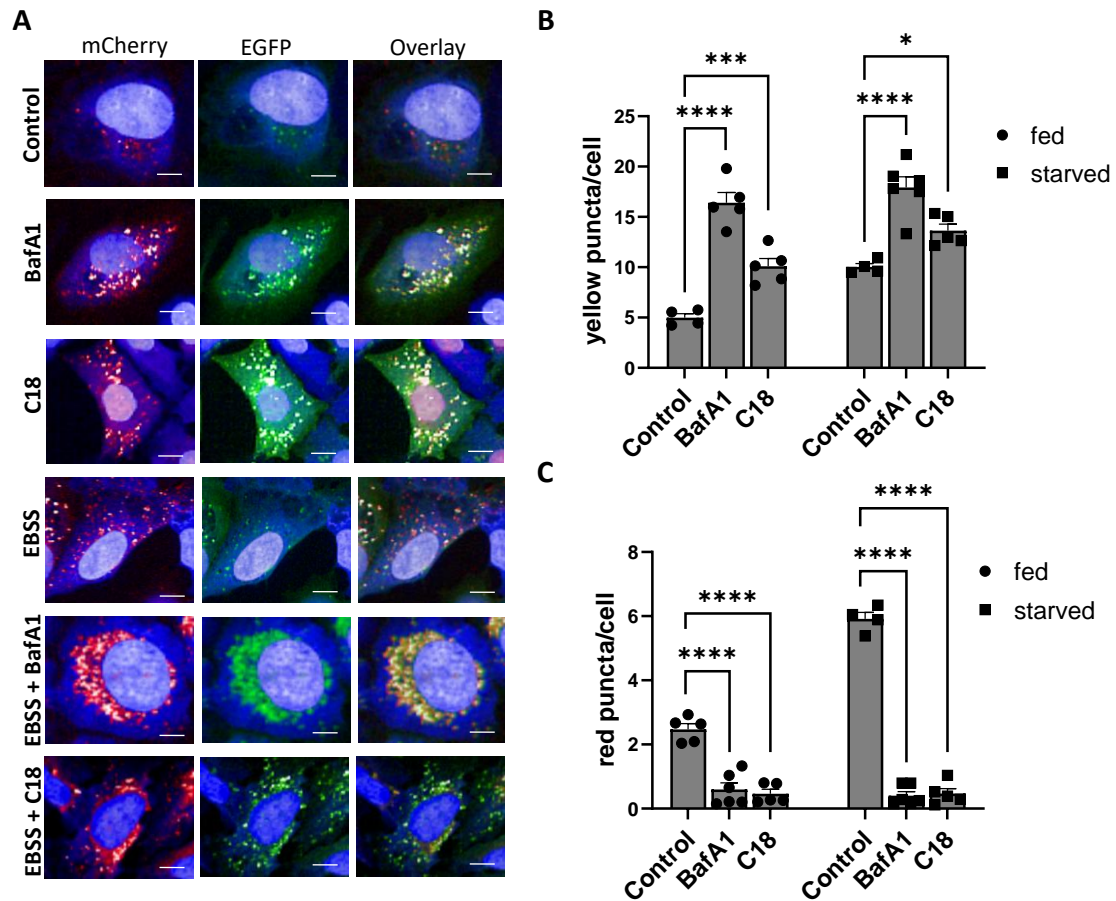


Figure 13: Autophagic flux modulation by C18. (A) U2OS cells expressing mCherry-EGFP-LC3B were treated with DMSO, BafA1 (100 nM), C18 (3 μ M), starvation (EBSS), and BafA1 and C18 in starvation media. Cells were then fixed and imaged with a confocal microscope. Images are representative of at least three independent experiments. Scale bar 50 μ m. (B-C) Quantification of autophagosomes (yellow puncta) and autolysosomes (red puncta). Only puncta $\geq 0.3 \mu$ m in size were counted. Individual values are indicated. Data are presented as mean \pm SEM of at least three independent biological replicates. At least 8 technical replicates per condition were quantified.

4.4.2 Inhibition of lysosome degradation

To corroborate further the effect of C18 on autophagic flux seen, lipidated LC3-II levels were measured by immunoblotting. Nutrient starved cells in presence of C18 were investigated for changes in LC3 protein levels to confirm that C18 can modulate starvation-induced autophagy. The number of autophagosomes increases by nutrient starvation and accordingly the amount of LC3-II should also increase. Consistently, C18 markedly increased LC3-II levels by 2.6-fold ($p = 0.0227$), which further increased to 3.1-fold in C18-treated starved cells ($p = 0.0212$). BafA1 caused a significant 3-fold increase in LC3-II levels ($p =$

0.0079), without further increase in starved cells (**Figure 14A-B**). The amount of LC3-II in standard conditions does not necessarily estimate the autophagic flux, because not only autophagy activation but also inhibition of autophagosome degradation greatly increases the amount of LC3-II. Therefore, it is essential to also determine how much LC3-II is degraded in a lysosome-dependent manner given a time point. This is achieved by quantifying the amount of LC3-II in the presence and absence of lysosomal inhibitors. Similar or less LC3-II levels in presence or absence of the lysosomal inhibitor are indicative of the impaired autophagic flux (Yoshii and Mizushima, 2017). To address this question, U2OS cells were treated with C18 (3 μ M), in presence or absence of BafA1 (100 nM), and probed for LC3. C18 treatment alone caused an accumulation of LC3-II, but the combined treatment with BafA1 did not cause further accumulation of LC3-II compared to C18 alone (**Figure 14C**).

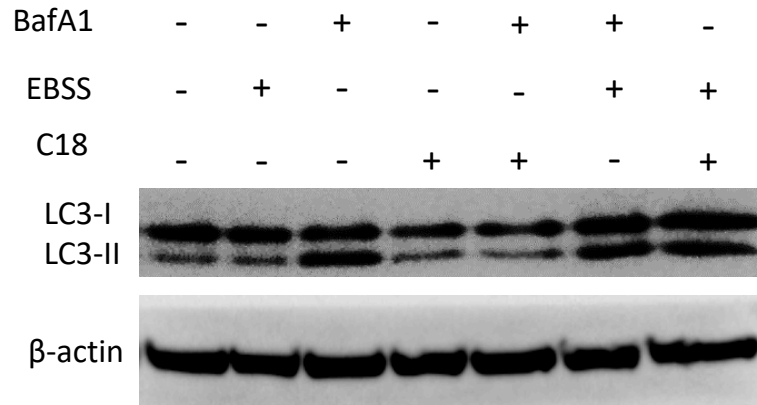
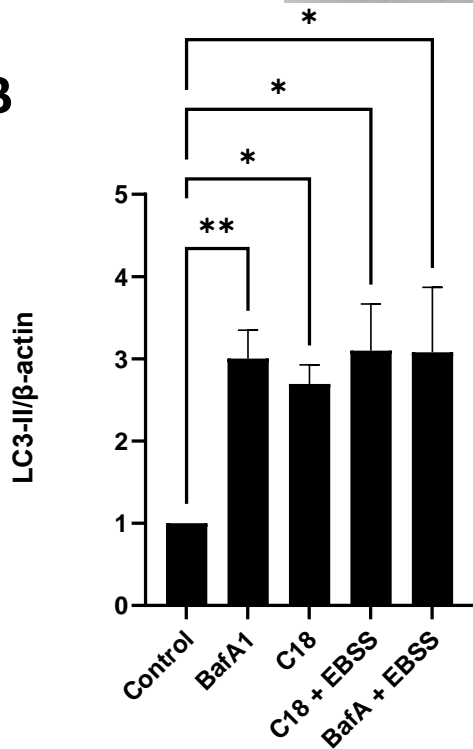
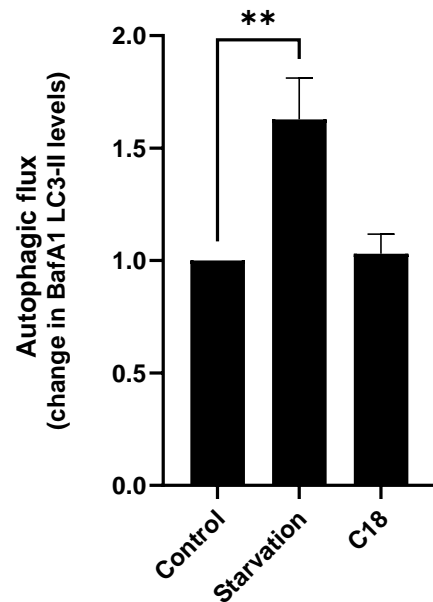
A**B****C**

Figure 14: C18 blockage of autophagic flux upon starvation-induced autophagy. (A) U2OS cells were incubated in complete media (control), starvation media (EBSS), complete media with BafA1 (100 nM), complete media with 3 μ M C18, 3 μ M C18 in presence of BafA1, starvation media with BafA1 and starvation media with 3 μ M C18 for 4 h. Quantitation of immunoblot data in **(B)** showing change in LC3-II levels relative to control (complete media) and **(C)** autophagic flux (change in LC3-II levels upon BafA1 treatment). Blots are representative. Data are presented as mean \pm SEM of at least three independent biological replicates normalized to the loading control.

4.4.3 p62/SQSTM1 upregulation

As explained previously, simultaneous with autophagosome maturation, cargo loading occurs⁷⁶. One particular adaptor protein, SQSTM1/p62, plays a critical role in recognizing and/or loading cargo. In U2OS cells, upon starvation, there is a reduction in p62 protein as it is delivered for lysosomal degradation upon autophagy induction. BafA1 and C18, on the other hand, prevented p62 degradation by increasing its levels compared to the control (**Figure 15A-B**). The accumulation of p62 protein is modest, compared to LC3-II accumulation. BafA1 caused a significant 1.5-fold increase in p62 levels ($p = 0.0407$). However, starving BafA1-treated cells causes a reduction in the protein level, compared to BafA1 alone. This is due to cargo loading occurring upon autophagy activation and BafA1 failing to inhibit autophagic flux. C18 caused 1.2-fold increase in p62 protein levels which upon starvation further increased. Starved cells treated with C18 caused a marked accumulation of p62 by 1.6-fold ($p = 0.0011$) (**Figure 15B**).

The above process can also be monitored by analyzing p62 and LC3 co-localization using confocal microscopy. Cells with active autophagy should demonstrate the co-localization of p62 and LC3²⁹⁰. In U2OS cells expressing EGFP-LC3, EGFP-LC3 punctate structures are occasionally observed, which co-localize with p62. This represents the basal level of autophagy in these cells. Upon starvation, there is a large increase in p62 and EGFP-LC3 puncta, most of which co-localize, indicating incorporation of specific p62-labeled cargo into autophagosomes. This process is inhibited upon BafA1 treatment and C18 treatment, where little colocalization between p62 and LC3 were observed (**Figure 15C**). Together these data indicate that C18 blocks the p62 cargo incorporation process and blocks autophagic flux.

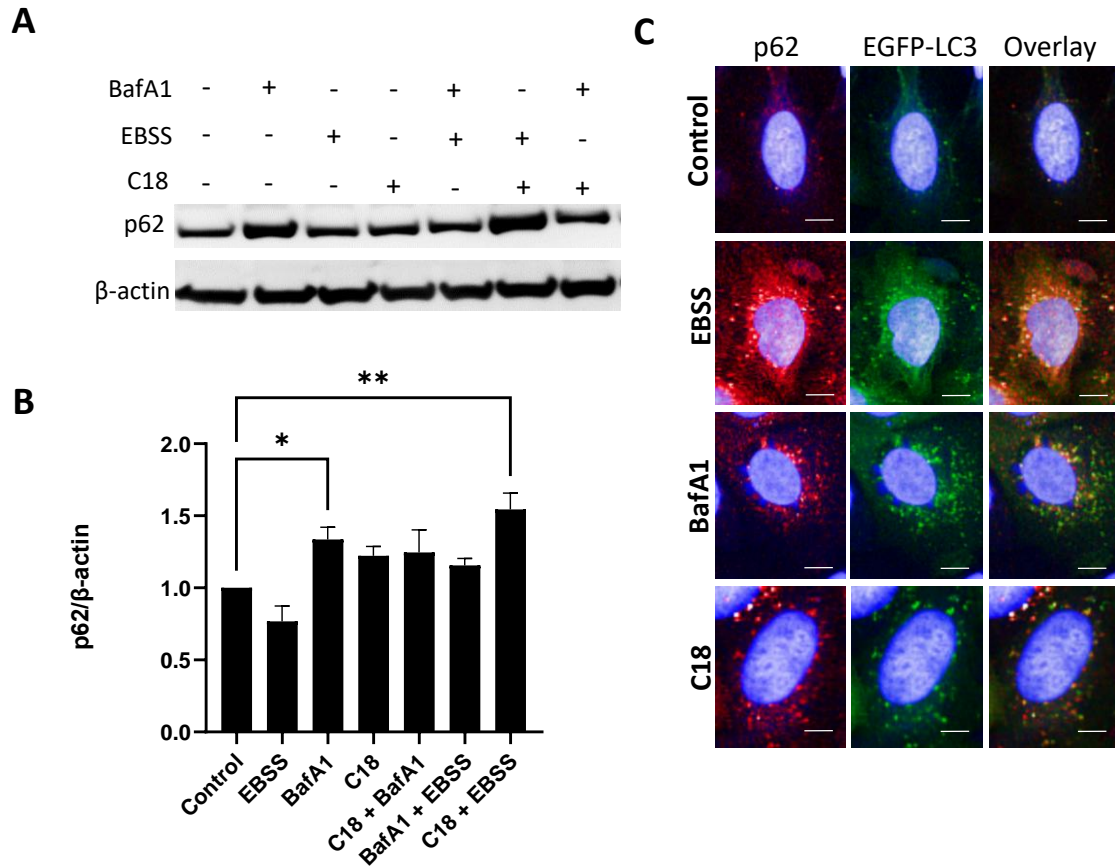


Figure 15: C18 inhibition of autophagosome formation. (A) U2OS cells were incubated in complete media (control), starvation media (EBSS), complete media with BafA1 (100 nM), complete media with 3 μ M C18, 3 μ M C18 in presence of BafA1, starvation media with BafA1 and starvation media with 3 μ M C18 for 4 h. Blots shown are representative of three independent biological replicates. (B) Quantitation of immunoblot data showing change in p62 levels relative to control (complete media). Data are presented as mean \pm SEM of at least three independent biological replicates normalized to the loading control. (C) U2OS cells expressing EGFP-LC3 were incubated in complete media (control), starvation media (EBSS), or 3 μ M C18 for 4 h, followed by staining with Hoechst (blue), anti-p62 (red) and EGFP (green). Bar, 50 μ m. Representative images from three independent biological replicates are shown.

Perturbation in p62/SQSTM1 protein levels should be complemented by respective RT-qPCR assessment of mRNA levels⁶². SQSTM1 mRNA levels were analysed by real-time PCR and are shown in **Figure 16**. BafA1, which inhibits autophagosome turnover, did not affect SQSTM1 transcription level. Starving cells, on the other hand, significantly increased SQSTM1 mRNA by 2-fold compared to the negative control (DMSO) ($p = 0.0430$). Starvation in BafA1-treated cells restored the expression of SQSTM1, causing a significant

2.5-fold upregulation in mRNA levels ($p = 0.0093$). On contrary to BafA1, C18 enhanced SQSTM1 transcription. C18 caused a significant 4-fold increase in mRNA levels ($p < 0.0001$). Furthermore, starving cells treated with C18 caused a significant transcriptional upregulation of SQSTM1 by 4.6-fold ($p < 0.0001$), more than C18 alone. In summary, the analysis of SQSTM1/p62 mRNA levels indicate that C18 not only did not suppress p62 transcription but was able to upregulate its transcription. This occurred despite inhibitory effect on the protein levels.

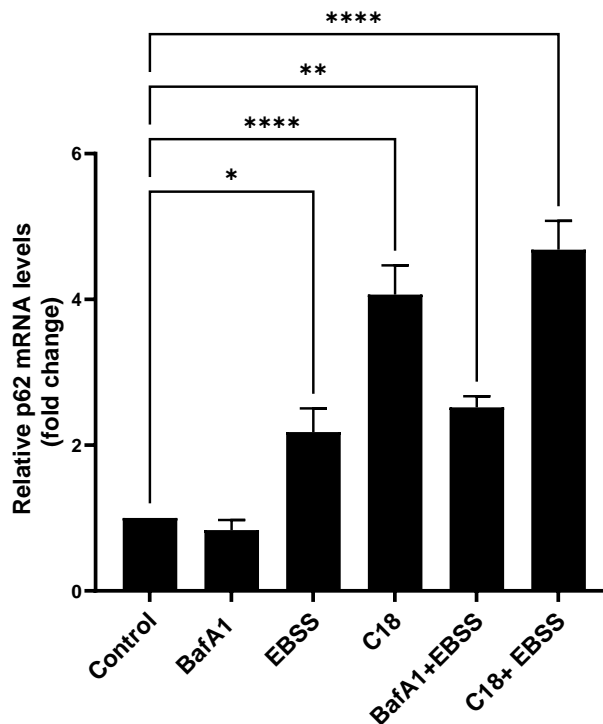


Figure 16: C18-induced upregulation of p62 mRNA. Quantification shown represents the mRNA levels of p62 relative to RPLPO by qRT-PCR after treatment of U2OS cells with DMSO (0.1%), BafA1 (100 nM), EBSS, C18 (3 μ M), BafA1 with EBSS and C18 with EBSS. Data are presented as mean \pm SEM of at least three independent biological replicates.

4.4.3 Effect of C18 on autophagosome-lysosome fusion

To further understand the inhibitory action of C18 on autophagic flux, any changes in fusion between autophagosome and lysosomes were observed. To do this, mCherry-EGFP-LC3 tagged U2OS cells were probed with LysoTracker deep red (LTR) dye. LTR is a widely used dye to stain acidic organelles in live-cells²⁹¹. The number of cells that are positive for LTR and LC3 reflect the

amount of fused autophagosomes with lysosomes. Cells treated with BafA1 displayed an accumulation of EGFP-LC3 puncta that did not colocalize with LTR, suggesting blocked fusion of autophagosomes with lysosomes. A remarkable separation of EGFP-LC3 and LTR was observed in C18-exposed cells, similar to the result of BafA1-treated cells (**Figure 17A**). Quantitative analysis of confocal microscopy images showed that C18 caused a significant dose-dependent reduction in EGFP⁺LTR⁺ puncta compared to negative control (**Figure 17B**), with the highest concentration (5 μ M) causing a significant reduction of approximately 2-fold ($p < 0.0001$). Interestingly, this effect was equally potent and significant to that of BafA1 ($p < 0.0001$). 1 μ M and 3 μ M C18 were also able to significantly reduce the number of EGFP⁺LTR⁺ puncta by 1.5-fold ($p < 0.01$ and $p < 0.001$). In addition to this, quantification of the total number of LTR puncta per cell showed a dose-dependent decrease in total levels of acidic lysosomes and/or endosomes (**Figure 17C**). All concentrations of C18 tested displayed potent inhibitory effect on the fusion step.

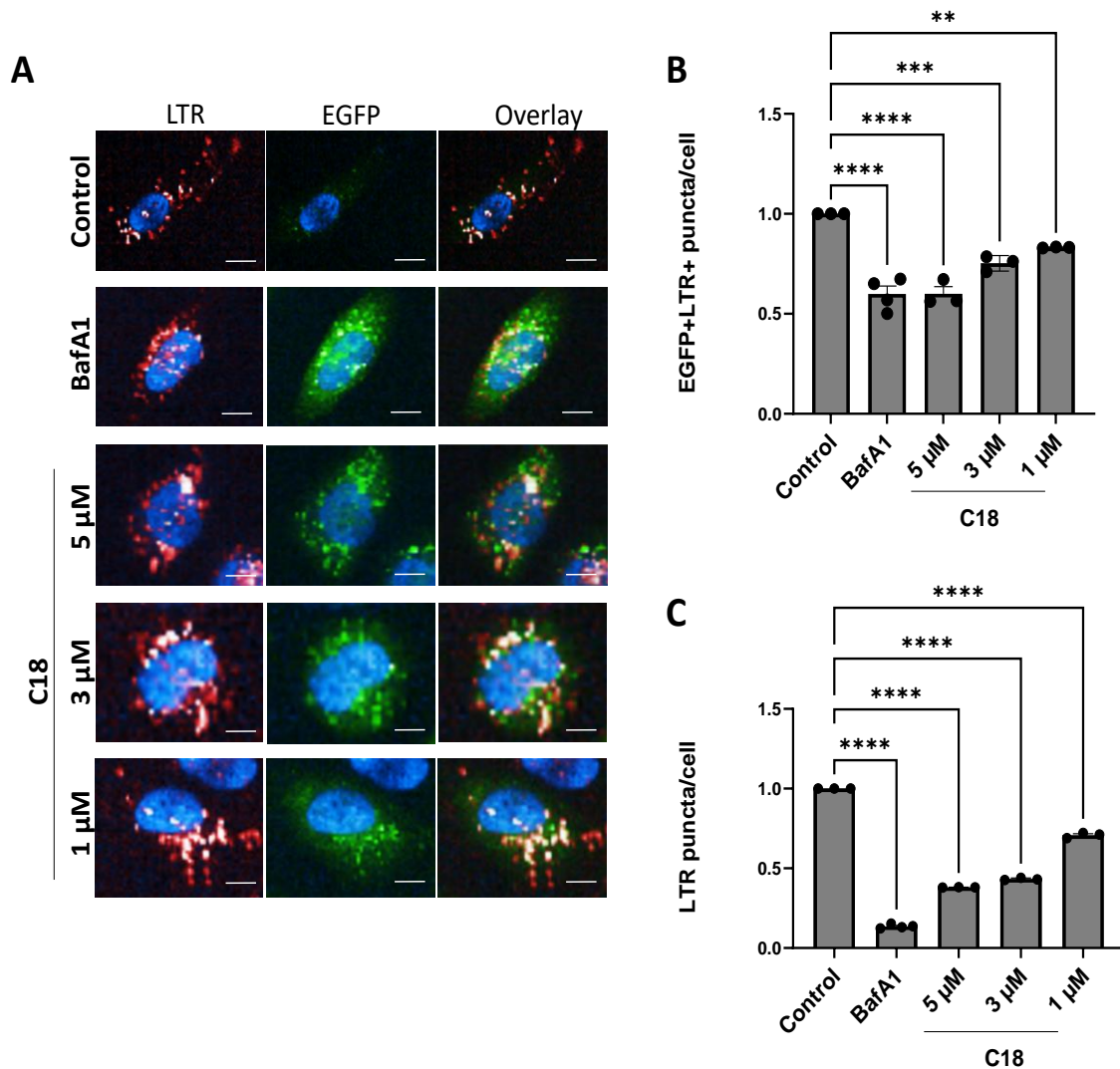


Figure 17: C18 inhibition of autophagosome-lysosome fusion. (A) Stably transfected U2OS cells with mCherry-EGFP-LC3 were treated with DMSO, BafA1 (100 nM) and C18 (5 μ M, 3 μ M and 1 μ M) for 4 h. After that, cells were stained LTR dye. Colocalization of EGFP-LC3 puncta with LTR was observed with the confocal microscope. Typical images are presented. Scale bar 50 μ m. **(B)** EGFP⁺LTR⁺ puncta per cell and **(C)** the number of LTR⁺ puncta per cell were quantified. Only puncta $\geq 0.3 \mu$ m in size were counted. Individual values are indicated. Data are represented as mean \pm SEM of at least three independent experiments. Data are presented as mean \pm SEM of at least three independent biological replicates. At least 8 technical replicates per condition were quantified.

4.4.4 Effect of C18 on lysosomal acidification

Because the impaired autophagic flux induced by C18 was caused by a blockade of fusion of autophagosomes with lysosomes or endosomes, next the effect of C18 on the endo-lysosomal pathway was assessed. For this purpose,

the quantitative ratiometric probe LysoSensor Yellow/Blue DND-160 was used. The dye produces yellow fluorescence in intracellular acidic vesicles, such as lysosomes, and blue fluorescence in alkaline environment thereby allowing one to investigate the functionality of lysosomes, which has a key role in autophagic degradation. The increase in fluorescence upon acidification is pH-dependent. To measure this, U2OS cells were treated with control (DMSO) and C18 (1 μ M, 3 μ M and 5 μ M) for 4 h and stained immediately after. A live cell image analysis was performed and the intensity of yellow and blue fluorescence were quantified. The ratio of yellow to blue fluorescence was plotted to assess intracellular pH (**Figure 18**). Following treatment with C18 U2OS cells exhibited lysosomal pH shifting toward more alkaline direction as compared with that in negative control. As expected, this change was dose dependent (**Figure 18A**). To confirm, the signal was quantified and the intensity ratio of yellow to blue fluorescence was determined as an indicator of how acidic the lysosomes are upon compound treatment. Results show a significant dose dependent decrease in the acidity of lysosomes following treatment with C18 following all the treatments (**Figure 18B**). 5 μ M C18 caused a significant reduction by 28% in acidity ($p < 0.0001$), while 3 μ M C18 and 1 μ M C18 also caused a significant decrease by 15% ($p = 0.0003$) and 10% respectively ($p = 0.0056$).

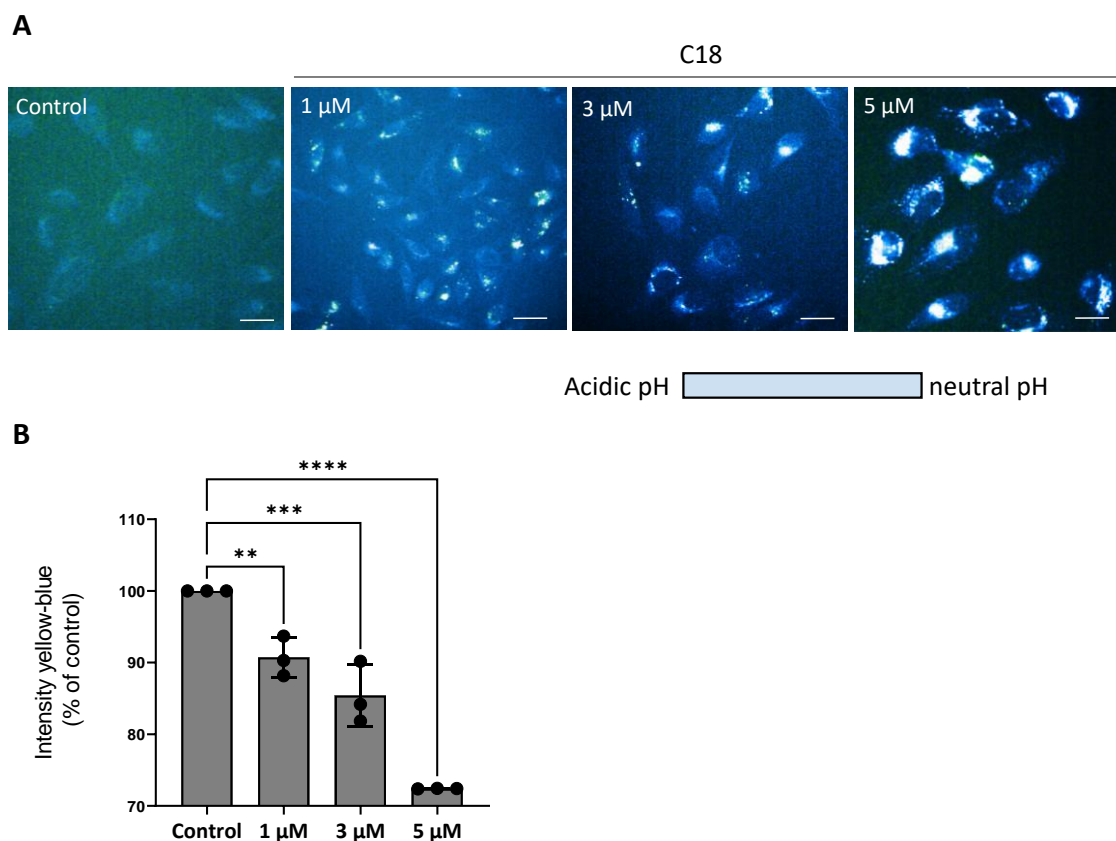


Figure 18: Lysosomal pH measurement. (A) Representative images of cultured U2OS cells treated with control (DMSO) and various concentrations of C18 (1 μ M, 3 μ M and 5 μ M). After 4 h incubated cells were labelled live with the pH-sensitive probe Lysosensor-DND-160. Scale bar 50 μ m. **(B)** The ratio of intensity of yellow to blue fluorescence was used to quantify lysosomal acidity. Individual values are indicated. Data are presented as mean \pm SEM of at least three independent biological replicates. At least 8 technical replicates per condition were quantified.

4.4.5 Effect of C18 on cathepsin B and cathepsin L

The aim of this part was to study the role of C18 on the expressions of cathepsin B (CTSB) and cathepsin L (CTSL) and determine whether C18 interferes with their function. U2OS cells were treated with DMSO, C18, BafA1 and torin2 for 4 h. After the designated treatment time, cells were incubated in fresh media containing the membrane permeable cathepsin B and Magic Red (MR) substrate. Upon hydrolysis, MR dye releases membrane-impermeable fluorescent cresyl violet within organelles containing catalytically active cathepsins. Using confocal microscopy, the fluorescent signal in living cells were detected. The intensity of MR signal is directly proportional with CTSB and/or CTSL activity and thereby is used as a measurement of proteolytically-

active lysosomes. Results indicate that BafA1 was able to significantly reduce the activity of CTSB and CTSL ($p < 0.0001$), whereas torin2 markedly increased their activity ($p < 0.0001$) due to autophagy induction. C18 did not affect levels of CSTB and CTSL despite increasing concentration. All concentrations caused similar effect to the control after 4 h incubation (**Figure 19**).

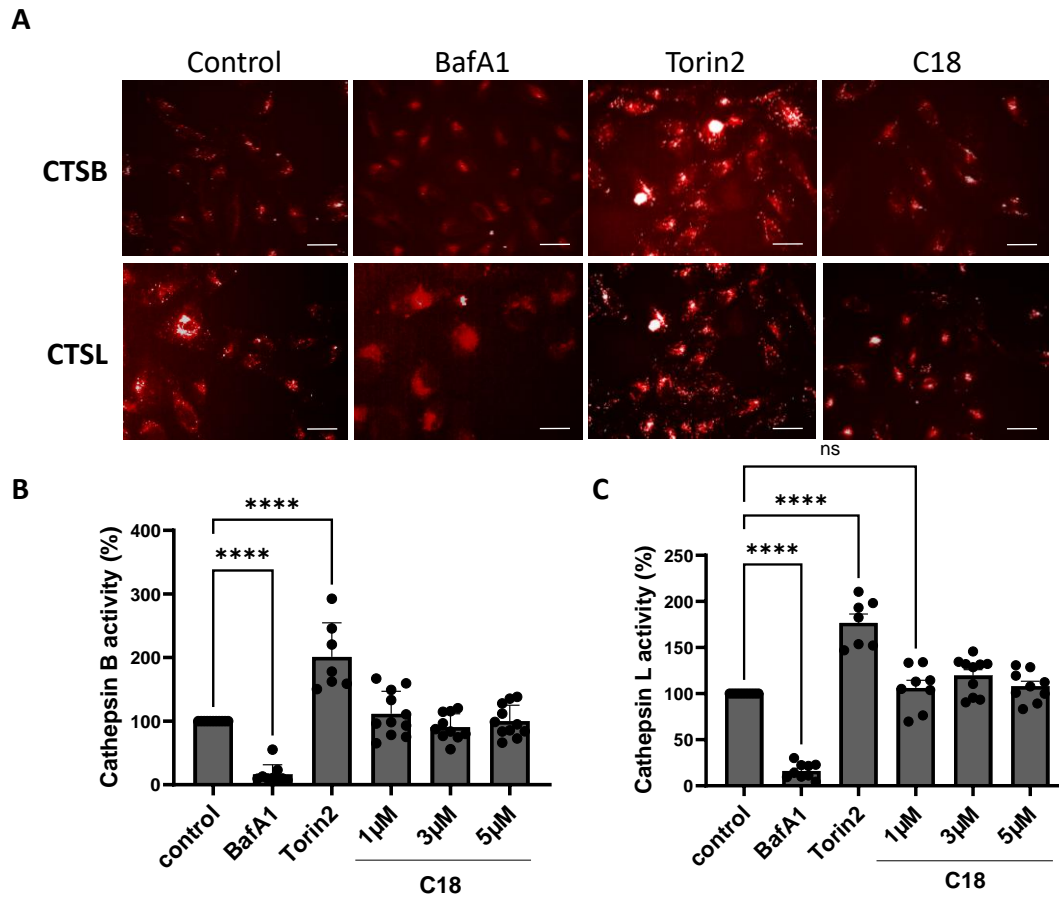


Figure 19: C18 inhibition of cathepsins. (A) Representative images of cells stained with cathepsin B Magic Red and cathepsin L Magic Red to visualize proteolytically active lysosomes. U2OS cells were incubated with DMSO, C18 (0.3 μ M, 1 μ M and 3 μ M), BafA1 (100 nM), torin2 (50 nM) and labelled with Magic Red for 30 min followed by live confocal microscopy. Image of C18 is representative of 3 μ M concentration. Scale bar 50 μ m. **(B-C)** Quantitation of Magic Red intensity, normalized to control (DMSO). Data are presented as mean \pm SEM of at least three independent biological replicates. At least 8 technical replicates per condition were quantified.

Following the same question, the effect of C18 at different time-points was examined. The hypothesis was that C18 may be affecting cathepsin levels in the early stage of compound treatment. The experiment was performed using 3

μM C18 at different time points, including 30 min, 1 h, 2 h and 4 h incubation. Interestingly, treatment with 3 μM C18 caused an initial drastic increase in both CTSB and CTSL at 30 min and 1 h (**Figure 20A**) but their expression was slowly suppressed in a time-dependent manner. However, the inhibitory effect on CTSB and CTSL was not statistically significant. Overall, C18 did not have a major influence on the proteolytic enzymes. There was a mild suppression of cathepsins with long-term C18-treatment but the effect is only secondary to effect on lysosomal acidification which happens through other pathways.

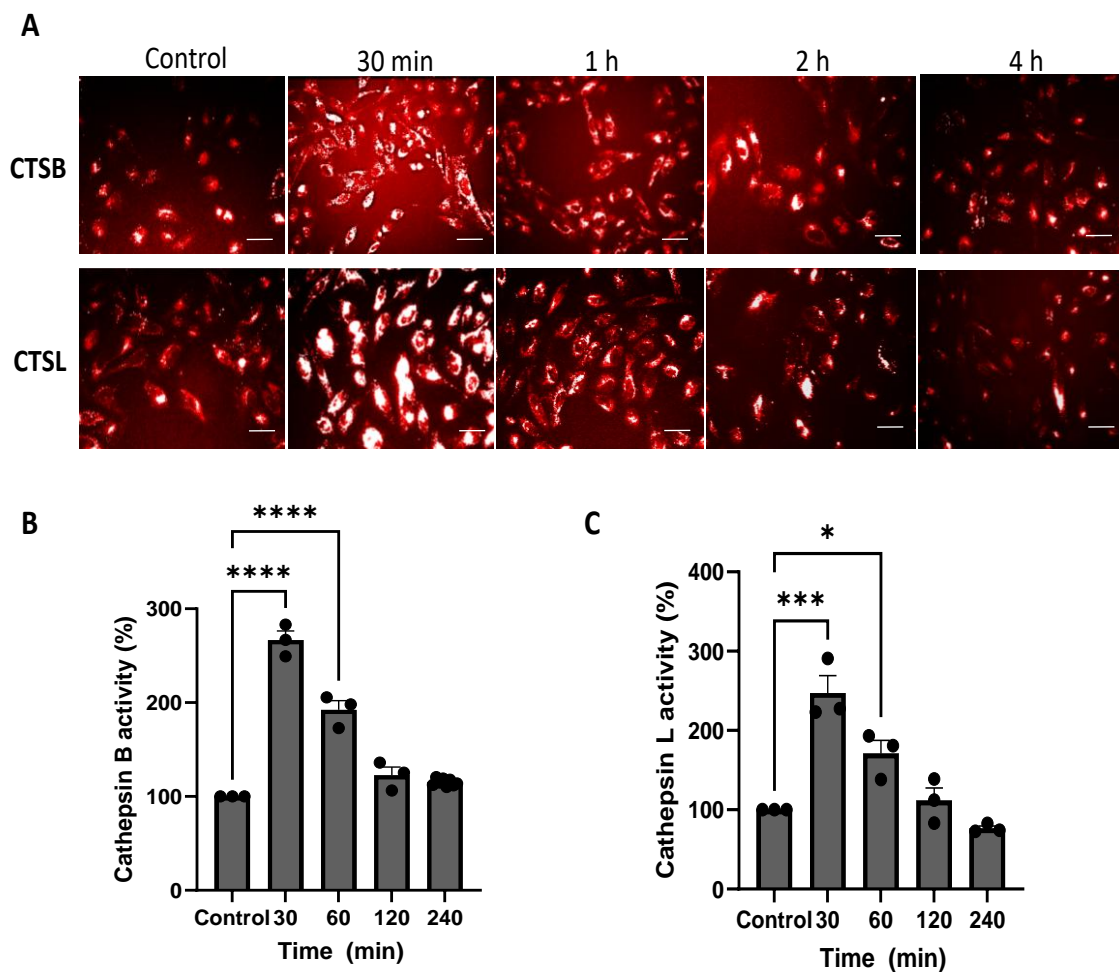


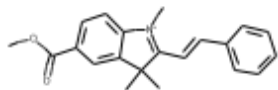
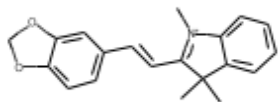
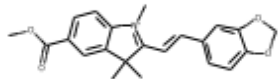
Figure 20: Time-dependent suppression of lysosomal hydrolases. (A) Representative images of cells stained with cathepsin B Magic Red and cathepsin L Magic Red to visualize proteolytically active lysosomes. U2OS cells were incubated with DMSO and C18 (3 μM) labelled with Magic Red for 30 min followed by live confocal microscopy. Scale bar 50 μm . (B-C) Quantitation of the time course experiments DMSO vs. C18. Magic Red intensity was normalized to control (DMSO). Data are presented as mean \pm SEM of at least three independent biological replicates. At least 8 technical replicates per condition were quantified.

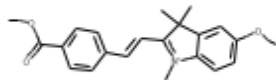
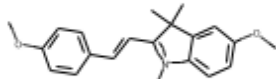
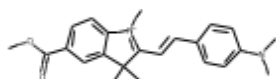
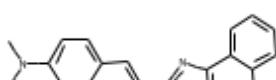
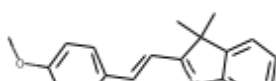
4.5 Hit expansion

4.5.1 Identification of C18 analogs

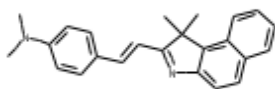
The SAR study lead to identification of 9 analogs of C18 (**Table 12**). The analysis was done by a colleague at the Institute, Andrea Zaliani. These compounds were commercially available and were purchased from MolPort (Riga, Latvia). 7 out of 9 compounds have at least Tanimoto > 0.7. MolPort-002-915-748 and MolPort-003-813-765 have Tanimoto of 0.61 but were chosen as scaffold molecules due to the increased chemical similarity.

Table 12: Structure–Activity Relationship (SAR) of C18 analogs.

MolPort ID	Structure	Tanimoto similarity	Comment
MolPort-007-566-707		0.83	Tan > 0.7
MolPort-007-569-322		0.73	Tan > 0.7
MolPort-007-569-323		0.77	Tan > 0.7

MolPort-007-570-230	0.93	Tan > 0.7
		
MolPort-007-570-267	0.87	Tan > 0.7
		
MolPort-007-571-916	0.78	Tan > 0.7
		
MolPort-002-915-748	0.61	Tan not similar but same scaffold family (different salt with different solubility)
		
MolPort-000-681-818	0.85	Tan > 0.7
		

MolPort-003-813-765	0.61	Tan	not similar but same scaffold family (different salt with different solubility)
---------------------	------	-----	---



4.5.2 Characterization of biological activity of the C18 analogs

After initial screening and the SAR analysis of the 9 analogs summarized above, two novel compounds that modulate autophagy were found. These compounds were tested in the same settings as the initial hit with the goal to find a more potent compound. Compounds MolPort-002-915-748 and MolPort-007-571-916 showed autophagy inhibition by increasing the number of yellow puncta in the cell, a marker for autophagosome accumulation (**Figure 21A-B**). In addition to this, MolPort-007-571-916 has a higher solubility than C18. MolPort-002-915-748, on the other hand, was unstable and oxidised in solution. Despite these findings, the IC_{50} analysis indicates that these two analogs are less potent than C18 ($IC_{50} = 1.9 \mu\text{M}$) and they did not improve potency. Thus, C18 was used as the lead compound from here forward.

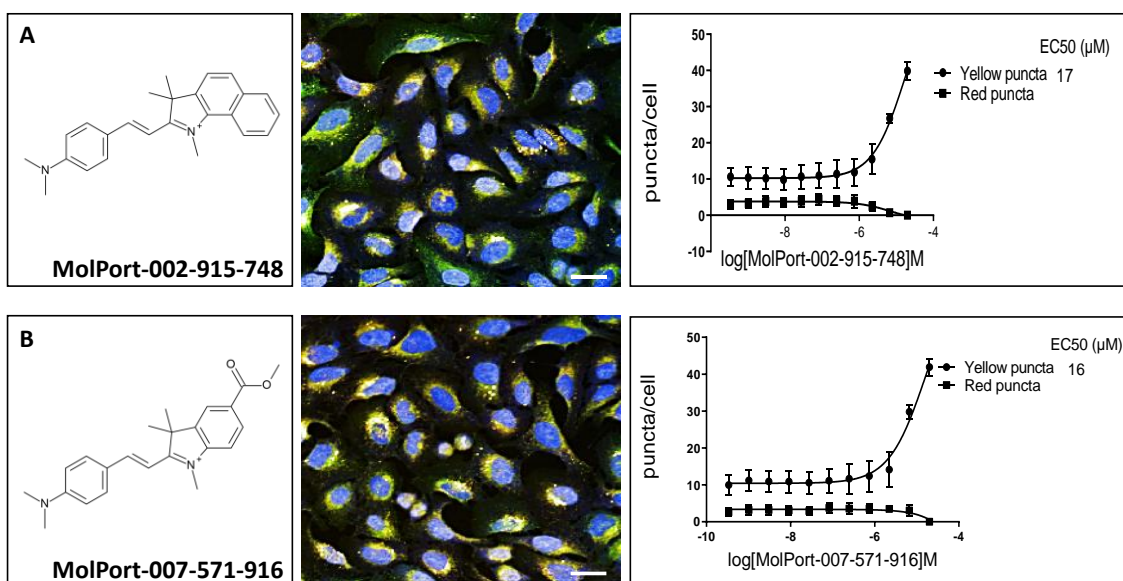


Figure 21: Structures, images and dose response curves for C18 analogs. (A-B) first column, chemical structures and names of each compound. Second column are representative

images of each hit compound at the most efficacious concentration showing Hoechst (blue), EGFP (green) and mCherry (red). Bar 50 μ M. Third column represents the dose response curves used for computing the IC_{50} for each hit compound. Nonlinear regression of the dose-response curves was used to determine the IC_{50} values. The yellow puncta represents colocalization of mCherry⁺ and EGFP⁺ puncta while red puncta represents only mCherry⁺ puncta. Data are presented as mean \pm SEM of at least three independent biological replicates. At least 8 technical replicates per condition were quantified.

4.6 mTOR signalling and interaction with Rab7 GTPase

To clarify the role of mTOR in C18-induced autophagy inhibition, western blot analysis of 4E-BP1 and its phosphorylation was performed. The results were expressed as ratio of phospho-4E-BP1 to total 4E-BP1. Additionally, Rab7 protein expression was checked. Western blot analysis revealed that C18 markedly increased phosphorylation of 4E-BP1 substrate by 1.4-fold ($p = 0.0291$), thus blocked autophagy induction. BafA1 caused a similar increase of 1.4-fold ($p = 0.0357$). On the other hand, starvation caused reduction of the p-4E-BP1 and higher expression levels of the total 4E-BP1. Starving C18-treated cells was able to suppress phosphorylation of 4E-BP1 and reduce the ratio of phospho-4E-BP1 to total 4E-BP1 levels. Interestingly, BafA1 followed the same pattern (**Figure 22B**).

Regarding Rab7, a significant increase in protein expression in starvation condition ($p = 0.0365$) was observed. On the other hand, C18 did not have a significant effect on Rab7 expression but was able to prevent its levels to increase following autophagy induction by EBSS (**Figure 22C**). This suggests that C18 does not block autolysosome maturation. Taken together, this data indicates that C18 impairs mTOR function by regulating important effectors of mTOR pathway and thereby blocking autophagy.

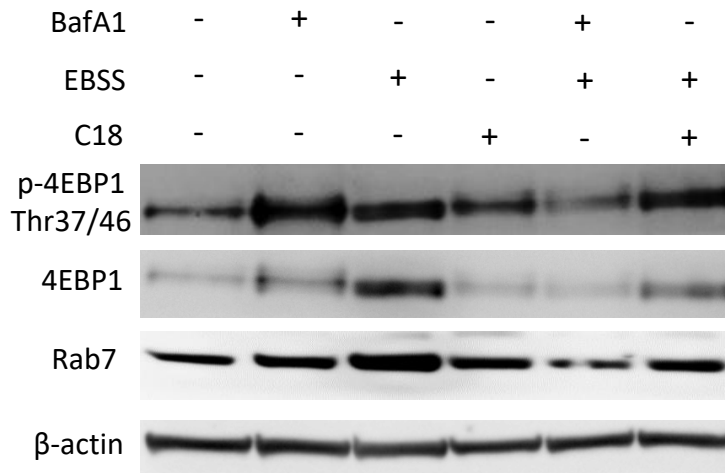
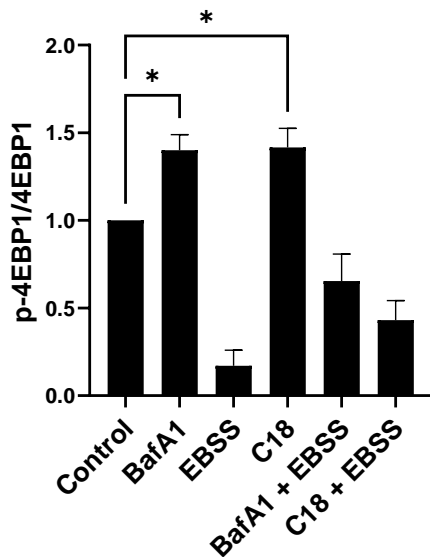
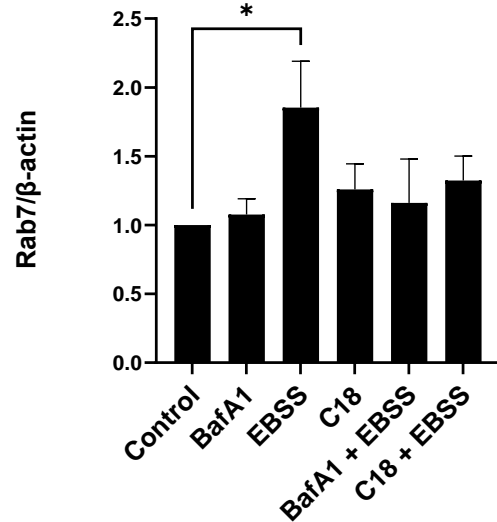
A**B****C**

Figure 22: C18 induced phosphorylation of 4E-BP1 and downregulation of Rab7. (A) Indicates phosphorylation of the mTORC1 downstream target, 4E-BP1 and the activation of Rab7. U2OS cells were incubated in complete media (control), complete media with BafA1 (100 nM), starvation media (EBSS), complete media with 3 μ M C18, 3 μ M C18 in presence of BafA1, starvation media with BafA1 and starvation media with 3 μ M C18 for 4 h. Blots shown are representative. Quantification of data shown in **(B)** phosphorylated proteins in respect to the respective total levels from the blots presented and **(C)** Rab7 levels relative to control. Data are presented as mean \pm SEM of at least three independent biological replicated normalized to the loading control.

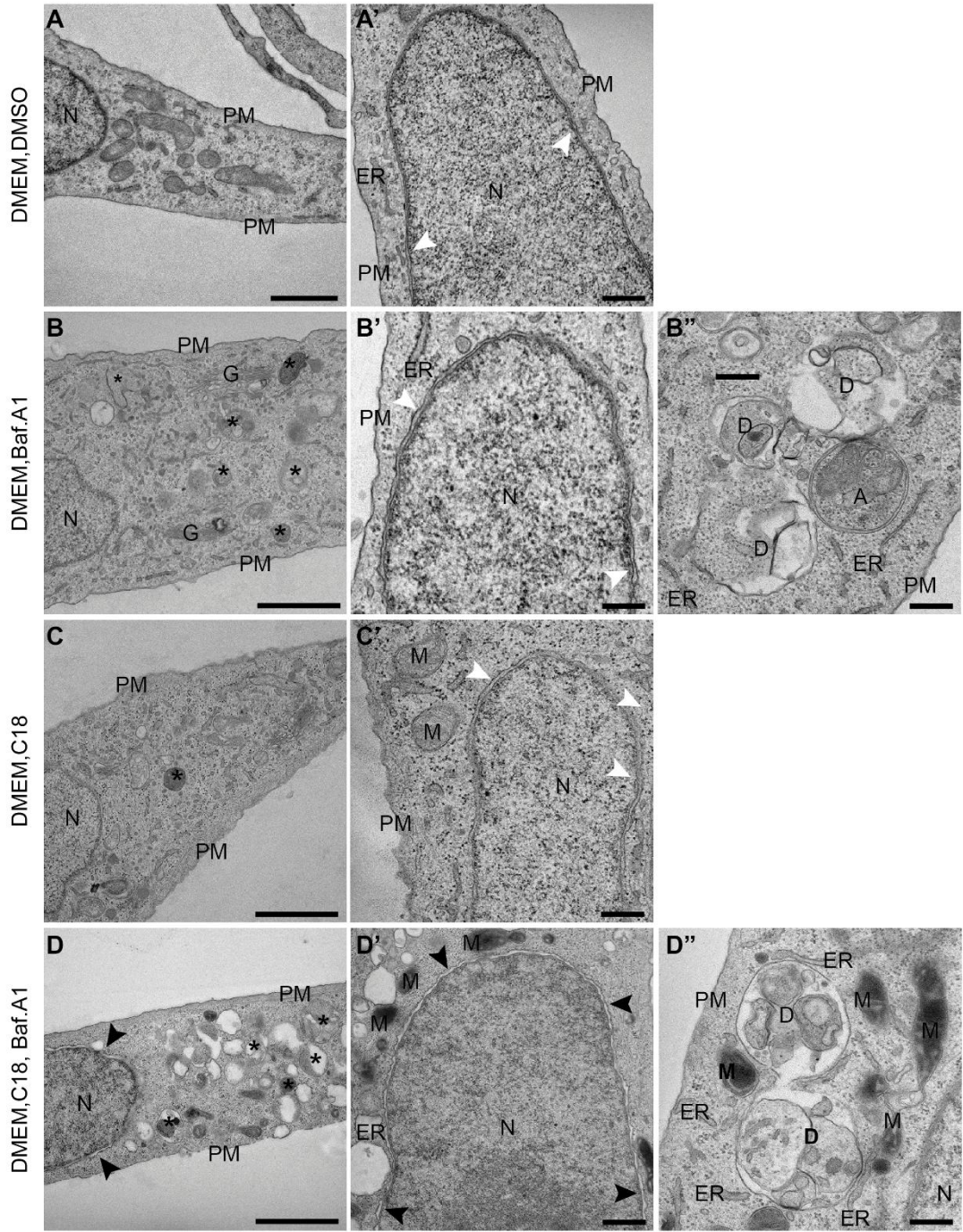
4.7 Endoplasmic reticulum stress and autophagy inhibition

4.7.1 Transmission electron microscopy analysis

Next, transmission electron microscopy was used to further investigate cellular autophagy phenotypes/structures and detect autophagic vacuoles (AVs). Under fed condition, U2OS cells treated with 0.1% DMSO have a fibroblastic shape (elongated cells) as expected. These cells barely show any degradative compartments and no autophagosomes could be observed, as expected. The ER is mostly tubular and the nuclear envelop is well preserved. The rest of the organelles have the classical ultrastructure. BafA1 treated cells under fed condition display more degradative compartments than DMSO cells. Occasionally some autophagosomes can be observed in the cell sections. The Golgi is swelling as expected. Like in DMSO-treated cells, the ER is mostly tubular and the nuclear envelop is well preserved. C18 cells still have a fibroblastic shape. A small proportion of the cells treated with C18 show some possible ER stress, leading to a mild swelling and expansion of the nuclear envelop (nuclear ER). The nuclear envelope look normal, similar to DMSO cells. However, most of the mitochondria do not appear healthy. Autophagosomes and/or degradative compartments were rarely observed. Finally, BafA1 treatment in cells treated with C18 seems to enhance the accumulation of autophagosomes and degradative compartments (lysosomes). Cells remain mostly fibroblastic. However, a swelling of the nuclear envelop was observed and, for some of these cells, the ER in the cytoplasm is expanding.

Furthermore, the accumulation of autophagic vacuoles under starvation condition was observed in order to estimate autophagic flux. In the control samples (EBSS, DMSO), cells have a fibroblastic shape (elongated cells) as expected. These cells contain numerous degradative compartments, most of them containing electron dense material. This is normal due to autophagy induction by EBSS. Autophagosomes are extremely rare. The ER is mostly tubular and the nuclear envelop is well preserved. The rest of the organelles have a classical ultrastructure. Starved cells treated with BafA1 led in two major differences in comparison to the control cells: an accumulation of autophagosomes and/or autolysosomes, and a change in the content of the degradative compartments which appear less dark than in absence of BafA1.

This is anticipated because dark content is a sign of degradation. The starved cells treated with C18 seem to lose, at least in part, their fibroblastic shape. Several cells become more round. There is a drastic ER stress response, leading to an accumulation of massively expanded ER. There is also a swelling and expansion of the nuclear envelop (nuclear ER). This ER/nuclear envelop expansion and proliferation is affecting mitochondria, as well as the lipid droplets biogenesis. There is an accumulation of autophagosomes and/or autolysosomes compared to DMSO cells but these structures appear to have a different shape than the ones observed in DMSO cells. Occasionally ER fragments in autophagosomes and/or autolysosomes were detected. In the last condition, BafA1 treatment of the C18-starved cells seems to enhance the already dramatic effect of the C18 compound, after cell starvation. The frequency of appearance of autophagosomes and/or autolysosomes seem to be similar to the C18 treated starved cells. Note that numerous of these autophagosomes/autolysosomes contain ER-fragments. In the presence of C18, it was even possible to occasionally see clear omegasomes, structures that are rarely detected in starved cells by experts in the field. There were no visible apoptotic cells observed following C18 treatment.



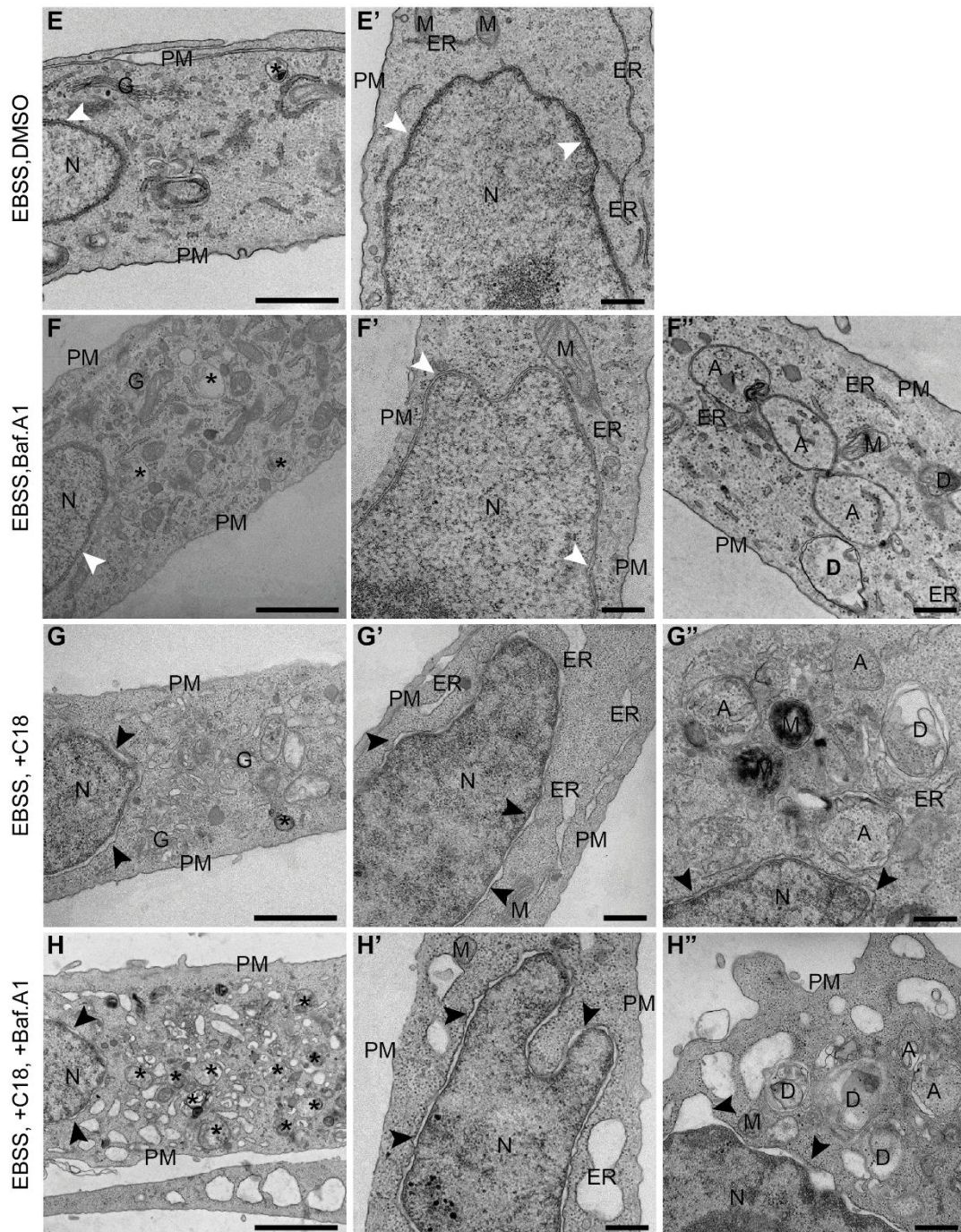


Figure 23: Effect of C18 on cell morphology. U2OS cells were incubated with DMSO (0.1%), BafA1 (100nM), C18 (3 μ M) and C18 in presence of BafA1 in complete media or EBSS (starvation media), and processed for transmission electron microscopy at 4 h post-incubation. Scale bars, 1 μ m (panels A, B, C, D, E, F, G and H) and 500 nm (panels A', B', B'', C', D', D'', E', F', F'', G', G'', H' and H''). Abbreviations: A, autophagosome; D, degradative compartments (lysosomes/autolysosomes/amphisome); ER, endoplasmic reticulum; G, Golgi apparatus; M, mitochondria; N, nucleus; PM, plasma membrane; asterisks, autophagosomes and/or degradative compartments, white arrows, nuclear ER with regular shape; black arrow, swelling nuclear ER.

4.7.2 Expression of ER stress-associated proteins

Examination of ER stress markers, BiP and CHOP, during 4 h treatment with C18 indicates a time-dependent increase in ER stress (**Figure 24A**). Densitometry analysis indicated that treatment with C18 caused a significant increase in BiP levels at 2 h ($p=0.0008$) and 4 h ($p < 0.0001$). CHOP protein expression also shows a tendency to increase ER stress, but levels were lower than BiP (**Figure 24B**). In addition, LC3-II and p62 protein levels were quantified and showed that there was a simultaneous increase in LC3-II and p62, confirming autophagy inhibition occurs at the same time with ER stress induction. Moreover, dose-dependency of the C18 effect was examined and compared it to EBSS and BafA1 (**Figure 24C**). Starvation increased BiP protein expression, whereas BafA1 suppressed BiP levels compared to control. On the other hand, starvation did not change CHOP protein expression, while BafA1 slightly suppressed it. C18 was able to increase BiP expression, regardless of the concentration. There was no significant difference in accumulation of BiP upon treatment with various concentrations of C18. On the other hand, CHOP protein expression failed to increase upon treatment with C18 (**Figure 24D**). Taken together, C18 activates ER stress mainly via BiP, without significant activation CHOP.

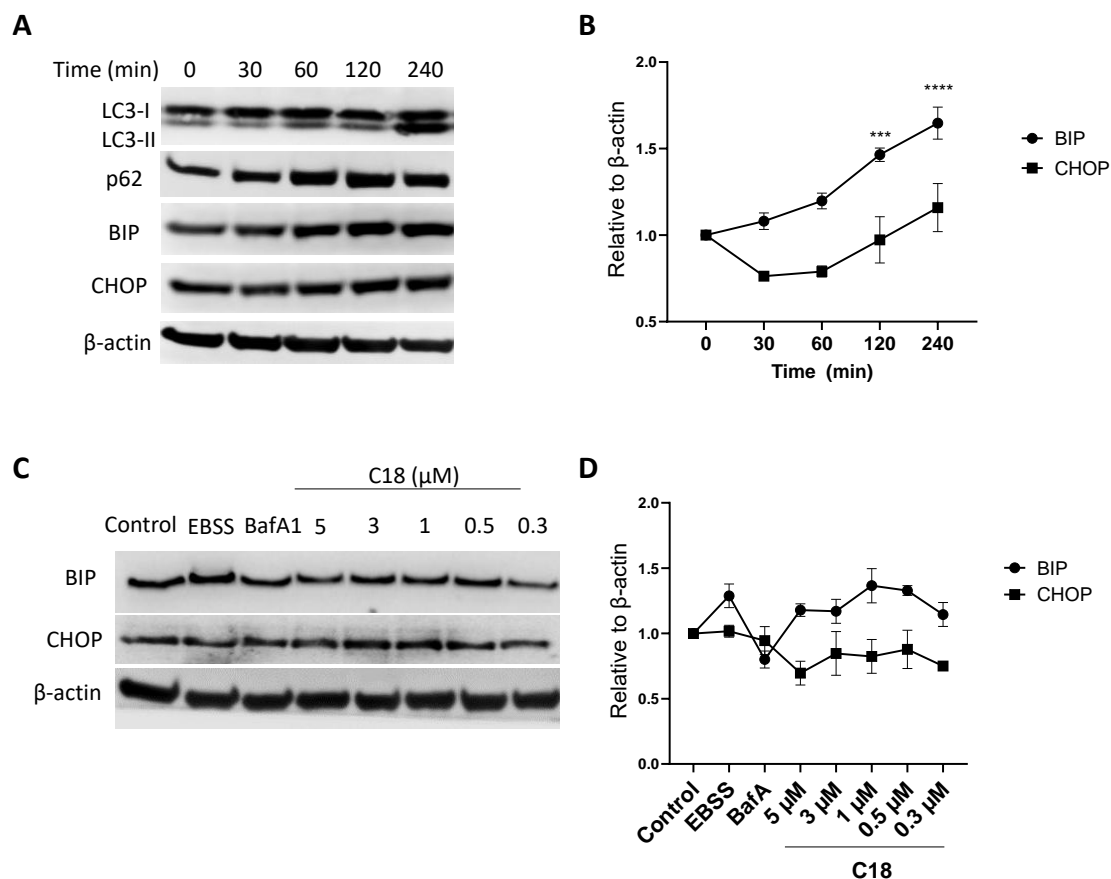


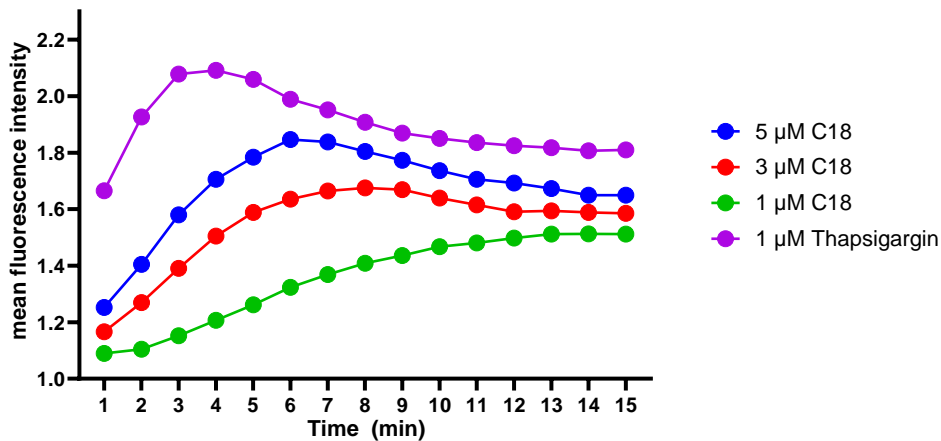
Figure 24: Time- and dose-dependent expression of BiP and CHOP. (A) Time-dependent expression of BiP and CHOP, endoplasmic reticulum (ER) stress markers, and co-activation of autophagy markers, LC3 and p62 in U2OS cells, and (B) its densitometry analysis in respect to the loading control. (C) Dose-dependent expression of BiP and CHOP after 4 h incubation and (D) its densitometry analysis in respect to the loading control. Blots shown are representative. Data are presented as mean \pm SEM of at least three independent biological replicates normalized to the loading control.

4.7.3 Direct measurement of intracellular calcium

Findings regarding C18 effect on ER suggest a possible perturbation of calcium homeostasis, according to previous findings²⁹². To Determine that C18 increases intracellular Ca^{2+} , Fluo-4 directTM calcium assay was used. As shown in **Figure 25A**, C18 elicited a calcium influx response in U2OS cells in a dose-dependent manner. This indicates that ER stress response involves an increase in cytosolic calcium concentration, possibly by depleting ER. To further investigate this theory, the effect of C18 on intracellular Ca^{2+} levels in presence

of thapsigargin (Tg) was examined. U2OS cells were pre-treated with 1 μM Tg and given enough time to deplete ER of calcium, followed by addition of various concentration of C18. Interestingly, pre-treatment with Tg prevented the fast increase in cytosolic Ca^{2+} but it was not able to completely inhibit C18 effect. **Figure 25B** shows a delayed release in intracellular Ca^{2+} , after depletion of ER Ca^{2+} stores, which suggests that C18 induces calcium buffering from other intracellular stores. The smaller the concentration of compound the longer the delay times were. The delay was less pronounced with 5 μM C18 which caused the highest Ca^{2+} release but the level gradually declined toward the same baseline values as before the Tg addition. 3 μM and 1 μM C18 caused a more noticeable delayed response.

A



B

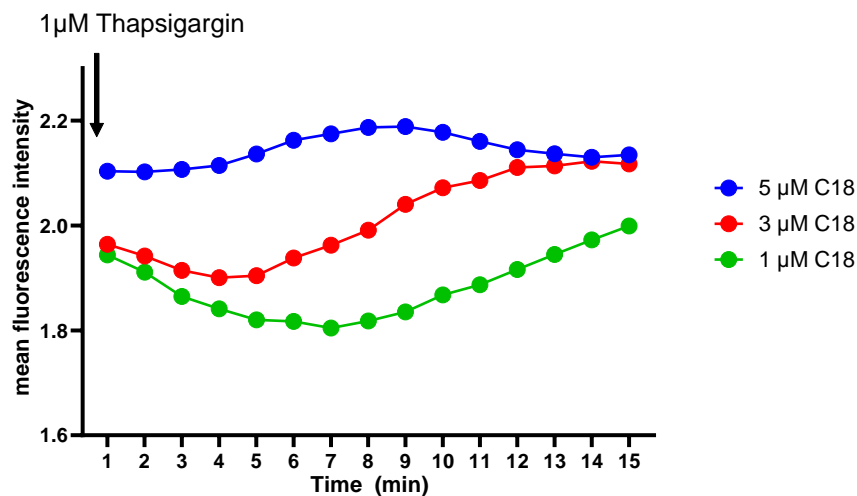


Figure 25: Intracellular calcium mobilization by C18. (A) Cells were incubated with Fluo-4 direct™ reagent solution at 37°C for 1 h and the fluorescence signals induced by the addition of

C18 at the indicated concentrations were measured for 15 min. **(B)** Cells were pre-treated with 1 μ M thapsigargin for 5 min prior to C18 stimulation. Data are representative of at least three independent biological replicates.

5 DISCUSSION

5.1 Phenotypic screening leads to the identification of a novel autophagy inhibitor

To date, a limited number of small molecule inhibitors of autophagy have been identified, which together provide very useful tools for studying the physiological role of autophagy. The complexity of the pathway and the tendency of inhibitors to show broad spectrum selectivity means that further research would significantly benefit the field. In an effort to promote drug discovery for autophagy modulators, a cell based image quantitative HTS assay developed for screening for autophagy modulators. Over 4,500 small molecules were screened for their ability to modulate autophagy in TagRFP-mWasabi-LC3 expressing HEK293 cells. A special advantage of the strategy was using Operetta, a highly advanced and automated confocal microscope which improves throughput and benefits of automated analysis of images. Another important advantage is the ability to easily adapt the assay and its analysis sequence in very little time for comparable programs, aiming at finding autophagy inhibitors.

There are various readily available drug libraries for HCS and HTS. Drug repositioning, or repurposing, is the application of an existing therapeutic to a new disease and is an important part of any drug discovery program that has led to identification of several blockbuster drugs such as Sildenafil²⁹³. There are commercially available FDA-approved drug libraries used for drug repurposing. These compounds have known and well-characterized bioactivity, safety and bioavailability which can significantly reduce the time spent on drug development and optimization^{294, 295}. There are also 'general purpose' library of compounds that can be used for screening. A good example is the ChemBioNet collection, which has been designed by Ronald Kühne group at the Leibniz-Forschungsinstitut für Molekulare Pharmakologie (FMP) in Berlin, Germany. This library aims at helping the academic community through the screening

centres of the ChemBioNet, which includes an interdisciplinary consortium of chemists and biologists, who worked together to exploit small molecules and created a compound library to study biological systems. The small-molecules in ChemBioNet library are chemically diverse, are arranged in novel combinations and have the ability to pass through biological membranes and thus are suitable for cellular assays²⁹⁶. There are various other libraries available for research use but based on the needs of the project these two were selected for the current screening program.

HCS approach led to the identification of compound 18, a small molecule from ChemBioNet collection, as the most potent novel autophagy modulator to increase the number of autophagic vacuoles in cells. Upon further validation and characterization of this compound, it was discovered that compound 18 (C18) significantly increases endogenous levels of both LC3-II and p62 proteins in HEK293 cells. Increase in LC3-II means an increase in autophagosome formation, or increased accumulation of autophagosomes due to inhibited flux downstream²⁹⁷, which could be either autophagy activation or inhibition. Since concomitantly p62 is accumulated when autophagy is inhibited⁸⁷, together with LC3-II data, it was concluded that C18 can inhibit autophagy in HEK293 cells.

Because it is important to confirm hit efficacy in secondary assays, a series of functional assays were used to ensure that C18 from the screening campaign can be reliably translated into a lead compound. First, it was sought to explore the ability of C18 in suppressing autophagy in osteosarcoma cell line (U2OS) with a stable doxycycline-inducible expression of mCherry-EGFP-tagged LC3. Special focus was put on the question if the effect seen here can be replicated in a similar cell model. For this purpose, an 11-point dose response study was performed which showed that increased concentrations of C18 increase the number of autophagosomes ($IC_{50} = 1.9 \mu\text{M}$), while reducing the number of autolysosomes. Furthermore, 3 compounds were identified from the Enzo FDA-approved drug library, ENZ_000713 (known as reserpine), ENZ_0000104 (known as idarubicin) and ENZ_0000735 (known as sunitinib). Reserpine, idarubicin and sunitinib are compounds that have already been acknowledged for their autophagic effect^{277, 278, 286}. Reserpine inhibits autophagic flux and leads to the accumulation of α -synuclein, as well as inducing cell death in

dopaminergic neurons²⁷⁷. Idarubicin and sunitinib on the other hand are studied in cancer context. Idarubicin induces mTOR-dependent in leukemic cells²⁷⁸ and sunitinib, which is the most studied in the field, is proposed to have a dual modulatory effect in cancer cells based on the dosage used²⁸⁶. Clinically relevant doses of sunitinib induce mTOR signalling in a panel of cancer cells and enhance the stability of the antiapoptotic protein MCL-1, while higher doses of sunitinib were cytotoxic, triggering a decline in MCL-1 levels and inhibiting mTOR signalling²⁸⁵. The current assay was able to detect these compounds, which further indicates that the established assay is robust enough to identify compounds that modulate autophagy. Since the aim of the study was finding a novel compound, all efforts were put in investigating C18, derived from ChemBioNet library.

Based on dose-response activity, various concentrations of C18 close to the IC₅₀ value were selected for investigation. Western blot analysis of endogenous LC3-II and the adaptor protein p62 using these concentrations revealed that C18 caused accumulation of LC3-II protein, suggesting an increase in autophagosomes. Simultaneous accumulation of the p62 also occurred, which suggests that the increase in autophagosomes observed following treatment with C18 is caused by blocking autophagy. The effects were both dose- and time-dependent. It is a known fact that BafA1 causes accumulation of both LC3-II and p62 as a consequence of inhibiting lysosomal degradation²⁸⁸, thus it can be hypothesised that C18 is a lysosomal inhibitor due its comparable effect.

5.2 C18 inhibits autophagic flux

Under normal cellular growth conditions, also called nutrient rich condition, autophagy occurs at a basal level. This happens mainly for house-keeping purposes, such as degradation of long-lived proteins and damaged cellular organelles. On the other hand, under nutrient starvation, autophagy is enhanced to provide cells with additional nutrients²⁹⁸. Starvation is also a classical inducer of autophagy and works by displacing mTOR from lysosomes, causing its inactivation²⁹⁹. A widely used strategy to measure autophagic flux is stimulating cells with starvation. This has been demonstrated using autophagy inhibitor BafA1, which inhibits autophagic flux under starvation in various cell lines^{76, 300, 301, 302, 303}. Next, C18 in cells with active autophagy induction by

nutrient starvation was studied. Interestingly, the results from C18 treatment showed further accumulation of autophagosomes in starved cells compared to non-starved cells while the number of autolysosomes stayed intact, which is a similar inhibitory activity to BafA1. This data was also confirmed in western blot analysis where endogenous levels of LC3-II and p62 were measured. C18 increased LC3-II levels, which further increased in C18-treated starved cells. The accumulation of p62 in C18-treated cells was more modest. However, starving C18-treated cells caused a marked accumulation of p62 protein, confirming that cells are more susceptible to C18 under nutritional stress conditions.

Another commonly used technique to confirm block in the autophagic flux is dual treatment with compound and BafA1^{304, 305, 306, 307}. In these studies, authors show that an autophagic flux inhibitor in combination treatment with BafA1 will not decrease or simply not change the LC3-II levels in the cell, compared to BafA1 treatment alone. Although in this experiment BafA1 had a significantly more potent effect than C18, dual treatment did not further increase LC-II compared to compound alone. While some studies^{160, 308} simply use GFP-LC3 or tandem fluorescent-tagged LC3 assays to conclude whether a compound inhibits autophagic flux within cells, this study has the advantage of using several endpoints related to autophagic flux, including starvation induced flux and usage of a lysosome inhibitor to block degradation. This is particularly important because LC3 can be incorporated in aggregates, which then can be mistaken with autophagic structures²⁸⁸. Collectively, current data indicates that C18 acts by inhibiting autophagic flux.

As C18 is supposed to block autophagic flux, a qualitative assessment of the fusion between autophagosomes and lysosomes was conducted and, consequently, the lysosomal acidity was determined. To determine whether C18 inhibits autophagic flux through blockage of autophagosome-lysosome fusion, confocal microscopy was used to detect the co-localization of EGFP-LC3 and LysoTracker Red, a pH-sensitive dye for live cell lysosome labelling³⁰⁹. In line with previous studies^{310, 306, 307}, a decrease in LysoTracker Red-positive puncta upon BafA1 treatment was observed. Strikingly, C18 exhibits similar potent inhibitory effect on acidic lysosomes at all the concentrations tested.

Furthermore, confocal microscopy assay was used to detect the colocalization of EGFP-LC3 and LysoTracker Red. A high magnification view of the U2OS cells treated with C18 showed few colocalized EGFP puncta with LysoTracker Red staining, suggesting that most of the EGFP puncta, but not all, are pre-lysosomal autophagic vesicles. However, LysoTracker stains all the acidic organelles, including late endosomes as well³¹¹, which makes it unspecific and hard to differentiate between lysosomes and endosomes. Although this dye is often used to estimate lysosomal pH, it is not a pH sensor and the intensity of its fluorescence signal does not correlate with the lysosomal pH but rather gives an estimation of the acidity by losing fluorescence at a pH above 6.5³¹². To overcome LysoTracker limitation, another lysosome stain, LysoSensor Yellow/Blue DND-160 was used. This probe allows one to check whether if the block in autophagosome-lysosome fusion also impaired lysosomal acidity and increased pH. Since LysoSensor Yellow/Blue is a ratiometric dye, it can measure pH-dependent acidification inside lysosomes as a marker for their functionality³¹³. As expected, a significant dose dependent decrease in the acidity of lysosomes following treatment with C18 following was observed. Since the pH in acidic compartments is dependent on the autophagosome-lysosome fusion³¹⁴, it was expected that C18 will diminish the acidity of lysosomal lumens.

Finally, it was assessed whether intralysosomal proteolytic activity was diminished or blocked by C18 by measuring the enzymatic activity of CTSB and CSTL in U2OS cells. Lysosomal proteases, also called cathepsins, are the largest group of proteolytic enzymes in the lysosomes³¹⁵. Dysfunction of lysosome also results in impaired activity of lysosomal proteases^{316, 317, 318}. Cathepsins B, D, and L are the major lysosomal proteases for degrading the lysosomal cargos and for maintaining lysosomal functions^{319, 320}. As study by Dennemarker et al.³²¹ demonstrated that cathepsin L deficient primary mouse embryonic fibroblasts have normal initiation of the autophagy process, autophagosome formation and even autophagosome–lysosome fusion, but impaired lysosomal degradation³²¹. On the other hand, cathepsin B is known to degrade the calcium channel MCOLN1/TRPML1 in the lysosomes, leading to the suppression of the transcription factor TFEB and inhibition of autophagy-

related proteins³²². Results indicate that CTSB and CTSL activities were not significantly affected in a dose-dependent manner following C18 treatment. However, C18 was able to slowly suppress their level if different time points are compared. This implies that impaired autophagic degradation is not dependent on CTSB and CTSL, and their modest suppression occurs only as a secondary event resulting from insufficient lysosomal function.

In conclusion, it was reported that C18-treated cells displays a reduced autophagosome-lysosome fusion and autolysosome degradation, which is enhanced by starvation. The effect on lysosome function was partially caused by the reduced enzymatic activity of CTSB and CTSD. Taken together, these results encourage the further investigation of C18 as a late stage lysosomal inhibitor.

5.3 Structure-activity relationship and lead optimisation

C18 is part of a wider series of small-molecules from ChemBioNet library that were screened in this program. Two other compounds from the same series sharing the same core structure, 31505_ChemDiv_5018-0020 and 31511_ChemDiv_5018-0024, were identified and validated, but with a more modest effect than C18. These compounds were categorised as hits in HEK293 cells but were not active in U2OS cells. There is a chance that they could be active in other cell lines but screening a panel of cancer cell lines is necessary for this purpose. However, data from the screen suggests that molecules showing only minor variations in structure, but with the same core structure as C18, might also be active.

To investigate this theory, an SAR study of C18 analogs was performed. Compounds with chemical similarities to C18 were systematically extracted from the public domain compound databases and analysed in the established assay. Overall 9 analogs of C18 were selected for the study. First, they were subjected to a core scoring method, called the Tanimoto coefficient, to assess molecular similarity. A Tanimoto score of 0.7 is a reasonable cut-off for most chemicals³²³ and it was used as a starting point in the program. 7 out of 9 analogs investigated exhibited a Tanimoto score above the cut-off, while 2 analogs had slightly lower score. This first part of the SAR study provided hope

that one of these molecules could be also active, thus dose-response studies for all 9 compounds were conducted with the aim to find equally or more potent compounds than C18.

As above mentioned, the second part of the optimization process involved a dose-response study for the 9 analogs using previously established assay. 11-point dose response curves were generated for all of them using the mCherry-EGFP-LC3B tagged U2OS cells and compared results to the dose-response curve of C18. Two analogs, MolPort-002-915-748 and MolPort-007-571-916 showed autophagy inhibition by increasing the number of yellow puncta in the cell, a marker for autophagosome accumulation. However, the IC₅₀ values were 17 μ M and 16 μ M, respectively, both lower than the IC₅₀ of C18. This indicates that these compounds were unable to improve potency. However, it is worthy to note that these compounds were indeed active and a thorough SAR analysis could potentially lead to a significant discovery.

Unfortunately due to limited chemical synthesis resources, only a small number of commercially available analogs were tested, which makes it difficult to predict the binding site or mechanism of action. However, these compounds are very similar in their structures. Thus, it cannot be excluded that the real mechanism of action could be either binding to same binding site as they have similar shape and volume, or a methylation transfer process which can be absolved by all of them in a similar manner. Moreover, another strategy was to study the binding site by covalent labelling and mass spectrometry (MS) analysis¹⁴⁷. However, the efforts to obtain the necessary support for investigation within the PhD program timeframe were unsuccessful.

5.4 Regulation mechanisms and signalling pathways

5.4.1 Implication of cell death and apoptosis

Autophagy inhibitors have the intrinsic capacity to trigger cell death³²⁴. The Ribas group investigated the consequences of various autophagy inhibitors, acting at the initiation, nucleation, or completion phases of autophagy, on cell viability under normal growth conditions. The results evidenced that some autophagy inhibitors such as 3-MA, BafA1, SBI-0206965 and CQ reduced cell viability to 70%, 96%, 40% and 80% respectively in MEF cells at 24 h post-

treatment. These inhibitors caused the most significant levels of cell lethality in growing medium and triggered caspase activation. On the other hand, treatment with MHY1485, Cpd18, SAR405 and Spautin-1 preserved the integrity of the plasma membrane in MEF cells and did not cause cytotoxic effects³²⁴. With that in mind, it was decided to investigate the consequences of autophagy inhibition with C18 on cell viability and caspase activation.

Cell viability up to 72 h treatment with various concentrations of C18 was explored through quantification of RealTime-Glo (RT-Glo), which is an ATP-independent live-cell assay. Results revealed that after long incubation times (above 24 h) C18 reduces cell viability in both HEK293 and U2OS cell lines and engages cell death as part of its autophagy inhibitory effect. Considering that autophagic activity was seen at concentrations below 5 μ M, the active concentration under 24 h treatment is 4-fold and 5-fold lower than the IC₅₀ in U2OS cells and HEK293 cells. Thus, it was proposed that C18 can potentially inhibit autophagy without cytotoxic effects, and that the cytotoxicity is both cell and time dependent.

One of the major hallmarks of cancer is escaping cell death pathways, such as apoptosis, that act as a barrier against tumour growth³²⁵. This can occur by loss of the classic death receptors, inactivation of caspases, and impaired mitochondrial-mediated intrinsic death pathways³²⁶. During apoptosis, the major mediators of cellular destruction are effectors caspase-3 and caspase-7, members of the cysteine aspartate proteases family, which cleave proteins after an aspartate residue^{327, 328}. They are primary drivers of apoptotic cell death, but also play a critical role in mediating autophagy because activated caspases can degrade autophagy proteins to shut down the autophagic response^{329, 330, 331}. In this line, the implication of caspase activation and apoptosis were evaluated. The assay explored caspase-3 and caspase-7 activation upon treatment with C18. Data suggests that caspases-3/7 gradually increased post treatment, with the highest accumulation observed at 14 h upon treatment with C18. This suggests that prolonged treatment with C18 pushes cells closer to their cell death threshold through accumulation of apoptotic proteins. However, caspase activation is probably not an initiating event in this system.

Inhibition of autophagy with lysomotropic agents has been shown to induce apoptosis and activate caspases⁸². Similarly, novel early-stage autophagy inhibitors can also enhance apoptosis and have shown antiproliferative effect in cancer³³². Furthermore, an interesting work by Amaravadi and colleagues in 2007 studied the impact of autophagy inhibition on Trp53-mediated cell death. In this model, using CQ markedly increased tumour regression and delayed tumour recurrence following activation of p53 and administration of tamoxifen. Activation of p53 was associated with the rapid appearance of apoptotic cells²³⁶. Other research groups have also shown that treatment with CQ causes apoptosis in glioma initiating cells and patient-derived stem-like glioma cells^{333, 334}. These studies provide evidence that chemical inhibition of autophagy and the subsequent apoptosis induction play cytoprotective roles in cancer. Because C18 has similar inhibitory effect to CQ, it could be a potent anti-cancer agent. On the other hand, one should remember that tumour development is a multistep and complex process and autophagy inhibitors can have different roles depending on the tumour stage. Sun et al.³³⁵ showed a stage-dependent role in the rat model with N-diethylnitrosamine-induced hepatocarcinogenesis. In the dysplastic stage (Ds), CQ administration enhanced cell proliferation, DNA damage and inflammatory cytokines in the liver, while in the tumour-forming stage CQ restrained tumour formation and lead to excessive ROS accumulation and apoptosis. Hence, each stage of the cancer requires a different treatment plan and the window in which an autophagy inhibitor can be used must be assessed thoroughly.

5.4.2 mTOR-dependent autophagy inhibition

Both mTOR complexes, mTORC1 and mTORC2, are essential effectors of the most common oncogenic drivers, including those in the Ras-driven MAPK and PI3K–AKT pathways³³⁶. Constant activation of mTORC1 signalling has been shown to cause drug resistance in lung cancer, breast cancer and melanoma^{337, 338, 339, 340}. Additionally, a growing body of evidence indicates that mTORC1 signalling is involved in the DNA damage response and determines cell survival or cell death based on the amount of DNA damage³⁴¹. As a result, mTORC1-dependent inhibitors or activators can be valuable addition to chemotherapy or targeted cancer therapy, based on the given cancer and stage. According to the

results that C18 affected autophagic flux, it was hypothesised that C18 may interfere with mTORC1 signalling. mTORC1 phosphorylates S6 kinase 1 (S6K1) and eukaryotic translation initiation factor 4E-binding protein 1 (4E-BP1) to activate mTORC1 signalling³⁴². The priming phosphorylation sites for 4E-BP1 are at Thr37/46³⁴³ and measuring the phosphorylation level serves as a reliable readout of mTORC1 activity. Therefore, a comparative analysis of C18 in nutrient rich or nutrient deprived cells was made. Protein quantification revealed that C18 increases phosphorylation of 4E-BP1 substrate while inhibiting total levels of 4E-BP1. On the other hand, starvation suppressed this phosphorylation by increasing expression levels of the total 4E-BP1, which was expected as nutrient deprivation will trigger mTORC1 inhibition and the subsequent phosphorylation of the downstream targets³⁴⁴. Starving C18-treated cells triggered mTORC1 inhibition, thus rescuing total levels of 4E-BP1 to some extent and decreasing phosphorylated protein levels. However, the ratio of phosphorylated to total 4E-BP1 protein remained higher than starvation alone and the rescuing effect was not significant, suggesting that C18 can suppress mTORC1 inhibition caused by starvation-induced autophagy. It is therefore possible that C18 interferes with mTORC1 signalling by a mechanism related to amino acid supply.

Lysosomal inhibitors such as BafA1 can modulate mTORC1 signalling³¹⁰, but there is some controversy around the molecular basis of why and how this occurs. BafA1 is a V-ATPase inhibitor and V-ATPase can interact with Ragulator which controls mTORC1³⁴⁵. Consequently, the inhibition of mTORC1 signalling by BafA1 could be due to its effect on the V-ATPase/Ragulator axis, rather than lysosomal alkalisation via autophagy. Fedele and Proud³¹⁰ demonstrate that BafA1 inhibits lysosomal acidity as early as 1 h after in A549 cells, but there was no reduction in rpS6 phosphorylation at this time point, a downstream target of mTORC1. Hence, suggesting that reduced mTORC1 signalling is not a direct consequence of lysosomal alkalisation itself. Interestingly, their results conclude that lysosomal alkalisation occurs within a comparable timeframe in CQ-treated cells, which negatively influences mTORC1 signalling. CQ is not a V-ATPase inhibitor so this also means that the phenomena can occur independently of interference with the V-ATPase. The

decline in mTORC1 activity seems not to be directly due to either inhibition of the v-ATPase or the change in pH, as these effects are occur before the reduction in mTORC1 signalling. In this study, cells were treated for 4 h with C18 and it is thus important to study C18 at earlier timepoints and assess whether the effect on mTORC1 takes place alongside lysosomal alkalinisation, which was shown already to take place, or as an indirect consequence of altered luminal pH. Furthermore, as previously shown, assessment of intralysosomal proteolytic activity of cathepsins indicated that C18 did not alter CTSB and CTSL activity significantly and it is therefore likely that C18 reduced mTORC1 signalling and deacidifies lysosomes through indirect mechanisms. It would also be curious to experimentally evaluate C18 effect after knockdown of BECN1, which causes reduction of autophagosome number, to verify whether inhibition of autophagosomes will reflect on the impairment of mTORC1 signalling. Since the ultimate goal is anti-cancer therapy and BECN1 is an important gene in human cancer, assessing both its transcription and protein levels would be useful. Furthermore, it would also be curious to explore the PI3K/AKT pathway and ULK1 phosphorylation which are often deregulated in human cancers leading to unrestrained cell proliferation and tumour formation^{131, 346}.

In this study, the protein levels of Rab7 after treatment with C18 were investigated as a marker for presence of matured autolysosomes. Rab7 is a small GTPase involved in the fusion machinery. Some studies suggest that Rab7 is required for autophagosome-lysosome fusion^{347, 304} while other studies indicate that Rab7 is not essential for autophagosome lysosome fusion and is only a requisite for autolysosome maturation by recruiting tethers and SNARE proteins^{348, 349}. Results indicated that C18 slightly increased Rab7 expression under nutrient rich conditions but effect was not significant. This was expected as it was observed previously that C18 blocks autophagosome-lysosome fusion. On the contrary, when cells were nutrient starved, C18 was able to prevent Rab7 further accumulation. This indicates that does not interfere with autolysosome maturation under normal conditions but under cellular stress conditions such as nutrient deprivation is able to trigger its suppression to prevent autophagy. Combined with previous observations, this supports the

hypothesis that nutrient-stressed cells are particularly susceptible to C18-inhibition of autophagy. The rapid tumour growth in a given cancer will deplete cells from nutrients³⁵⁰, creating a unique vulnerability for autophagy inhibition with C18. Furthermore, there are other proteins involved in the fusion, such as Stx17 and YKT6, known as SNARE proteins that may selectively be translocated upon autophagy inhibition^{304, 351}. Matsui et al.³⁵¹ report that two distinct SNARE complexes mediate autophagosome–lysosome fusion, Stx17–SNAP29–VAMP7/8 and YKT6–SNAP29–Stx7. The role of Rab7 in these complexes remains to be elucidated. Overall, C18 may serve as a useful tool to study autophagosomal SNARE trafficking.

5.4.3 p62 regulation

During the last decade, research has shown that p62 has a vital role in autophagy by interacting with LC3 and ensuring the cargo selectivity for autophagy degradation³⁵². In liver cancer, p62 has been found to be elevated and deletion of it was reported to greatly diminish the growth of tumors^{353, 354}. Menon et al.³⁵⁵ show that p62 ablation completely inhibits HCC development in mice. c-Myc expression in both mouse and human HCC, driven by mTORC1 activation, is also ameliorated by p62 ablation³⁵⁶. Altogether, this suggests the importance of p62 regulation in autophagy and cancer. Nonetheless, these conclusions are complicated by the fact that p62 is also a TFEB target gene. Under normal conditions, mTORC1 causes retention of TFEB in the cytoplasm³⁵⁷ but under conditions of cellular stress, such as nutrient starvation or lysosomal stress, mTORC1 is released from the lysosomal membrane and unable to cause TFEB phosphorylation. Thus allowing translocation of TFEB to the nucleus and increased expression of target genes linked to autophagy and lysosomal function, such as p62³¹⁰. Together with high levels of p62 protein detected, it was decided to evaluate p62 transcript levels by qPCR to check for any changes in the gene expression levels.

p62 is regulated transcriptionally and post-translationally^{358, 359} by a number of factors such as NFE2L2, SPDEF/PDEF, MAPK8/9/10 (mitogen-activated protein kinase 8/9/10), NFkB and XBP-1⁹². Elevated p62 expression without changes in SQSTM1 mRNA levels is generally used as an indicator of autophagy impairment³⁵³. Results show that BafA1 did not change SQSTM1

mRNA levels. However, C18 data revealed increased p62 mRNA levels upon C18 treatment which indicates that inhibition of p62 protein degradation occurs despite transcriptional upregulation. A possible explanation would be that transcription is induced by TFEB nuclear translocation.

Another interesting observation when protein analysis was carried out was significant p62 accumulation upon starvation. In qPCR analysis, an increased mRNA transcription in C18 starved cells was observed, which was further enhanced in C18-treated starved cells. During starvation, the protein level of p62 does not always inversely correlate with autophagy activity. Under short-term starvation (up to 2 h), autophagy is induced, which degrades p62 protein. Under these circumstances, there is a limited supply of intracellular and extracellular amino acids, as well as reduced mRNA levels. However, after prolonged starvation (more than 4 h), sufficient amounts of intracellular amino acids, produced by autophagy, are available and the transcription is upregulated. Thus, p62 protein level is restored to basal levels by de novo protein synthesis⁹². This is most likely the reason for high levels of p62 mRNA detected after 4 h of starvation. Additionally, preliminary data from immunoprecipitation assay (data not shown) have been obtained, showing that C18 increases endogenous p62 colocalization with ubiquitinated proteins. Since manipulation of cellular p62 level changes the quantity and location pattern of ubiquitinated proteins³⁶⁰, an explanation for increased p62 transcription upon C18 treatment could be that C18 simultaneously impairs the ubiquitin-proteasome system (UPS) and autophagy. Furthermore, it is known that there is a positive feedback loop between p62 and mTORC1. mTORC1 activation increases p62 levels, further promoting mTORC1 activity³⁶⁰. mTORC1 activation has been detected in this study, which could explain increased p62 transcription despite a blocked degradation. The kinetics of SQSTM1 restoration are similar between treatment with C18 and long-term starvation, which suggest a complex role of C18 in autophagy that has to be investigated further in various conditions and cell lines.

5.5 Implication of ER stress and calcium signalling

For further evidence of C18-regulated autophagy, an ultrastructural investigation of C18-treated U2OS cells in nutrient-rich versus starvation

condition was performed using transmission electron microscopy. As compared with the control cells, few autophagosomes were observed in C18-treated cells, with mild ER stress. On the contrary, the starved cells treated with C18 caused an increase in the number of autophagosomes/autolysosomes compared to starvation alone. Moreover, results indicate a drastic ER stress, leading to an accumulation of massively expanded ER, as well as swelling and expansion of the nuclear envelop (nuclear ER). BafA1 addition to C18-treated cells enhances the ER stress, suggesting a synthetic effect due to manipulation of connected pathways such as calcium-dependent pathways³⁶¹. Numerous of the observed autophagosomes/autolysosomes in C18-treated cells contain ER-fragments. Thus, the autophagy inhibition observed after C18 treatment may very likely be the consequence of the dramatic ER defect induced. Current transmission electron microscopy (TEM) data is based on morphological observations and quantitative analysis remains to be performed.

Inhibition of autophagy results in the accumulation of large quantities of protein in the cytoplasm, which cannot be degraded and will inevitably result in further cytotoxic effects, including ER stress^{362, 363}. Given this information and the TEM observations, it was determined whether C18-treated cells are undergoing ER stress by measuring ER stress markers, Grp78/BiP and CHOP/GADD153. The glucose-regulated protein-78, known as Grp78 and/or BiP, is a master regulator of ER stress and promotes cell survival. C/EBP homologous protein (CHOP), also known as GADD153, mediates ER stress by activating apoptosis³⁶⁴. Under severe ER stress, where the steady state of ER cannot be restored, CHOP will activate apoptosis signalling pathways²⁶⁰. Both BiP and CHOP are involved in ER-stress mediated autophagy, which if unresolved can activate the unfolded protein response and, hence, apoptosis^{269, 363, 364, 365}. Simultaneous examination of BiP with autophagy markers, LC3-II and p62, showed increased autophagy inhibition with ER stress occurrence. CHOP levels also increased with increasing incubation time but were not as enhanced as with BiP. As a result, regardless of the C18 concentration, the accumulation of BiP can be induced without significant activation of CHOP. Neither nutrient deprivation nor BafA1 treatment had an effect on CHOP expression, as shown previously⁷⁶. Collectively, this suggests that C18 increased ER stress in a time-dependent manner but higher

concentrations and/or longer incubation times are required to induce a significant increase in CHOP expression.

Currently, ER stress inducers are an attractive therapeutic strategy for killing cancer cells. Autophagy inhibitor CQ which is used in clinical trials has shown to induce apoptosis in primary effusion lymphoma both *in vitro* and *in vivo* by triggering ER stress and increasing CHOP expression³⁶⁶. Jia et al.³⁶⁷ support this theory and believe that the ER stress is what causes apoptosis. Although caspase activation, a hallmark of apoptosis, has been indicated upon C18 treatment apoptosis induction seems to be lower than what is observed with CQ. Therefore, it was considered that autophagy inhibition was not dependent on apoptosis but C18 may induce CHOP and initiate apoptosis depending on the time and dose used. Alternatively, C18 can be used in combination with therapies to induce a stronger apoptotic effect in human cancers.

It is a known fact that calcium (Ca^{2+}) is one of the key regulators of cell survival and its perturbations can induce ER stress²⁹². Increased levels of cytosolic Ca^{2+} lead to the activation of the ER stress response and impaired autophagy^{267, 269}. For this reason, measuring changes in the intracellular calcium signalling serves as a confirmation for presence of ER stress. Direct measurement of intracellular calcium following treatment with various concentrations of C18 revealed an increase in calcium release from cells. Next, the presence of any disruption in intracellular calcium upon C18 treatment was investigated, first by inducing calcium release with Tg³⁶⁸. Five min exposure to Tg prior to C18 addition blocked the sharp rise in cytosolic calcium however a delayed broader and flatter peaks were observed compared with those obtained with Tg. Since Tg depletes ER calcium stores, C18 possibly induces calcium buffering from other intracellular stores, such as mitochondria, or an influx from the plasma membrane³⁶⁹.

Thapsigargin inhibits SERCA (the sarco/endoplasmic reticulum Ca^{2+} ATPase) and exerts a major effect on ER and cellular calcium signalling⁷⁶. Through the inhibition of SERCA pump, Tg acts as an anti-cancer agent³⁷⁰. There are many similarities between C18 and Tg. Ganley group⁷⁶ report that Tg blocks both basal and starvation-induced autophagy by inhibiting autophagosome fusion

with lysosomes, similar to C18. In a previous part of this study was shown that caspase-3 and caspase-7, two drivers of apoptotic cell death^{329, 330, 331}, were activated. Hu et al.³⁷¹ report that apoptotic cell death via upregulation of CHOP occurs via UPR when ER protein homeostasis is not restored over long period of times. Therefore, C18 may be initiating cell death via caspase-3/7 activation but does not cause chronic ER stress necessary to trigger CHOP activation. Moreover, studies suggest cell dependent accumulation of BiP and CHOP upon Tg treatment^{372, 373}. For this reason, a panel of cell lines must be tested to check accumulation of CHOP. Most of the commonly used chemotherapy drugs, such as paclitaxel, doxorubicin and 5-fluorouracil, are ineffective against cancers that have a low rate of proliferation. Although Tg overcomes this issue, it is highly cytotoxic and lacks selectivity^{374, 375, 370}, therefore is not suitable as a drug candidate. Consequently, there is a high demand for safe and selective chemotherapeutics. C18 could fill this gap, providing potential for the development of a new target treatment strategy and can be used as a drug or combination therapy for cancer.

Furthermore, examination of intracellular Ca^{2+} levels indicated that C18 increased Ca^{2+} levels, which could be originating from ER. Drugs that can modify Ca^{2+} signalling are commonly used to treat various types of cancers, including sarcomas, carcinomas, lymphomas, and germ cell tumours and are considered a new class of chemotherapeutics. Various research programs in fact propose that it is useful to induce ER stress to obtain an anti-cancer effect^{376, 377, 378, 379}. Dual combination of autophagy inhibitors with calcium-mobilizing compounds also provide a novel therapeutic strategy in oncology field³⁸⁰. C18 could mobilize intracellular calcium stores. Thus, through its dual effect on autophagy and calcium mobilization, C18 could be a promising drug candidate for either single-agent or combination chemotherapy. Additionally, one of the hypothesis was that C18 interferes with mitochondrial Ca^{2+} release. Studies suggest that anti-cancer properties of molecules that increase mitochondrial Ca^{2+} release, such as resveratrol³⁸¹ and ABT-737³⁸². Taken together, these data strengthen the image of C18 as a potent compound for the oncology research.

5.6 Concluding remarks

The described findings show the ability of C18 to inhibit autophagic flux via inhibition of autophagosome-lysosome fusion in an mTOR-dependent manner. Further experiments support the hypothesis that the ER stress is implicated in autophagy inhibition by C18. This was confirmed by protein levels of ER stress markers that were affected, as well as fluctuations in intracellular calcium. C18 could also have antiproliferative activity against cancer by inducing apoptosis. Therefore, it is proposed that C18 is a multi-target compound that can be effective in cancer therapy.

Nevertheless, more comprehensive investigation of the signalling pathways modulated by C18 might provide new insights into its mechanism of action, allowing to selectively target specific cancers. Additional studies will elucidate the exact link between C18-induced inhibition of autophagy, ER stress and the onset of apoptosis. The role of BECN1, as well as other ATG genes involved in human cancer also need to be studied. Continuing research should focus on preclinical and clinical trials because a big challenge in autophagy field is findings drugs that can potently and selectively inhibit various stages of the process without causing cytotoxicity.

6 SUMMARY

Macroautophagy, herein referred to as autophagy, is an evolutionarily conserved homeostatic process that normally occurs inside eukaryotic cells which involves degradation of cytoplasmic substances via lysosomes. It can be induced by various conditions such as starvation and drug exposure, as well as be inhibited by numerous compounds. Under normal conditions, the double-membrane autophagosomes engulf the cytosolic substrates and deliver them to lysosomes for digestion. These substrates include unnecessary or dysfunctional cell components, such as faulty macromolecules, organelles and even invading pathogens. Autophagosomes are formed through the co-operative work of various autophagy-related (ATG) proteins organized into complexes. Upon closure of the autophagosomes, they fuse with the acidic lysosomes, resulting in formation of autolysosomes and the delivery of lysosomal hydrolases to degrade the engulfed contents. The fusion of the autophagosome with lysosome is carried out by specific SNARE proteins, small GTPases and their effectors including tethers, adaptors and motor proteins. Autophagy is impaired in many human diseases including cancer, neurodegenerative diseases, aging

and inflammation. Therefore, manipulation of autophagy pathway holds a great promise for new therapeutic applications.

In the case of cancer, autophagy has been shown to play a dual role, both as tumor suppressor and tumor promoter. On one hand, autophagy facilitates the clearance of damaged macromolecules and organelles, preventing excessive reactive oxygen species production and DNA damage, and thus preventing normal cells to become cancerous. However, once the cells become malignant, autophagy plays a pro-survival role and protects cancer cells from metabolic and therapeutic stresses thereby promoting their growth. Extensive research data shows that autophagy is upregulated in different cancer types and chemical inhibition can limit cancer cell survival and progression. Therefore, inhibiting autophagy is currently being developed as a new strategy for cancer treatment. The most widely used autophagy inhibitor in clinical trials include chloroquine (CQ) and its derivative hydroxychloroquine (HCQ), either alone or in combination with other cancer drugs or radiation. The results indicate some improvements in cancer patients but high micromolar concentrations of CQ and HCQ are required to inhibit autophagy which cause toxic effects and thereby limiting their clinical use. Consequently, the search for more potent autophagy inhibitors continues.

For this purpose, research on the topic of high-throughput and high-content screening for discovery of autophagy modulators is continuing to grow. There are a number of established techniques to identify autophagy modulators based on the activity of autophagy reporters or clearance of cargo. Some of these assays are compatible with high-throughput screening to identify pharmacological modulators of autophagy, which can be followed up by secondary assays that have lower throughput aiming at the independent validation of the modulatory effect. In the past years, significant number of drug candidates have been initiated from such screens and clinical trials are ongoing to prove efficacy and safety in humans. Our aim was to use a combination of high-throughput image-based screen and additional secondary assays to identify small-molecule compounds that modulate autophagy selectively without disruption of other necessary cellular components.

First, we set out to identify autophagy modulating small-molecule compounds from two chemical libraries including an FDA-approved drug library and the ChemBioNet library using a high-content image screen. The first part of this study involved screening a total of 4153 compounds in TagRFP-mWassabi-LC3B tagged HEK293T cells. Once hit confirmation and validation were performed, the selected hits were evaluated in western blot experiments to assess endogenous levels of autophagy protein LC3 and the substrate p62. Phenotypic screening led to the identification of 12 compounds, from which 4 were confirmed in western blot. Compound 18 (C18), from ChemBioNet collection, was identified as the compound that potently increases the number of TagRFP⁺mWassabi⁺ puncta, referred to as yellow puncta, reflecting increased autophagosomes in cells. Further characterization on C18 revealed that it significantly increases endogenous levels of LC3 and a concomitant increase in p62 which confirms that autophagy is impaired.

Because of the promising results, more comprehensive characterization of the C18 followed. The aim of this part was to assess C18 in orthogonal assays by testing various autophagy markers to unravel mechanism of action. We examined the activity of C18 in osteosarcoma U2OS cells. The previously established assay was optimised accordingly and C18 was confirmed in mCherry⁺EGFP⁺LC3B tagged U2OS cells to increase the number of mCherry⁺EGFP⁺ (yellow puncta) in a dose-dependent manner. Furthermore, the most active concentration (approximately the IC₅₀ value) was selected and the endogenous levels of LC3 and p62 were investigated. Our data supports previous findings and confirmed that C18 significantly increases the number of autophagosomes in the cell and prevents p62 degradation. These observations strengthened the image of C18 as an autophagy inhibitor and encourages additional investigations.

During the next part of the experiments, we assessed cytotoxicity of C18 at various time points in U2OS cells and HEK293 cells respectively. We could demonstrate that C18 is non-toxic at the concentrations used in our autophagy assays in both cell lines. In addition, the implication of caspase activation and apoptosis were evaluated. Data suggests that prolonged treatment with C18 pushes cells closer to their cell death threshold through accumulation of

caspase-3 and caspase-7. It should be noted that autophagy and apoptosis are closely interconnected, thus this outcome was expected. We can induce autophagy inhibition with C18 with short incubation times, without significantly interfering with apoptosis, but might be able to also selectively trigger apoptosis to inhibit cancer cell growth and proliferation.

Once C18 was confirmed as an autophagy inhibitor and the necessary cytotoxicity data were obtained, we moved forward to the hit expansion step and extracted structure-activity relationship from our high-content screening (HCS) campaign with the aim to discover C18 analogs with similar or higher potency. We were successfully able to identify structurally-related analogs with medium potency that inhibit autophagy. Our SAR analysis proposes a series of functional analogs of C18, which can then be used to find the target. Furthermore, we investigated if C18 inhibits autophagic flux by interfering with autophagosome-lysosome fusion and the following lysosomal degradation mechanisms, as compound effect in amino acid starvation conditions. We report that C18 reduced autophagosome-lysosome fusion and decreased the number of acidic lysosomes. The effect was enhanced by starvation. Our experiments also demonstrated that amino acid starvation increased autophagic flux and C18 was able to inhibit starvation-induced autophagic flux. Moreover, literature research reveals that autophagic flux inhibition should be studied in presence or absence of a lysosomal inhibitor, such as bafilomycin A1 (BafA1) or CQ. We found that combined treatment with C18 and BafA1 did not increase LC3 lipidation more than C18 alone, indicative of the impaired autophagic flux. Taken together, these data clearly show that C18 is a late stage lysosomal inhibitor.

The mechanistic target of rapamycin complex 1 (mTORC1) is responsible for preserving cellular homeostasis and is a major negative regulator of autophagy. We determined whether the mTORC1 pathway was inhibited in C18-treated osteosarcoma cancer cells. First, we examined the phosphorylation status of 4E-BP1, one of the best characterized targets of mTORC1. mTORC1 activation causes phosphorylation of 4E-BP1. Since autophagy inhibitors prevent mTORC1 inhibition, we anticipated that C18 will cause a marked increase in phosphorylation of 4E-BP1 substrate. C18 markedly increased phosphorylation

of 4E-BP1, thereby blocking autophagy induction. On the contrary, induction of autophagy by starving C18-treated cells was able to rescue autophagy to some extent but this effect was not significant. Taken together, C18 was able to block autophagy in an mTORC1-dependent manner. Other experiments evaluating p62/SQSTM1 mRNA transcript were conducted because our observations suggest that C18 has a major effect on this substrate. C18 prevents p62 degradation, marked by accumulation of protein levels. However, mRNA analysis indicated an upregulation of SQSTM1. Based on our findings, we assume that prolonged stress induced by C18 restores SQSTM1 transcription. The role of p62/SQSTM1 is complex in C18-mediated autophagic inhibition which needs further investigations.

Clear evidence of C18 mechanism came from transmission electron microscopy experiments. TEM experiments were conducted in collaboration with Prof. Dr. Fulvio Reggiori and Dr. Muriel Mari (Department of Biomedical Sciences of Cells and Systems, University of Groningen, Netherlands) to directly measure cellular changes upon C18 treatment. Data showed that C18 induces endoplasmic reticulum (ER) stress and ER fragmentation which may potentially be the cause of autophagy inhibition. Given the significance of ER stress in the cell, we exploited this effect by measuring endogenous levels of ER stress markers, BiP and CHOP, which confirmed presence of ER stress. Furthermore, since ER is the biggest Ca^{2+} storage, we performed a direct measurement of intracellular calcium (Ca^{2+}). As expected, results indicated an increase in cytosolic calcium concentration. To check whether this effect is specific to ER, we used thapsigargin (Tg) to deplete ER Ca^{2+} stores, followed by C18 treatment. Live cell analysis indicated that Tg pre-treatment failed to inhibit C18-mediated increase in intracellular Ca^{2+} but, interestingly, it caused a delay in the onset of the effect. We assume that C18 induces calcium buffering from other important intracellular Ca^{2+} stores, such as mitochondria. It has been previously observed that ER stressors inhibit autophagy which encourages the fact that C18 mediates autophagy inhibition through its effect on the ER.

In summary, we achieved our aim to identify a novel autophagy modulator, providing promising data that C18 acts as a late-stage lysosomal inhibitor with potential therapeutic benefits for cancer patients. We concluded that mTORC1

pathway is involved in this effect, as well as ER stress. Autophagy regulates Ca^{2+} signalling by developmentally maintaining the homeostasis of the ER. We see that C18 interferes with Ca^{2+} stores in the cell, which we assume is the reason for ER stress and fragmentation. ER stress in turn contributes to autophagy inhibition. Nevertheless, more mechanistic studies will further elucidate the autophagy inhibitory mechanism and provide valuable information for continuing autophagy research.

7 ZUSAMMENFASSUNG

Die Makroautophagie, im Folgenden als Autophagie bezeichnet, ist ein evolutionär konservierter homöostatischer Prozess, der normalerweise in eukaryontischen Zellen abläuft und den Abbau von zytoplasmatischen Substanzen über Lysosomen beinhaltet. Er kann durch verschiedene Bedingungen wie Hunger und Pharmazeutika ausgelöst und durch zahlreiche Substanzen gehemmt werden. Unter normalen Bedingungen umschließen die aus Doppelmembranen gebildeten Autophagosomen die zytosolischen Substrate und fusionieren zu deren Verdauung mit Lysosomen. Zu diesen Substraten gehören überflüssige oder funktionsuntüchtige Zellbestandteile, wie fehlerhafte Makromoleküle, Organellen und sogar eingedrungene Krankheitserreger. Autophagosomen werden durch das Zusammenwirken verschiedener Autophagie-Proteine (ATG) gebildet, die in Komplexen organisiert sind. Nach dem Schließen der Autophagosomen verschmelzen diese mit den sauren Lysosomen, was zur Bildung von Autolysosomen und zur Freisetzung von lysosomalen Hydrolasen zum Abbau des eingeschlossenen Inhalts führt. Die Verschmelzung des Autophagosoms mit dem Lysosom wird

durch spezifische SNARE-Proteine, kleine GTPasen und ihre Effektoren, einschließlich Bindeproteinen, Adaptoren und Motorproteinen, durchgeführt. Die Autophagie ist bei vielen menschlichen Krankheiten wie Krebs, neurodegenerativen Erkrankungen, Alterung und Entzündungen beeinträchtigt. Daher verspricht die Beeinflussung von Autophagieprozessen neue therapeutische Anwendungen.

Im Falle von Krebs hat sich gezeigt, dass die Autophagie eine doppelte Rolle spielt, sowohl als Tumorsuppressor als auch als Tumorpromotor. Einerseits erleichtert die Autophagie die Beseitigung geschädigter Makromoleküle und Organellen, indem sie eine übermäßige Produktion reaktiver Sauerstoffspezies und DNA-Schäden verhindert und somit verhindert, dass normale Zellen zu Krebszellen werden. Sobald die Zellen jedoch bösartig werden, dient die Autophagie als Überlebensfunktion und schützt die Krebszellen vor metabolischen und therapeutischen Belastungen, wodurch ihr Wachstum gefördert wird. Umfangreiche Forschungsdaten zeigen, dass die Autophagie bei verschiedenen Krebsarten hochreguliert ist und eine chemische Hemmung das Überleben und Fortschreiten von Krebszellen einschränken kann. Daher wird die Hemmung der Autophagie derzeit als neue Strategie für die Krebsbehandlung entwickelt. Zu den in klinischen Studien am häufigsten eingesetzten Autophagie-Inhibitoren gehören Chloroquin (CQ) und dessen Derivat Hydroxychloroquin (HCQ), entweder allein oder in Kombination mit anderen Krebsmedikamenten oder Bestrahlung. Die Ergebnisse deuten auf gewisse Verbesserungen bei Krebspatienten hin, doch sind hohe mikromolare Konzentrationen von CQ und HCQ erforderlich, um die Autophagie zu hemmen, was toxische Wirkungen hat und somit deren klinische Anwendung einschränkt. Daher wird die Suche nach wirksameren Autophagie-Inhibitoren fortgesetzt.

Zu diesem Zweck wird die Forschung zum Thema Hochdurchsatz- und High-Content-Screening zur Entdeckung von Autophagie-Modulatoren weiter ausgebaut. Es gibt eine Reihe etablierter Techniken zur Identifizierung von Autophagie-Modulatoren auf der Grundlage der Aktivität von Autophagie-Reportern oder der Beseitigung von Autophagie-Substraten. Einige dieser Assays sind mit einem Hochdurchsatz-Screening zur Identifizierung pharmakologischer Modulatoren der Autophagie kompatibel, an das sich

sekundäre Assays mit geringerem Durchsatz anschließen können, die auf eine unabhängige Validierung der modulatorischen Wirkung abzielen. In den letzten Jahren wurde eine beträchtliche Anzahl von Wirkstoffkandidaten auf der Grundlage solcher Screenings entwickelt, und es laufen klinische Studien zum Nachweis der Wirksamkeit und Sicherheit beim Menschen. Unser Ziel war es, mit einer Kombination aus bildbasierten Hochdurchsatz-Screens und zusätzlichen sekundären Assays niedermolekulare Wirkstoffe zu identifizieren, die die Autophagie selektiv modulieren, ohne andere wichtige zelluläre Mechanismen zu beeinträchtigen.

Zunächst haben wir uns vorgenommen, die Autophagie modulierende niedermolekulare Verbindungen aus zwei chemischen Bibliotheken zu identifizieren, darunter eine von der FDA zugelassene Arzneimittelbibliothek und die ChemBioNet-Bibliothek, und zwar mithilfe eines bildbasierten High-Content-Screens. Der erste Teil dieser Studie umfasste das Screening von insgesamt 4153 Verbindungen in TagRFP-mWasabi-LC3B-exprimierenden HEK293T-Zellen. Nach der Hit-Bestätigung und -Validierung wurden die ausgewählten Hits in Western-Blot-Experimenten getestet, um die endogenen Spiegel des Autophagie-spezifischen Proteins LC3 und p62 zu bestimmen. Das phänotypische Screening führte zur Identifizierung von 12 Verbindungen, von denen 4 in ihrer Wirkung mittels Western-Blot bestätigt werden konnten. Verbindung 18 (C18) aus der ChemBioNet-Sammlung wurde als diejenige Verbindung identifiziert, die die Anzahl der intrazellulären TagRFP+mWasabi-Punktstrukturen (gelb) stark erhöht, was auf eine Zunahme der Autophagosomen in den Zellen hinweist. Die weitere Charakterisierung von C18 ergab, dass es die endogenen LC3-Spiegel signifikant erhöht und gleichzeitig zu einem Anstieg von p62 führt, was bestätigt, dass die Autophagie beeinflusst ist.

Aufgrund der vielversprechenden Ergebnisse folgte eine umfassendere Charakterisierung von C18. Ziel dieses Teils war es, C18 in orthogonalen Assays zu bewerten, indem verschiedene Autophagie-Marker getestet wurden, um den Wirkmechanismus zu entschlüsseln. Wir untersuchten die Aktivität von C18 in U2OS Osteosarkomzellen. Der zuvor etablierte Assay wurde entsprechend optimiert, und es wurde bestätigt, dass C18 in

mCherry+EGFP+LC3B-markierten U2OS-Zellen die Anzahl der mCherry+EGFP+ (gelbe Punktstrukturen) dosisabhängig erhöht. Außerdem wurde die aktivste Konzentration (ungefähr der IC_{50} -Wert) ausgewählt und die endogenen LC3- und p62-Konzentrationen untersucht. Unsere Daten unterstützen die vorherigen Erkenntnisse und bestätigen, dass C18 die Anzahl der Autophagosomen in der Zelle deutlich erhöht und den Abbau von p62 verhindert. Diese Beobachtungen stärkten das Bild von C18 als Autophagie-Inhibitor und ermutigen zu weiteren Untersuchungen.

Im nächsten Teil der Experimente haben wir die Zytotoxizität von C18 zu verschiedenen Zeitpunkten in U2OS-Zellen bzw. HEK293-Zellen untersucht. Wir konnten zeigen, dass C18 bei den in unseren Autophagie-Assays verwendeten Konzentrationen in beiden Zelllinien nicht toxisch ist. Darüber hinaus wurden die Auswirkungen von Caspase-Aktivierung und Apoptose untersucht. Die Daten deuten darauf hin, dass eine längere Behandlung mit C18 die Zellen durch die Akkumulation von Caspase-3 und Caspase-7 näher an die Zelltodschwelle bringt. Es sei darauf hingewiesen, dass Autophagie und Apoptose eng miteinander verknüpft sind, so dass dieses Ergebnis zu erwarten war. Mit C18 können wir die Autophagie mit kurzen Inkubationszeiten hemmen, ohne die Apoptose wesentlich zu beeinträchtigen, aber auch selektiv Apoptose auslösen, um das Wachstum und die Vermehrung von Krebszellen zu hemmen.

Nachdem C18 als Autophagie-Inhibitor bestätigt wurde und die erforderlichen Zytotoxizitätsdaten vorlagen, gingen wir zum Schritt der Hit-Expansion über und leiteten Struktur-Aktivitäts-Beziehungen aus unserem High-Content-Screening-Datensatz ab mit dem Ziel, C18-Analoga mit ähnlicher oder höherer Wirksamkeit zu entdecken. Es ist uns gelungen, strukturell verwandte Analoga mit mittlerer Wirksamkeit zu identifizieren, die die Autophagie hemmen. Unsere SAR-Analyse schlägt eine Reihe von funktionellen Analoga von C18 vor, die verwendet werden können, um Zielmolekül zu finden. Darüber hinaus haben wir untersucht, ob C18 den autophagischen Flux hemmt, indem es die Autophagosom-Lysosom-Fusion und die nachfolgenden lysosomalen Abbaumechanismen stört, wie es bei Aminosäuremangel der Fall ist. Wir berichten, dass C18 die Autophagosomen-Lysosomen-Fusion reduziert und die Anzahl der sauren Lysosomen verringert. Dieser Effekt wurde durch das

Hungern der Zellen noch verstärkt. Unsere Experimente haben auch gezeigt, dass Aminosäuredepletion durch Hunger den autophagischen Fluss erhöht und C18 in der Lage war, den durch Hunger induzierten autophagischen Flux zu hemmen. Darüber hinaus zeigt die Literaturrecherche, dass die Hemmung des autophagischen Fluxes in Gegenwart oder Abwesenheit eines lysosomalen Inhibitors, wie Bafilomycin A1 (BafA1) oder CQ, untersucht werden sollte. Wir fanden heraus, dass die kombinierte Behandlung mit C18 und BafA1 die LC3-Lipidierung nicht stärker erhöhte als C18 allein, was auf den beeinträchtigten autophagischen Flux hindeutet. Zusammengenommen zeigen diese Daten eindeutig, dass C18 ein lysosomaler Inhibitor der späten Autophagiephasen ist.

Der Mechanistic Target of Rapamycin Complex 1 (mTORC1) ist für die Aufrechterhaltung der zellulären Homöostase verantwortlich und ist ein wichtiger negativer Regulator der Autophagie. Wir untersuchten, ob der mTORC1-Signalweg in C18-behandelten U2OS Osteosarkomzellen gehemmt wurde. Zunächst untersuchten wir den Phosphorylierungsstatus von 4E-BP1, einem der am besten charakterisierten Ziele von mTORC1. Die Aktivierung von mTORC1 führt zur Phosphorylierung von 4E-BP1. Da Autophagie-Inhibitoren die mTORC1-Hemmung verhindern, erwarteten wir, dass C18 einen deutlichen Anstieg der Phosphorylierung des 4E-BP1-Substrats verursachen würde. C18 erhöhte die Phosphorylierung von 4E-BP1 deutlich und blockierte damit die Autophagie-Induktion. Im Gegensatz dazu konnte die Induktion der Autophagie durch Aushungern der mit C18 behandelten Zellen die Autophagie bis zu einem gewissen Grad retten, aber dieser Effekt war nicht signifikant. Insgesamt war C18 in der Lage, die Autophagie auf eine mTORC1-abhängige Weise zu blockieren. Da unsere Beobachtungen darauf hindeuten, dass C18 eine wichtige Wirkung auf dieses Substrat hat, wurden weitere Experimente zur Bewertung des p62/SQSTM1-mRNA-Transkripts durchgeführt. C18 verhindert den Abbau von p62, was sich in einer Anhäufung der Proteinkonzentrationen zeigt. Die mRNA-Analyse zeigte jedoch eine Hochregulierung von SQSTM1. Aufgrund unserer Ergebnisse gehen wir davon aus, dass anhaltender Stress, der durch C18 induziert wird, die SQSTM1-Transkription wiederherstellt. Die Rolle von p62/SQSTM1 bei der C18-vermittelten Autophagiehemmung ist komplex und muss weiter untersucht werden.

Wichtige Hinweise zum Wirkmechanismus von C18 lieferten transmissionselektronenmikroskopische (TEM) Experimente. In Zusammenarbeit mit Prof. Dr. Fulvio Reggiori und Dr. Muriel Mari (Department of Biomedical Sciences of Cells and Systems, Universität Groningen, Niederlande) wurden TEM-Experimente durchgeführt, um die zellulären Veränderungen nach C18-Behandlung direkt zu messen. Die Daten zeigten, dass C18 Stress im endoplasmatischen Retikulum (ER) und ER-Fragmentierung auslöst, was möglicherweise die Ursache für die Hemmung der Autophagie ist. Angesichts der Bedeutung von ER-Stress in der Zelle nutzten wir diesen Effekt durch die Messung der endogenen Spiegel der ER-Stress-Marker BiP und CHOP, die das Vorhandensein von ER-Stress bestätigten. Da das ER der größte Ca^{2+} -Speicher ist, führten wir außerdem eine direkte Messung des intrazellulären Kalziums (Ca^{2+}) durch. Wie erwartet, zeigten die Ergebnisse einen Anstieg der zytosolischen Kalziumkonzentration. Um zu prüfen, ob dieser Effekt spezifisch für das ER ist, verwendeten wir Thapsigargin (Tg), um die Ca^{2+} -Speicher des ER zu leeren, und behandelten anschließend die Zellen mit C18. Die Analyse der lebenden Zellen zeigte, dass die Vorbehandlung mit Tg den C18-vermittelten Anstieg der intrazellulären Ca^{2+} -Konzentration nicht hemmte, aber interessanterweise eine Verzögerung des Einsetzens des Effekts bewirkte. Wir gehen davon aus, dass C18 die Kalziumausschüttung aus anderen wichtigen intrazellulären Ca^{2+} -Speichern wie den Mitochondrien induziert. Es wurde bereits beobachtet, dass ER-Stressoren die Autophagie hemmen, was die Tatsache unterstützt, dass C18 die Autophagie durch seine Wirkung auf das ER hemmt.

Zusammenfassend lässt sich sagen, dass wir unser Ziel, einen neuartigen Autophagie-Modulator zu identifizieren, erreicht haben und vielversprechende Daten dafür liefern, dass C18 als lysosomaler Inhibitor in der Spätphase der Autophagie wirkt. Dies hat potenziell einen therapeutischen Nutzen für Krebspatienten. Wir kamen zu dem Schluss, dass der mTORC1-Stoffwechselweg an dieser Wirkung beteiligt ist, ebenso wie ER-Stress. Autophagie reguliert Ca^{2+} -Signalwege, indem sie die Homöostase des ER aufrechterhält. Wir sehen, dass C18 in die Ca^{2+} -Speicher der Zelle eingreift, was vermutlich der Grund für ER-Stress und -Fragmentierung ist. Der ER-

Stress wiederum trägt zur Hemmung der Autophagie bei. Dennoch werden weitere mechanistische Studien den Mechanismus von C18 im Kontext der Hemmung der Autophagie weiter aufklären und wertvolle Informationen für die weitere translationale Autophagieforschung liefern.

8 REFERENCES

1. Klionsky DJ, Baehrecke EH, Brumell JH, et al. A comprehensive glossary of autophagy-related molecules and processes (2nd edition). *Autophagy*. 2011;7(11):1273-1294. doi:10.4161/auto.7.11.17661
2. de Duve C, Wattiaux R. Functions of Lysosomes. *Annu Rev Physiol*. 1966;28(1):435-492. doi:10.1146/annurev.ph.28.030166.002251
3. Shintani T, Klionsky DJ. Autophagy in Health and Disease: A Double-Edged Sword. *Science*. 2004;306(5698):990-995. doi:10.1126/science.1099993
4. Abada A, Elazar Z. Getting ready for building: signaling and autophagosome biogenesis. *EMBO Rep*. 2014;15(8):839-852. doi:10.15252/embr.201439076

5. Lamb CA, Yoshimori T, Tooze SA. The autophagosome: origins unknown, biogenesis complex. *Nat Rev Mol Cell Biol.* 2013;14(12):759-774. doi:10.1038/nrm3696
6. Mizushima N, Komatsu M. Autophagy: Renovation of Cells and Tissues. *Cell.* 2011;147(4):728-741. doi:10.1016/j.cell.2011.10.026
7. Li W wen, Li J, Bao J ku. Microautophagy: lesser-known self-eating. *Cell Mol Life Sci.* 2012;69(7):1125-1136. doi:10.1007/s00018-011-0865-5
8. Neff NT, Bourret L, Miao P, Dice JF. Degradation of proteins microinjected into IMR-90 human diploid fibroblasts. *J Cell Biol.* 1981;91(1):184-194. doi:10.1083/jcb.91.1.184
9. Kaushik S, Cuervo AM. The coming of age of chaperone-mediated autophagy. *Nat Rev Mol Cell Biol.* 2018;19(6):365-381. doi:10.1038/s41580-018-0001-6
10. Codogno P, Mehrpour M, Proikas-Cezanne T. Canonical and non-canonical autophagy: variations on a common theme of self-eating? *Nat Rev Mol Cell Biol.* 2012;13(1):7-12. doi:10.1038/nrm3249
11. Feng Y, He D, Yao Z, Klionsky DJ. The machinery of macroautophagy. *Cell Res.* 2014;24(1):24-41. doi:10.1038/cr.2013.168
12. Deffieu M, Bhatia-Kissová I, Salin B, Galinier A, Manon S, Camougrand N. Glutathione participates in the regulation of mitophagy in yeast. *J Biol Chem.* 2009;284(22):14828-14837. doi:10.1074/jbc.M109.005181
13. Dunn WA, Cregg JM, Kiel JAKW, et al. Pexophagy: the selective autophagy of peroxisomes. *Autophagy.* 2005;1(2):75-83. doi:10.4161/auto.1.2.1737
14. Klionsky DJ, Codogno P. The Mechanism and Physiological Function of Macroautophagy. *J Innate Immun.* 2013;5(5):427-433. doi:10.1159/000351979
15. Kocak M, Ezazi Erdi S, Jorba G, et al. Targeting autophagy in disease: established and new strategies. *Autophagy.* Published online July 9, 2021:1-23. doi:10.1080/15548627.2021.1936359

16. Hara K, Maruki Y, Long X, et al. Raptor, a binding partner of target of rapamycin (TOR), mediates TOR action. *Cell*. 2002;110(2):177-189. doi:10.1016/s0092-8674(02)00833-4
17. Kim DH, Sarbassov DD, Ali SM, et al. mTOR interacts with raptor to form a nutrient-sensitive complex that signals to the cell growth machinery. *Cell*. 2002;110(2):163-175. doi:10.1016/s0092-8674(02)00808-5
18. Loewith R, Jacinto E, Wullschleger S, et al. Two TOR complexes, only one of which is rapamycin sensitive, have distinct roles in cell growth control. *Mol Cell*. 2002;10(3):457-468. doi:10.1016/s1097-2765(02)00636-6
19. Sarbassov DD, Ali SM, Kim DH, et al. Rictor, a novel binding partner of mTOR, defines a rapamycin-insensitive and raptor-independent pathway that regulates the cytoskeleton. *Curr Biol CB*. 2004;14(14):1296-1302. doi:10.1016/j.cub.2004.06.054
20. Rabanal-Ruiz Y, Otten EG, Korolchuk VI. mTORC1 as the main gateway to autophagy. *Essays Biochem*. 2017;61(6):565-584. doi:10.1042/EBC20170027
21. Papandreou I, Lim AL, Laderoute K, Denko NC. Hypoxia signals autophagy in tumor cells via AMPK activity, independent of HIF-1, BNIP3, and BNIP3L. *Cell Death Differ*. 2008;15(10):1572-1581. doi:10.1038/cdd.2008.84
22. Rouschop KMA, van den Beucken T, Dubois L, et al. The unfolded protein response protects human tumor cells during hypoxia through regulation of the autophagy genes MAP1LC3B and ATG5. *J Clin Invest*. 2010;120(1):127-141. doi:10.1172/JCI40027
23. Lamming DW, Ye L, Katajisto P, et al. Rapamycin-Induced Insulin Resistance Is Mediated by mTORC2 Loss and Uncoupled from Longevity. *Science*. Published online March 30, 2012. doi:10.1126/science.1215135
24. Schreiber KH, Ortiz D, Academia EC, Anies AC, Liao CY, Kennedy BK. Rapamycin-mediated mTORC2 inhibition is determined by the relative expression of FK506-binding proteins. *Aging Cell*. 2015;14(2):265-273. doi:10.1111/acel.12313

25. Wen X, Klionsky DJ. An overview of macroautophagy in yeast. *J Mol Biol.* 2016;428(9 Pt A):1681-1699. doi:10.1016/j.jmb.2016.02.021
26. Koyama-Honda I, Itakura E, Fujiwara TK, Mizushima N. Temporal analysis of recruitment of mammalian ATG proteins to the autophagosome formation site. *Autophagy.* 2013;9(10):1491-1499. doi:10.4161/auto.25529
27. Suzuki K, Kubota Y, Sekito T, Ohsumi Y. Hierarchy of Atg proteins in pre-autophagosomal structure organization. *Genes Cells Devoted Mol Cell Mech.* 2007;12(2):209-218. doi:10.1111/j.1365-2443.2007.01050.x
28. Abounit K, Scarabelli TM, McCauley RB. Autophagy in mammalian cells. *World J Biol Chem.* 2012;3(1):1-6. doi:10.4331/wjbc.v3.i1.1
29. Zhang D, Wang W, Sun X, et al. AMPK regulates autophagy by phosphorylating BECN1 at threonine 388. *Autophagy.* 2016;12(9):1447-1459. doi:10.1080/15548627.2016.1185576
30. Papinski D, Kraft C. Regulation of Autophagy By Signaling Through the Atg1/ULK1 Complex. *J Mol Biol.* 2016;428(9):1725-1741. doi:10.1016/j.jmb.2016.03.030
31. Mizushima N. The role of the Atg1/ULK1 complex in autophagy regulation. *Curr Opin Cell Biol.* 2010;22(2):132-139. doi:10.1016/j.ceb.2009.12.004
32. Mercer CA, Kaliappan A, Dennis PB. A novel, human Atg13 binding protein, Atg101, interacts with ULK1 and is essential for macroautophagy. *Autophagy.* 2009;5(5):649-662. doi:10.4161/auto.5.5.8249
33. Hara T, Takamura A, Kishi C, et al. FIP200, a ULK-interacting protein, is required for autophagosome formation in mammalian cells. *J Cell Biol.* 2008;181(3):497-510. doi:10.1083/jcb.200712064
34. Hosokawa N, Sasaki T, Iemura S, Ichiro, Natsume T, Hara T, Mizushima N. Atg101, a novel mammalian autophagy protein interacting with Atg13. *Autophagy.* 2009;5(7):973-979. doi:10.4161/auto.5.7.9296

35. Jung CH, Jun CB, Ro SH, et al. ULK-Atg13-FIP200 Complexes Mediate mTOR Signaling to the Autophagy Machinery. *Mol Biol Cell*. 2009;20(7):1992-2003. doi:10.1091/mbc.E08-12-1249
36. Kim J, Kundu M, Viollet B, Guan KL. AMPK and mTOR regulate autophagy through direct phosphorylation of Ulk1. *Nat Cell Biol*. 2011;13(2):132-141. doi:10.1038/ncb2152
37. Di Bartolomeo S, Corazzari M, Nazio F, et al. The dynamic interaction of AMBRA1 with the dynein motor complex regulates mammalian autophagy. *J Cell Biol*. 2010;191(1):155-168. doi:10.1083/jcb.201002100
38. Russell RC, Tian Y, Yuan H, et al. ULK1 induces autophagy by phosphorylating Beclin-1 and activating Vps34 lipid kinase. *Nat Cell Biol*. 2013;15(7):741-750. doi:10.1038/ncb2757
39. Itakura E, Kishi C, Inoue K, Mizushima N. Beclin 1 Forms Two Distinct Phosphatidylinositol 3-Kinase Complexes with Mammalian Atg14 and UVRAG. *Mol Biol Cell*. 2008;19(12):5360-5372. doi:10.1091/mbc.E08-01-0080
40. Kihara A, Noda T, Ishihara N, Ohsumi Y. Two Distinct Vps34 Phosphatidylinositol 3-Kinase Complexes Function in Autophagy and Carboxypeptidase Y Sorting in *Saccharomyces cerevisiae*. *J Cell Biol*. 2001;152(3):519-530.
41. Axe EL, Walker SA, Manifava M, et al. Autophagosome formation from membrane compartments enriched in phosphatidylinositol 3-phosphate and dynamically connected to the endoplasmic reticulum. *J Cell Biol*. 2008;182(4):685-701. doi:10.1083/jcb.200803137
42. Pattingre S, Tassa A, Qu X, et al. Bcl-2 antiapoptotic proteins inhibit Beclin 1-dependent autophagy. *Cell*. 2005;122(6):927-939. doi:10.1016/j.cell.2005.07.002
43. Wei Y, Pattingre S, Sinha S, Bassik M, Levine B. JNK1-mediated phosphorylation of Bcl-2 regulates starvation-induced autophagy. *Mol Cell*. 2008;30(6):678-688. doi:10.1016/j.molcel.2008.06.001

44. Dooley HC, Razi M, Polson HEJ, Girardin SE, Wilson MI, Tooze SA. WIPI2 Links LC3 Conjugation with PI3P, Autophagosome Formation, and Pathogen Clearance by Recruiting Atg12–5-16L1. *Mol Cell*. 2014;55(2):238-252. doi:10.1016/j.molcel.2014.05.021
45. Proikas-Cezanne T, Takacs Z, Dönnies P, Kohlbacher O. WIPI proteins: essential PtdIns3 P effectors at the nascent autophagosome. *J Cell Sci*. Published online January 1, 2015;jcs.146258. doi:10.1242/jcs.146258
46. Kabeya Y, Mizushima N, Ueno T, et al. LC3, a mammalian homologue of yeast Apg8p, is localized in autophagosome membranes after processing. *EMBO J*. 2000;19(21):5720-5728. doi:10.1093/emboj/19.21.5720
47. Mizushima N, Yamamoto A, Hatano M, et al. Dissection of autophagosome formation using Apg5-deficient mouse embryonic stem cells. *J Cell Biol*. 2001;152(4):657-668. doi:10.1083/jcb.152.4.657
48. Ariosa AR, Klionsky DJ. Autophagy core machinery: overcoming spatial barriers in neurons. *J Mol Med*. 2016;94(11):1217-1227. doi:10.1007/s00109-016-1461-9
49. Schaaf MBE, Keulers TG, Vooijs MA, Rouschop KMA. LC3/GABARAP family proteins: autophagy-(un)related functions. *FASEB J*. 2016;30(12):3961-3978. doi:10.1096/fj.201600698R
50. Tanida I, Ueno T, Kominami E. Human light chain 3/MAP1LC3B is cleaved at its carboxyl-terminal Met121 to expose Gly120 for lipidation and targeting to autophagosomal membranes. *J Biol Chem*. 2004;279(46):47704-47710. doi:10.1074/jbc.M407016200
51. Kabeya Y, Mizushima N, Yamamoto A, Oshitani-Okamoto S, Ohsumi Y, Yoshimori T. LC3, GABARAP and GATE16 localize to autophagosomal membrane depending on form-II formation. *J Cell Sci*. 2004;117(13):2805-2812. doi:10.1242/jcs.01131
52. Grunwald DS, Otto NM, Park JM, Song D, Kim DH. GABARAPs and LC3s have opposite roles in regulating ULK1 for autophagy induction. *Autophagy*. 2020;16(4):600-614. doi:10.1080/15548627.2019.1632620

53. Birgisdottir ÁB, Mouilleron S, Bhujabal Z, et al. Members of the autophagy class III phosphatidylinositol 3-kinase complex I interact with GABARAP and GABARAPL1 via LIR motifs. *Autophagy*. 2019;15(8):1333-1355. doi:10.1080/15548627.2019.1581009
54. Kirkin V, Rogov VV. A Diversity of Selective Autophagy Receptors Determines the Specificity of the Autophagy Pathway. *Mol Cell*. 2019;76(2):268-285. doi:10.1016/j.molcel.2019.09.005
55. Xie Z, Klionsky DJ. Autophagosome formation: core machinery and adaptations. *Nat Cell Biol*. 2007;9(10):1102-1109. doi:10.1038/ncb1007-1102
56. Young ARJ, Chan EYW, Hu XW, et al. Starvation and ULK1-dependent cycling of mammalian Atg9 between the TGN and endosomes. *J Cell Sci*. 2006;119(Pt 18):3888-3900. doi:10.1242/jcs.03172
57. Orsi A, Razi M, Dooley HC, et al. Dynamic and transient interactions of Atg9 with autophagosomes, but not membrane integration, are required for autophagy. *Mol Biol Cell*. 2012;23(10):1860-1873. doi:10.1091/mbc.E11-09-0746
58. Puri C, Renna M, Bento CF, Moreau K, Rubinsztein DC. Diverse autophagosome membrane sources coalesce in recycling endosomes. *Cell*. 2013;154(6):1285-1299. doi:10.1016/j.cell.2013.08.044
59. Yamada T, Carson AR, Caniggia I, et al. Endothelial nitric-oxide synthase antisense (NOS3AS) gene encodes an autophagy-related protein (APG9-like2) highly expressed in trophoblast. *J Biol Chem*. 2005;280(18):18283-18290. doi:10.1074/jbc.M413957200
60. Combs CA. Fluorescence Microscopy: A Concise Guide to Current Imaging Methods. *Curr Protoc Neurosci Editor Board Jacqueline N Crawley Al*. 2010;0 2:Unit2.1. doi:10.1002/0471142301.ns0201s50
61. Zanella F, Lorens JB, Link W. High content screening: seeing is believing. *Trends Biotechnol*. 2010;28(5):237-245. doi:10.1016/j.tibtech.2010.02.005

62. Panda PK, Fahrner A, Vats S, et al. Chemical Screening Approaches Enabling Drug Discovery of Autophagy Modulators for Biomedical Applications in Human Diseases. *Front Cell Dev Biol.* 2019;7:38. doi:10.3389/fcell.2019.00038
63. Swinney DC, Anthony J. How were new medicines discovered? *Nat Rev Drug Discov.* 2011;10(7):507-519. doi:10.1038/nrd3480
64. Wawer M, Bajorath J. Extraction of structure-activity relationship information from high-throughput screening data. *Curr Med Chem.* 2009;16(31):4049-4057. doi:10.2174/092986709789378189
65. Bender A, Glen RC. Molecular similarity: a key technique in molecular informatics. *Org Biomol Chem.* 2004;2(22):3204. doi:10.1039/b409813g
66. Young DW, Bender A, Hoyt J, et al. Integrating high-content screening and ligand-target prediction to identify mechanism of action. *Nat Chem Biol.* 2008;4(1):59-68. doi:10.1038/nchembio.2007.53
67. Rubinsztein DC, Frake RA. Yoshinori Ohsumi's Nobel Prize for mechanisms of autophagy: from basic yeast biology to therapeutic potential. *J R Coll Physicians Edinb.* 2016;46(4):228-233. doi:10.4997/jrcpe.2016.403
68. Kimura S, Noda T, Yoshimori T. Dissection of the autophagosome maturation process by a novel reporter protein, tandem fluorescent-tagged LC3. *Autophagy.* 2007;3(5):452-460. doi:10.4161/auto.4451
69. Kaizuka T, Morishita H, Hama Y, et al. An Autophagic Flux Probe that Releases an Internal Control. *Mol Cell.* 2016;64(4):835-849. doi:10.1016/j.molcel.2016.09.037
70. Shvets E, Fass E, Elazar Z. Utilizing flow cytometry to monitor autophagy in living mammalian cells. *Autophagy.* 2008;4(5):621-628. doi:10.4161/auto.5939
71. Kovács J, Fellingner E, Kárpáti AP, Kovács AL, László L, Réz G. Morphometric evaluation of the turnover of autophagic vacuoles after treatment with Triton X-100 and vinblastine in murine pancreatic acinar and seminal

vesicle epithelial cells. *Virchows Arch B Cell Pathol Incl Mol Pathol*. 1987;53(3):183-190. doi:10.1007/BF02890242

72. Kovács J, Fellingner E, Kárpáti PA, Kovács AL, László L. The turnover of autophagic vacuoles: evaluation by quantitative electron microscopy. *Biomed Biochim Acta*. 1986;45(11-12):1543-1547.

73. Kovács J, László L, Kovács AL. Regression of autophagic vacuoles in pancreatic acinar, seminal vesicle epithelial, and liver parenchymal cells: a comparative morphometric study of the effect of vinblastine and leupeptin followed by cycloheximide treatment. *Exp Cell Res*. 1988;174(1):244-251. doi:10.1016/0014-4827(88)90158-9

74. Mizushima N, Yoshimori T, Levine B. Methods in mammalian autophagy research. *Cell*. 2010;140(3):313-326. doi:10.1016/j.cell.2010.01.028

75. Klionsky DJ, Abeliovich H, Agostinis P, et al. Guidelines for the use and interpretation of assays for monitoring autophagy in higher eukaryotes. *Autophagy*. 2008;4(2):151-175. doi:10.4161/auto.5338

76. Ganley IG, Wong PM, Gammoh N, Jiang X. DISTINCT AUTOPHAGOSOMAL-LYSOSOMAL FUSION MECHANISM REVEALED BY THAPSIGARGIN-INDUCED AUTOPHAGY ARREST. *Mol Cell*. 2011;42(6):731-743. doi:10.1016/j.molcel.2011.04.024

77. Geng J, Klionsky DJ. Direct quantification of autophagic flux by a single molecule-based probe. *Autophagy*. 2017;13(4):639-641. doi:10.1080/15548627.2017.1280646

78. Klionsky DJ, Abdalla FC, Abeliovich H, et al. Guidelines for the use and interpretation of assays for monitoring autophagy. *Autophagy*. 2012;8(4):445-544. doi:10.4161/auto.19496

79. Pankiv S, Clausen TH, Lamark T, et al. p62/SQSTM1 binds directly to Atg8/LC3 to facilitate degradation of ubiquitinated protein aggregates by autophagy. *J Biol Chem*. 2007;282(33):24131-24145. doi:10.1074/jbc.M702824200

80. Zhou C, Zhong W, Zhou J, et al. Monitoring autophagic flux by an improved tandem fluorescent-tagged LC3 (mTagRFP-mWasabi-LC3) reveals that high-dose rapamycin impairs autophagic flux in cancer cells. *Autophagy*. 2012;8(8):1215-1226. doi:10.4161/auto.20284
81. Klionsky DJ, Abdelmohsen K, Abe A, et al. Guidelines for the use and interpretation of assays for monitoring autophagy (3rd edition). *Autophagy*. 2016;12(1):1-222. doi:10.1080/15548627.2015.1100356
82. Boya P, González-Polo RA, Casares N, et al. Inhibition of Macroautophagy Triggers Apoptosis. *Mol Cell Biol*. 2005;25(3):1025-1040. doi:10.1128/MCB.25.3.1025-1040.2005
83. Rubinsztein DC, Cuervo AM, Ravikumar B, et al. In search of an “autophagometer.” *Autophagy*. 2009;5(5):585-589. doi:10.4161/auto.5.5.8823
84. Farkas T, Jäättelä M. Renilla Luciferase-LC3 Based Reporter Assay for Measuring Autophagic Flux. *Methods Enzymol*. 2017;588:1-13. doi:10.1016/bs.mie.2016.09.072
85. Farkas T, Høyer-Hansen M, Jäättelä M. Identification of novel autophagy regulators by a luciferase-based assay for the kinetics of autophagic flux. *Autophagy*. 2009;5(7):1018-1025. doi:10.4161/auto.5.7.9443
86. Bresciani A, Spiezia MC, Boggio R, et al. Quantifying autophagy using novel LC3B and p62 TR-FRET assays. Ulasov I, ed. *PLOS ONE*. 2018;13(3):e0194423. doi:10.1371/journal.pone.0194423
87. Bjørkøy G, Lamark T, Brech A, et al. p62/SQSTM1 forms protein aggregates degraded by autophagy and has a protective effect on huntingtin-induced cell death. *J Cell Biol*. 2005;171(4):603-614. doi:10.1083/jcb.200507002
88. Larsen KB, Lamark T, Øvervatn A, Harneshaug I, Johansen T, Bjørkøy G. A reporter cell system to monitor autophagy based on p62/SQSTM1. *Autophagy*. 2010;6(6):784-793. doi:10.4161/auto.6.6.12510

89. Brown A, Patel S, Ward C, et al. PEG-lipid micelles enable cholesterol efflux in Niemann-Pick Type C1 disease-based lysosomal storage disorder. *Sci Rep*. 2016;6(1):31750. doi:10.1038/srep31750
90. Min Z, Ting Y, Mingtao G, et al. Monitoring autophagic flux using p62/SQSTM1 based luciferase reporters in glioma cells. *Exp Cell Res*. 2018;363(1):84-94. doi:10.1016/j.yexcr.2017.12.027
91. Kuo SY, Castoreno AB, Aldrich LN, et al. Small-molecule enhancers of autophagy modulate cellular disease phenotypes suggested by human genetics. *Proc Natl Acad Sci U S A*. 2015;112(31):E4281-E4287. doi:10.1073/pnas.1512289112
92. Sahani MH, Itakura E, Mizushima N. Expression of the autophagy substrate SQSTM1/p62 is restored during prolonged starvation depending on transcriptional upregulation and autophagy-derived amino acids. *Autophagy*. 2014;10(3):431-441. doi:10.4161/auto.27344
93. El-Khoury V, Pierson S, Szwarcbart E, et al. Disruption of autophagy by the histone deacetylase inhibitor MGCD0103 and its therapeutic implication in B-cell chronic lymphocytic leukemia. *Leukemia*. 2014;28(8):1636-1646. doi:10.1038/leu.2014.19
94. Piracs K, Nagy P, Varga A, et al. Advantages and limitations of different p62-based assays for estimating autophagic activity in *Drosophila*. *PLoS One*. 2012;7(8):e44214. doi:10.1371/journal.pone.0044214
95. Mizushima N, Yoshimori T. How to Interpret LC3 Immunoblotting. *Autophagy*. 2007;3(6):542-545. doi:10.4161/auto.4600
96. Jung M, Choi H, Mun JY. The autophagy research in electron microscopy. *Appl Microsc*. 2019;49:11. doi:10.1186/s42649-019-0012-6
97. Chen L, Wang FY, Zeng ZY, et al. MicroRNA-199a acts as a potential suppressor of cardiomyocyte autophagy through targeting Hspa5. *Oncotarget*. 2017;8(38):63825-63834. doi:10.18632/oncotarget.19133
98. Tarique I, Vistro WA, Bai X, et al. LIPOPHAGY: a novel form of steroidogenic activity within the LEYDIG cell during the reproductive cycle of

turtle. *Reprod Biol Endocrinol RBE*. 2019;17(1):19. doi:10.1186/s12958-019-0462-2

99. Schrader M, Fahimi HD. The peroxisome: still a mysterious organelle. *Histochem Cell Biol*. 2008;129(4):421-440. doi:10.1007/s00418-008-0396-9

100. Cheng XT, Zhou B, Lin MY, Cai Q, Sheng ZH. Axonal autophagosomes recruit dynein for retrograde transport through fusion with late endosomes. *J Cell Biol*. 2015;209(3):377-386. doi:10.1083/jcb.201412046

101. D'Assante R, Fusco A, Palamaro L, et al. Abnormal cell-clearance and accumulation of autophagic vesicles in lymphocytes from patients affected with Ataxia-Teleangiectasia. *Clin Immunol Orlando Fla*. 2017;175:16-25. doi:10.1016/j.clim.2016.11.015

102. Martin KR, Xu Y, Looyenga BD, et al. Identification of PTPsigma as an autophagic phosphatase. *J Cell Sci*. 2011;124(Pt 5):812-819. doi:10.1242/jcs.080341

103. Bustos V, Pulina MV, Bispo A, et al. Phosphorylated Presenilin 1 decreases β -amyloid by facilitating autophagosome-lysosome fusion. *Proc Natl Acad Sci U S A*. 2017;114(27):7148-7153. doi:10.1073/pnas.1705240114

104. Rubinsztein DC, Codogno P, Levine B. Autophagy modulation as a potential therapeutic target for diverse diseases. *Nat Rev Drug Discov*. 2012;11(9):709-730. doi:10.1038/nrd3802

105. Sarkar S. Chemical screening platforms for autophagy drug discovery to identify therapeutic candidates for Huntington's disease and other neurodegenerative disorders. *Drug Discov Today Technol*. 2013;10(1):e137-144. doi:10.1016/j.ddtec.2012.09.010

106. Levine B, Packer M, Codogno P. Development of autophagy inducers in clinical medicine. *J Clin Invest*. 2015;125(1):14-24. doi:10.1172/JCI73938

107. Sehgal SN, Baker H, Vézina C. RAPAMYCIN (AY-22, 989), A NEW ANTIFUNGAL ANTIBIOTIC II. FERMENTATION, ISOLATION AND CHARACTERIZATION. *J Antibiot (Tokyo)*. 1975;28(10):727-732. doi:10.7164/antibiotics.28.727

108. Douros J, Suffness M. New antitumor substances of natural origin. *Cancer Treat Rev.* 1981;8(1):63-87. doi:10.1016/s0305-7372(81)80006-0
109. Seto B. Rapamycin and mTOR: a serendipitous discovery and implications for breast cancer. *Clin Transl Med.* 2012;1:29. doi:10.1186/2001-1326-1-29
110. Heitman J, Movva NR, Hall MN. Targets for Cell Cycle Arrest by the Immunosuppressant Rapamycin in Yeast. *Science.* 1991;253(5022):905-909. doi:10.1126/science.1715094
111. Sabatini DM, Erdjument-Bromage H, Lui M, Tempst P, Snyder SH. RAFT1: a mammalian protein that binds to FKBP12 in a rapamycin-dependent fashion and is homologous to yeast TORs. *Cell.* 1994;78(1):35-43. doi:10.1016/0092-8674(94)90570-3
112. Choi J, Chen J, Schreiber SL, Clardy J. Structure of the FKBP12-rapamycin complex interacting with the binding domain of human FRAP. *Science.* 1996;273(5272):239-242. doi:10.1126/science.273.5272.239
113. Wan X, Harkavy B, Shen N, Grohar P, Helman LJ. Rapamycin induces feedback activation of Akt signaling through an IGF-1R-dependent mechanism. *Oncogene.* 2007;26(13):1932-1940. doi:10.1038/sj.onc.1209990
114. Aoki M, Blazek E, Vogt PK. A role of the kinase mTOR in cellular transformation induced by the oncoproteins P3k and Akt. *Proc Natl Acad Sci U S A.* 2001;98(1):136-141.
115. Galluzzi L, Bravo-San Pedro JM, Levine B, Green DR, Kroemer G. Pharmacological modulation of autophagy: therapeutic potential and persisting obstacles. *Nat Rev Drug Discov.* 2017;16(7):487-511. doi:10.1038/nrd.2017.22
116. Carracedo A, Ma L, Teruya-Feldstein J, et al. Inhibition of mTORC1 leads to MAPK pathway activation through a PI3K-dependent feedback loop in human cancer. *J Clin Invest.* 2008;118(9):3065-3074. doi:10.1172/JCI34739
117. Thoreen CC, Kang SA, Chang JW, et al. An ATP-competitive Mammalian Target of Rapamycin Inhibitor Reveals Rapamycin-resistant Functions of

mTORC1 *. *J Biol Chem.* 2009;284(12):8023-8032.
doi:10.1074/jbc.M900301200

118. Jacinto E, Loewith R, Schmidt A, et al. Mammalian TOR complex 2 controls the actin cytoskeleton and is rapamycin insensitive. *Nat Cell Biol.* 2004;6(11):1122-1128. doi:10.1038/ncb1183

119. Liu Q, Wang J, Kang SA, et al. Discovery of 9-(6-aminopyridin-3-yl)-1-(3-(trifluoromethyl)phenyl)benzo[h][1,6]naphthyridin-2(1H)-one (Torin2) as a potent, selective and orally available mTOR inhibitor for treatment of cancer. *J Med Chem.* 2011;54(5):1473-1480. doi:10.1021/jm101520v

120. Liu Q, Xu C, Kirubakaran S, et al. Characterization of Torin2, an ATP-Competitive Inhibitor of mTOR, ATM, and ATR. *Cancer Res.* 2013;73(8):2574-2586. doi:10.1158/0008-5472.CAN-12-1702

121. Feldman ME, Apsel B, Uotila A, et al. Active-Site Inhibitors of mTOR Target Rapamycin-Resistant Outputs of mTORC1 and mTORC2. *PLoS Biol.* 2009;7(2):e1000038. doi:10.1371/journal.pbio.1000038

122. Janes MR, Limon JJ, So L, et al. Effective and selective targeting of leukemia cells using a TORC1/2 kinase inhibitor. *Nat Med.* 2010;16(2):205-213. doi:10.1038/nm.2091

123. Cordaro M, Paterniti I, Siracusa R, Impellizzeri D, Esposito E, Cuzzocrea S. KU0063794, a Dual mTORC1 and mTORC2 Inhibitor, Reduces Neural Tissue Damage and Locomotor Impairment After Spinal Cord Injury in Mice. *Mol Neurobiol.* 2017;54(4):2415-2427. doi:10.1007/s12035-016-9827-0

124. Zhang H, Berel D, Wang Y, et al. A Comparison of Ku0063794, a Dual mTORC1 and mTORC2 Inhibitor, and Temsirolimus in Preclinical Renal Cell Carcinoma Models. *PLOS ONE.* 2013;8(1):e54918. doi:10.1371/journal.pone.0054918

125. Chresta CM, Davies BR, Hickson I, et al. AZD8055 is a potent, selective, and orally bioavailable ATP-competitive mammalian target of rapamycin kinase inhibitor with in vitro and in vivo antitumor activity. *Cancer Res.* 2010;70(1):288-298. doi:10.1158/0008-5472.CAN-09-1751

126. Liao H, Huang Y, Guo B, et al. Dramatic antitumor effects of the dual mTORC1 and mTORC2 inhibitor AZD2014 in hepatocellular carcinoma. *Am J Cancer Res.* 2015;5(1):125-139.
127. Wang L, Zhu YR, Wang S, Zhao S. Autophagy inhibition sensitizes WYE-354-induced anti-colon cancer activity in vitro and in vivo. *Tumor Biol.* 2016;37(9):11743-11752. doi:10.1007/s13277-016-5018-x
128. Xie J, Wang X, Proud CG. mTOR inhibitors in cancer therapy. *F1000Research.* 2016;5:F1000 Faculty Rev-2078. doi:10.12688/f1000research.9207.1
129. Waetzig R, Matthes M, Leister J, et al. Comparing mTOR inhibitor Rapamycin with Torin-2 within the RIST molecular-targeted regimen in neuroblastoma cells. *Int J Med Sci.* 2021;18(1):137-149. doi:10.7150/ijms.48393
130. He S, Li Q, Jiang X, et al. Design of Small Molecule Autophagy Modulators: A Promising Druggable Strategy. *J Med Chem.* 2018;61(11):4656-4687. doi:10.1021/acs.jmedchem.7b01019
131. Sabbah DA, Brattain MG, Zhong H. Dual inhibitors of PI3K/mTOR or mTOR-selective inhibitors: which way shall we go? *Curr Med Chem.* 2011;18(36):5528-5544. doi:10.2174/092986711798347298
132. Park S, Chapuis N, Bardet V, et al. PI-103, a dual inhibitor of Class IA phosphatidylinositide 3-kinase and mTOR, has antileukemic activity in AML. *Leukemia.* 2008;22(9):1698-1706. doi:10.1038/leu.2008.144
133. Simioni C, Cani A, Martelli AM, et al. The novel dual PI3K/mTOR inhibitor NVP-BGT226 displays cytotoxic activity in both normoxic and hypoxic hepatocarcinoma cells. *Oncotarget.* 2015;6(19):17147-17160. doi:10.18632/oncotarget.3940
134. Chang KY, Tsai SY, Wu CM, Yen CJ, Chuang BF, Chang JY. Novel Phosphoinositide 3-Kinase/mTOR Dual Inhibitor, NVP-BGT226, Displays Potent Growth-Inhibitory Activity against Human Head and Neck Cancer Cells In Vitro and In Vivo. *Clin Cancer Res.* 2011;17(22):7116-7126. doi:10.1158/1078-0432.CCR-11-0796

135. Fan QW, Cheng C, Hackett C, et al. Akt and Autophagy Cooperate to Promote Survival of Drug-Resistant Glioma. *Sci Signal*. 2010;3(147):ra81-ra81. doi:10.1126/scisignal.2001017
136. Fei HR, Tian H, Zhou XL, et al. Inhibition of autophagy enhances effects of PF-04691502 on apoptosis and DNA damage of lung cancer cells. *Int J Biochem Cell Biol*. 2016;78:52-62. doi:10.1016/j.biocel.2016.06.023
137. Mallon R, Feldberg LR, Lucas J, et al. Antitumor Efficacy of PKI-587, a Highly Potent Dual PI3K/mTOR Kinase Inhibitor. *Clin Cancer Res*. 2011;17(10):3193-3203. doi:10.1158/1078-0432.CCR-10-1694
138. Powles T, Lackner MR, Oudard S, et al. Randomized Open-Label Phase II Trial of Apatolisib (GDC-0980), a Novel Inhibitor of the PI3K/Mammalian Target of Rapamycin Pathway, Versus Everolimus in Patients With Metastatic Renal Cell Carcinoma. *J Clin Oncol*. 2016;34(14):1660-1668. doi:10.1200/JCO.2015.64.8808
139. Fruman DA, Chiu H, Hopkins BD, Bagrodia S, Cantley LC, Abraham RT. The PI3K Pathway in Human Disease. *Cell*. 2017;170(4):605-635. doi:10.1016/j.cell.2017.07.029
140. Lamoureux F, Zoubeidi A. Dual inhibition of autophagy and the AKT pathway in prostate cancer. *Autophagy*. 2013;9(7):1119-1120. doi:10.4161/auto.24921
141. Jeong EH, Choi HS, Lee TG, Kim HR, Kim CH. Dual Inhibition of PI3K/Akt/mTOR Pathway and Role of Autophagy in Non-Small Cell Lung Cancer Cells. *Tuberc Respir Dis*. 2012;72(4):343-351. doi:10.4046/trd.2012.72.4.343
142. Zorea J, Prasad M, Cohen L, et al. IGF1R upregulation confers resistance to isoform-specific inhibitors of PI3K in PIK3CA-driven ovarian cancer. *Cell Death Dis*. 2018;9(10):1-12. doi:10.1038/s41419-018-1025-8
143. Lin J, Sampath D, Nannini MA, et al. Targeting Activated Akt with GDC-0068, a Novel Selective Akt Inhibitor That Is Efficacious in Multiple Tumor Models. *Clin Cancer Res*. 2013;19(7):1760-1772. doi:10.1158/1078-0432.CCR-12-3072

144. Cheng Y, Ren X, Zhang Y, et al. eEF-2 Kinase Dictates Cross-Talk between Autophagy and Apoptosis Induced by Akt Inhibition, Thereby Modulating Cytotoxicity of Novel Akt Inhibitor MK-2206. *Cancer Res.* 2011;71(7):2654-2663. doi:10.1158/0008-5472.CAN-10-2889
145. Degtyarev M, De Mazière A, Orr C, et al. Akt inhibition promotes autophagy and sensitizes PTEN-null tumors to lysosomotropic agents. *J Cell Biol.* 2008;183(1):101-116. doi:10.1083/jcb.200801099
146. Walter C, Clemens LE, Müller AJ, et al. Activation of AMPK-induced autophagy ameliorates Huntington disease pathology in vitro. *Neuropharmacology.* 2016;108:24-38. doi:10.1016/j.neuropharm.2016.04.041
147. Liu T, Marcinko TM, Kiefer PA, Vachet RW. Using Covalent Labeling and Mass Spectrometry to Study Protein Binding Sites of Amyloid Inhibiting Molecules. *Anal Chem.* 2017;89(21):11583-11591. doi:10.1021/acs.analchem.7b02915
148. Huang SC, Adhikari S, Brownell JE, et al. Discovery and optimization of pyrazolopyrimidine sulfamates as ATG7 inhibitors. *Bioorg Med Chem.* 2020;28(19):115681. doi:10.1016/j.bmc.2020.115681
149. Vucicevic L, Misirkic M, Janjetovic K, et al. Compound C induces protective autophagy in cancer cells through AMPK inhibition-independent blockade of Akt/mTOR pathway. *Autophagy.* 2011;7(1):40-50. doi:10.4161/auto.7.1.13883
150. Lee JW, Park S, Takahashi Y, Wang HG. The Association of AMPK with ULK1 Regulates Autophagy. *PLOS ONE.* 2010;5(11):e15394. doi:10.1371/journal.pone.0015394
151. Robert G, Sahra IB, Puissant A, et al. Acadesine Kills Chronic Myelogenous Leukemia (CML) Cells through PKC-Dependent Induction of Autophagic Cell Death. *PLOS ONE.* 2009;4(11):e7889. doi:10.1371/journal.pone.0007889
152. Baur JA, Sinclair DA. Therapeutic potential of resveratrol: the in vivo evidence. *Nat Rev Drug Discov.* 2006;5(6):493-506. doi:10.1038/nrd2060

153. Pineda-Ramírez N, Alquisiras-Burgos I, Ortiz-Plata A, Ruiz-Tachiquín ME, Espinoza-Rojo M, Aguilera P. Resveratrol Activates Neuronal Autophagy Through AMPK in the Ischemic Brain. *Mol Neurobiol.* 2020;57(2):1055-1069. doi:10.1007/s12035-019-01803-6
154. Sarkar S, Davies JE, Huang Z, Tunnacliffe A, Rubinsztein DC. Trehalose, a novel mTOR-independent autophagy enhancer, accelerates the clearance of mutant huntingtin and alpha-synuclein. *J Biol Chem.* 2007;282(8):5641-5652. doi:10.1074/jbc.M609532200
155. Sarkar S, Perlstein EO, Imarisio S, et al. Small molecules enhance autophagy and reduce toxicity in Huntington's disease models. *Nat Chem Biol.* 2007;3(6):331-338. doi:10.1038/nchembio883
156. Sarkar S, Floto RA, Berger Z, et al. Lithium induces autophagy by inhibiting inositol monophosphatase. *J Cell Biol.* 2005;170(7):1101-1111. doi:10.1083/jcb.200504035
157. Sarkar S, Korolchuk VI, Renna M, et al. Complex inhibitory effects of nitric oxide on autophagy. *Mol Cell.* 2011;43(1):19-32. doi:10.1016/j.molcel.2011.04.029
158. Williams A, Sarkar S, Cuddon P, et al. Novel targets for Huntington's disease in an mTOR-independent autophagy pathway. *Nat Chem Biol.* 2008;4(5):295-305. doi:10.1038/nchembio.79
159. Sarkar S, Ravikumar B, Floto RA, Rubinsztein DC. Rapamycin and mTOR-independent autophagy inducers ameliorate toxicity of polyglutamine-expanded huntingtin and related proteinopathies. *Cell Death Differ.* 2009;16(1):46-56. doi:10.1038/cdd.2008.110
160. Li Y, McGreal S, Zhao J, et al. A cell-based quantitative high-throughput image screening identified novel autophagy modulators. *Pharmacol Res.* 2016;110:35-49. doi:10.1016/j.phrs.2016.05.004
161. Sarkar S, Krishna G, Imarisio S, Saiki S, O'Kane CJ, Rubinsztein DC. A rational mechanism for combination treatment of Huntington's disease using lithium and rapamycin. *Hum Mol Genet.* 2008;17(2):170-178. doi:10.1093/hmg/ddm294

162. Steelman LS, Martelli AM, Cocco L, et al. The therapeutic potential of mTOR inhibitors in breast cancer. *Br J Clin Pharmacol*. 2016;82(5):1189-1212. doi:10.1111/bcp.12958
163. Pasquier B. Autophagy inhibitors. *Cell Mol Life Sci*. 2016;73(5):985-1001. doi:10.1007/s00018-015-2104-y
164. Seglen PO, Gordon PB. 3-Methyladenine: Specific inhibitor of autophagic/lysosomal protein degradation in isolated rat hepatocytes. *Proc Natl Acad Sci*. 1982;79(6):1889-1892. doi:10.1073/pnas.79.6.1889
165. Arcaro A, Wymann MP. Wortmannin is a potent phosphatidylinositol 3-kinase inhibitor: the role of phosphatidylinositol 3,4,5-trisphosphate in neutrophil responses. *Biochem J*. 1993;296 (Pt 2):297-301. doi:10.1042/bj2960297
166. Vlahos CJ, Matter WF, Hui KY, Brown RF. A specific inhibitor of phosphatidylinositol 3-kinase, 2-(4-morpholinyl)-8-phenyl-4H-1-benzopyran-4-one (LY294002). *J Biol Chem*. 1994;269(7):5241-5248.
167. Wu Y, Wang X, Guo H, et al. Synthesis and screening of 3-MA derivatives for autophagy inhibitors. *Autophagy*. 2013;9(4):595-603. doi:10.4161/auto.23641
168. Caro LHP, Plomp PJAM, Wolvetang EJ, Kerkhof C, Meijer AJ. 3-Methyladenine, an inhibitor of autophagy, has multiple effects on metabolism. *Eur J Biochem*. 1988;175(2):325-329. doi:10.1111/j.1432-1033.1988.tb14200.x
169. Hou H, Zhang Y, Huang Y, et al. Inhibitors of Phosphatidylinositol 3'-Kinases Promote Mitotic Cell Death in HeLa Cells. *PLOS ONE*. 2012;7(4):e35665. doi:10.1371/journal.pone.0035665
170. Sheng Y, Sun B, Guo WT, et al. 3-Methyladenine induces cell death and its interaction with chemotherapeutic drugs is independent of autophagy. *Biochem Biophys Res Commun*. 2013;432(1):5-9. doi:10.1016/j.bbrc.2013.01.106
171. Wiesinger D, Gubler HU, Haefliger W, Hauser D. Antiinflammatory activity of the new mould metabolite 11-desacetoxy-wortmannin and of some of its derivatives. *Experientia*. 1974;30(2):135-136. doi:10.1007/BF01927691

172. Powis G, Bonjouklian R, Berggren MM, et al. Wortmannin, a potent and selective inhibitor of phosphatidylinositol-3-kinase. *Cancer Res.* 1994;54(9):2419-2423.
173. Thelen M, Wymann MP, Langen H. Wortmannin binds specifically to 1-phosphatidylinositol 3-kinase while inhibiting guanine nucleotide-binding protein-coupled receptor signaling in neutrophil leukocytes. *Proc Natl Acad Sci U S A.* 1994;91(11):4960-4964. doi:10.1073/pnas.91.11.4960
174. Blommaert EF, Krause U, Schellens JP, Vreeling-Sindelárová H, Meijer AJ. The phosphatidylinositol 3-kinase inhibitors wortmannin and LY294002 inhibit autophagy in isolated rat hepatocytes. *Eur J Biochem.* 1997;243(1-2):240-246. doi:10.1111/j.1432-1033.1997.0240a.x
175. Chude CI, Amaravadi RK. Targeting Autophagy in Cancer: Update on Clinical Trials and Novel Inhibitors. *Int J Mol Sci.* 2017;18(6):1279. doi:10.3390/ijms18061279
176. Miller S, Tavshanjian B, Oleksy A, et al. Shaping development of autophagy inhibitors with the structure of the lipid kinase Vps34. *Science.* 2010;327(5973):1638-1642. doi:10.1126/science.1184429
177. Knight SD, Adams ND, Burgess JL, et al. Discovery of GSK2126458, a Highly Potent Inhibitor of PI3K and the Mammalian Target of Rapamycin. *ACS Med Chem Lett.* 2010;1(1):39-43. doi:10.1021/ml900028r
178. Vakifahmetoglu-Norberg H, Xia H guang, Yuan J. Pharmacologic agents targeting autophagy. *J Clin Invest.* 2015;125(1):5-13. doi:10.1172/JCI73937
179. Redmann M, Benavides GA, Berryhill TF, et al. Inhibition of autophagy with bafilomycin and chloroquine decreases mitochondrial quality and bioenergetic function in primary neurons. *Redox Biol.* 2016;11:73-81. doi:10.1016/j.redox.2016.11.004
180. Bowman EJ, Siebers A, Altendorf K. Bafilomycins: a class of inhibitors of membrane ATPases from microorganisms, animal cells, and plant cells. *Proc Natl Acad Sci U S A.* 1988;85(21):7972-7976. doi:10.1073/pnas.85.21.7972

181. Werner G, Hagenmaier H, Drautz H, Baumgartner A, Zähler H. Metabolic products of microorganisms. 224. Bafilomycins, a new group of macrolide antibiotics. Production, isolation, chemical structure and biological activity. *J Antibiot (Tokyo)*. 1984;37(2):110-117. doi:10.7164/antibiotics.37.110
182. Yoshimori T, Yamamoto A, Moriyama Y, Futai M, Tashiro Y. Bafilomycin A1, a specific inhibitor of vacuolar-type H(+)-ATPase, inhibits acidification and protein degradation in lysosomes of cultured cells. *J Biol Chem*. 1991;266(26):17707-17712.
183. Ochiai H, Sakai S, Hirabayashi T, Shimizu Y, Terasawa K. Inhibitory effect of bafilomycin A1, a specific inhibitor of vacuolar-type proton pump, on the growth of influenza A and B viruses in MDCK cells. *Antiviral Res*. 1995;27(4):425-430. doi:10.1016/0166-3542(95)00040-s
184. Lim JH, Park JW, Kim MS, Park SK, Johnson RS, Chun YS. Bafilomycin induces the p21-mediated growth inhibition of cancer cells under hypoxic conditions by expressing hypoxia-inducible factor-1alpha. *Mol Pharmacol*. 2006;70(6):1856-1865. doi:10.1124/mol.106.028076
185. Hernández-Breijo B, Monserrat J, Román ID, et al. Azathioprine desensitizes liver cancer cells to insulin-like growth factor 1 and causes apoptosis when it is combined with bafilomycin A1. *Toxicol Appl Pharmacol*. 2013;272(3):568-578. doi:10.1016/j.taap.2013.07.024
186. Li Z, Du L, Zhang W, et al. Complete elucidation of the late steps of bafilomycin biosynthesis in *Streptomyces lohii*. *J Biol Chem*. 2017;292(17):7095-7104. doi:10.1074/jbc.M116.751255
187. Tripathy S, Dassarma B, Roy S, Chabalala H, Matsabisa MG. A review on possible modes of action of chloroquine/hydroxychloroquine: repurposing against SAR-CoV-2 (COVID-19) pandemic. *Int J Antimicrob Agents*. 2020;56(2):106028. doi:10.1016/j.ijantimicag.2020.106028
188. Homewood CA, Warhurst DC, Peters W, Baggaley VC. Lysosomes, pH and the anti-malarial action of chloroquine. *Nature*. 1972;235(5332):50-52. doi:10.1038/235050a0

189. Steinman RM, Mellman IS, Muller WA, Cohn ZA. Endocytosis and the recycling of plasma membrane. *J Cell Biol.* 1983;96(1):1-27. doi:10.1083/jcb.96.1.1
190. Verbaanderd C, Maes H, Schaaf MB, et al. Repurposing Drugs in Oncology (ReDO)—chloroquine and hydroxychloroquine as anti-cancer agents. *ecancermedicalscience.* 2017;11:781. doi:10.3332/ecancer.2017.781
191. McAfee Q, Zhang Z, Samanta A, et al. Autophagy inhibitor Lys05 has single-agent antitumor activity and reproduces the phenotype of a genetic autophagy deficiency. *Proc Natl Acad Sci U S A.* 2012;109(21):8253-8258. doi:10.1073/pnas.1118193109
192. Choi HS, Jeong EH, Lee TG, Kim SY, Kim HR, Kim CH. Autophagy Inhibition with Monensin Enhances Cell Cycle Arrest and Apoptosis Induced by mTOR or Epidermal Growth Factor Receptor Inhibitors in Lung Cancer Cells. *Tuberc Respir Dis.* 2013;75(1):9-17. doi:10.4046/trd.2013.75.1.9
193. Carew JS, Espitia CM, Esquivel JA, et al. Lucanthone is a novel inhibitor of autophagy that induces cathepsin D-mediated apoptosis. *J Biol Chem.* 2011;286(8):6602-6613. doi:10.1074/jbc.M110.151324
194. Carew JS, Espitia CM, Zhao W, et al. Disruption of autophagic degradation with ROC-325 antagonizes renal cell carcinoma pathogenesis. *Clin Cancer Res Off J Am Assoc Cancer Res.* 2017;23(11):2869-2879. doi:10.1158/1078-0432.CCR-16-1742
195. Wang Z, Zhang J, Wang Y, et al. Matrine, a novel autophagy inhibitor, blocks trafficking and the proteolytic activation of lysosomal proteases. *Carcinogenesis.* 2013;34(1):128-138. doi:10.1093/carcin/bgs295
196. Renna M, Schaffner C, Brown K, et al. Azithromycin blocks autophagy and may predispose cystic fibrosis patients to mycobacterial infection. *J Clin Invest.* 2011;121(9):3554-3563. doi:10.1172/JCI46095
197. Yang Y ping, Hu L fang, Zheng H fen, et al. Application and interpretation of current autophagy inhibitors and activators. *Acta Pharmacol Sin.* 2013;34(5):625-635. doi:10.1038/aps.2013.5

198. Vahsen BF, Ribas VT, Sundermeyer J, et al. Inhibition of the autophagic protein ULK1 attenuates axonal degeneration in vitro and in vivo, enhances translation, and modulates splicing. *Cell Death Differ.* 2020;27(10):2810-2827. doi:10.1038/s41418-020-0543-y
199. Dyczynski M, Yu Y, Otrocka M, et al. Targeting autophagy by small molecule inhibitors of vacuolar protein sorting 34 (Vps34) improves the sensitivity of breast cancer cells to Sunitinib. *Cancer Lett.* 2018;435:32-43. doi:10.1016/j.canlet.2018.07.028
200. Akin D, Wang SK, Habibzadegah-Tari P, et al. A novel ATG4B antagonist inhibits autophagy and has a negative impact on osteosarcoma tumors. *Autophagy.* 2014;10(11):2021-2035. doi:10.4161/auto.32229
201. Kurdi A, Cleenewerck M, Vangestel C, et al. ATG4B inhibitors with a benzotropolone core structure block autophagy and augment efficiency of chemotherapy in mice. *Biochem Pharmacol.* 2017;138:150-162. doi:10.1016/j.bcp.2017.06.119
202. Liu PF, Tsai KL, Hsu CJ, et al. Drug Repurposing Screening Identifies Tioconazole as an ATG4 Inhibitor that Suppresses Autophagy and Sensitizes Cancer Cells to Chemotherapy. *Theranostics.* 2018;8(3):830-845. doi:10.7150/thno.22012
203. Bosc D, Vezenkov L, Bortnik S, et al. A new quinoline-based chemical probe inhibits the autophagy-related cysteine protease ATG4B. *Sci Rep.* 2018;8(1):11653. doi:10.1038/s41598-018-29900-x
204. Fu Y, Hong L, Xu J, et al. Discovery of a small molecule targeting autophagy via ATG4B inhibition and cell death of colorectal cancer cells in vitro and in vivo. *Autophagy.* 2019;15(2):295-311. doi:10.1080/15548627.2018.1517073
205. Barnard RA, Wittenburg LA, Amaravadi RK, Gustafson DL, Thorburn A, Thamm DH. Phase I clinical trial and pharmacodynamic evaluation of combination hydroxychloroquine and doxorubicin treatment in pet dogs treated for spontaneously occurring lymphoma. *Autophagy.* 2014;10(8):1415-1425. doi:10.4161/auto.29165

206. Manic G, Obrist F, Kroemer G, Vitale I, Galluzzi L. Chloroquine and hydroxychloroquine for cancer therapy. *Mol Cell Oncol*. 2014;1(1):e29911. doi:10.4161/mco.29911
207. Rosenfeld MR, Ye X, Supko JG, et al. A phase I/II trial of hydroxychloroquine in conjunction with radiation therapy and concurrent and adjuvant temozolomide in patients with newly diagnosed glioblastoma multiforme. *Autophagy*. 2014;10(8):1359-1368. doi:10.4161/auto.28984
208. Yang S, Kimmelman AC. A critical role for autophagy in pancreatic cancer. *Autophagy*. 2011;7(8):912-913. doi:10.4161/auto.7.8.15762
209. Wolpin BM, Rubinson DA, Wang X, et al. Phase II and pharmacodynamic study of autophagy inhibition using hydroxychloroquine in patients with metastatic pancreatic adenocarcinoma. *The Oncologist*. 2014;19(6):637-638. doi:10.1634/theoncologist.2014-0086
210. Kinsey CG, Camolotto SA, Boespflug AM, et al. Protective autophagy elicited by RAF→MEK→ERK inhibition suggests a treatment strategy for RAS-driven cancers. *Nat Med*. 2019;25(4):620-627. doi:10.1038/s41591-019-0367-9
211. Mahalingam D, Mita M, Sarantopoulos J, et al. Combined autophagy and HDAC inhibition. *Autophagy*. 2014;10(8):1403-1414. doi:10.4161/auto.29231
212. Rangwala R, Leone R, Chang YC, et al. Phase I trial of hydroxychloroquine with dose-intense temozolomide in patients with advanced solid tumors and melanoma. *Autophagy*. 2014;10(8):1369-1379. doi:10.4161/auto.29118
213. Vogl DT, Stadtmauer EA, Tan KS, et al. Combined autophagy and proteasome inhibition: a phase 1 trial of hydroxychloroquine and bortezomib in patients with relapsed/refractory myeloma. *Autophagy*. 2014;10(8):1380-1390. doi:10.4161/auto.29264
214. Boulware DR, Pullen MF, Bangdiwala AS, et al. A Randomized Trial of Hydroxychloroquine as Postexposure Prophylaxis for Covid-19. *N Engl J Med*. 2020;383(6):517-525. doi:10.1056/NEJMoa2016638

215. Shoji-Kawata S, Sumpter R, Leveno M, et al. Identification of a candidate therapeutic autophagy-inducing peptide. *Nature*. 2013;494(7436):201-206. doi:10.1038/nature11866
216. Roy J, Paquette JS, Fortin JF, Tremblay MJ. The immunosuppressant rapamycin represses human immunodeficiency virus type 1 replication. *Antimicrob Agents Chemother*. 2002;46(11):3447-3455. doi:10.1128/AAC.46.11.3447-3455.2002
217. Nicoletti F, Lapenta C, Lamenta C, et al. Inhibition of human immunodeficiency virus (HIV-1) infection in human peripheral blood leucocytes-SCID reconstituted mice by rapamycin. *Clin Exp Immunol*. 2009;155(1):28-34. doi:10.1111/j.1365-2249.2008.03780.x
218. Underwood BR, Green-Thompson ZW, Pugh PJ, et al. An open-label study to assess the feasibility and tolerability of rilmenidine for the treatment of Huntington's disease. *J Neurol*. 2017;264(12):2457-2463. doi:10.1007/s00415-017-8647-0
219. Wirth M, Benson G, Schwarz C, et al. The effect of spermidine on memory performance in older adults at risk for dementia: A randomized controlled trial. *Cortex J Devoted Study Nerv Syst Behav*. 2018;109:181-188. doi:10.1016/j.cortex.2018.09.014
220. Amaravadi R, Kimmelman AC, White E. Recent insights into the function of autophagy in cancer. *Genes Dev*. 2016;30(17):1913-1930. doi:10.1101/gad.287524.116
221. Mathew R, Karantza-Wadsworth V, White E. Role of autophagy in cancer. *Nat Rev Cancer*. 2007;7(12):961-967. doi:10.1038/nrc2254
222. Virgin HW, Levine B. Autophagy genes in immunity. *Nat Immunol*. 2009;10(5):461-470. doi:10.1038/ni.1726
223. Mainz L, Rosenfeldt MT. Autophagy and cancer - insights from mouse models. *FEBS J*. 2018;285(5):792-808. doi:10.1111/febs.14274

224. Kuma A, Hatano M, Matsui M, et al. The role of autophagy during the early neonatal starvation period. *Nature*. 2004;432(7020):1032-1036. doi:10.1038/nature03029
225. Komatsu M, Waguri S, Ueno T, et al. Impairment of starvation-induced and constitutive autophagy in Atg7-deficient mice. *J Cell Biol*. 2005;169(3):425-434. doi:10.1083/jcb.200412022
226. Yoshii SR, Kuma A, Akashi T, et al. Systemic Analysis of Atg5-Null Mice Rescued from Neonatal Lethality by Transgenic ATG5 Expression in Neurons. *Dev Cell*. 2016;39(1):116-130. doi:10.1016/j.devcel.2016.09.001
227. Saito T, Ichimura Y, Taguchi K, et al. p62/Sqstm1 promotes malignancy of HCV-positive hepatocellular carcinoma through Nrf2-dependent metabolic reprogramming. *Nat Commun*. 2016;7(1):12030. doi:10.1038/ncomms12030
228. Xiang X, Qin H, You X, et al. Expression of P62 in hepatocellular carcinoma involving hepatitis B virus infection and aflatoxin B1 exposure. *Cancer Med*. 2017;6(10):2357-2369. doi:10.1002/cam4.1176
229. Michaud M, Martins I, Sukkurwala AQ, et al. Autophagy-Dependent Anticancer Immune Responses Induced by Chemotherapeutic Agents in Mice. *Science*. Published online December 16, 2011. doi:10.1126/science.1208347
230. Masuelli L, Granato M, Benvenuto M, et al. Chloroquine supplementation increases the cytotoxic effect of curcumin against Her2/neu overexpressing breast cancer cells in vitro and in vivo in nude mice while counteracts it in immune competent mice. *Oncoimmunology*. 2017;6(11):e1356151. doi:10.1080/2162402X.2017.1356151
231. Carew JS, Medina EC, Esquivel JA, et al. Autophagy inhibition enhances vorinostat-induced apoptosis via ubiquitinated protein accumulation. *J Cell Mol Med*. 2010;14(10):2448-2459. doi:10.1111/j.1582-4934.2009.00832.x
232. Vyas AR, Hahm ER, Arlotti JA, et al. Chemoprevention of prostate cancer by d,l-sulforaphane is augmented by pharmacological inhibition of autophagy. *Cancer Res*. 2013;73(19):5985-5995. doi:10.1158/0008-5472.CAN-13-0755

233. Balic A, Sørensen MD, Trabulo SM, et al. Chloroquine targets pancreatic cancer stem cells via inhibition of CXCR4 and hedgehog signaling. *Mol Cancer Ther.* 2014;13(7):1758-1771. doi:10.1158/1535-7163.MCT-13-0948
234. Golden EB, Cho HY, Jahanian A, et al. Chloroquine enhances temozolomide cytotoxicity in malignant gliomas by blocking autophagy. *Neurosurg Focus.* 2014;37(6):E12. doi:10.3171/2014.9.FOCUS14504
235. Lefort S, Joffre C, Kieffer Y, et al. Inhibition of autophagy as a new means of improving chemotherapy efficiency in high-LC3B triple-negative breast cancers. *Autophagy.* 2014;10(12):2122-2142. doi:10.4161/15548627.2014.981788
236. Amaravadi RK, Yu D, Lum JJ, et al. Autophagy inhibition enhances therapy-induced apoptosis in a Myc-induced model of lymphoma. *J Clin Invest.* 2007;117(2):326-336. doi:10.1172/JCI28833
237. Xie X, White EP, Mehnert JM. Coordinate autophagy and mTOR pathway inhibition enhances cell death in melanoma. *PloS One.* 2013;8(1):e55096. doi:10.1371/journal.pone.0055096
238. Zhang HQ, Fang N, Liu XM, et al. Antitumor activity of chloroquine in combination with Cisplatin in human gastric cancer xenografts. *Asian Pac J Cancer Prev APJCP.* 2015;16(9):3907-3912. doi:10.7314/apjcp.2015.16.9.3907
239. Zou Y, Ling YH, Sironi J, Schwartz EL, Perez-Soler R, Piperdi B. The autophagy inhibitor chloroquine overcomes the innate resistance of wild-type EGFR non-small-cell lung cancer cells to erlotinib. *J Thorac Oncol Off Publ Int Assoc Study Lung Cancer.* 2013;8(6):693-702. doi:10.1097/JTO.0b013e31828c7210
240. Ding ZB, Hui B, Shi YH, et al. Autophagy Activation in Hepatocellular Carcinoma Contributes to the Tolerance of Oxaliplatin via Reactive Oxygen Species Modulation. *Clin Cancer Res.* 2011;17(19):6229-6238. doi:10.1158/1078-0432.CCR-11-0816
241. Pavlova NN, Thompson CB. THE EMERGING HALLMARKS OF CANCER METABOLISM. *Cell Metab.* 2016;23(1):27-47. doi:10.1016/j.cmet.2015.12.006

242. Weeks SE, Metge BJ, Samant RS. The nucleolus: a central response hub for the stressors that drive cancer progression. *Cell Mol Life Sci CMLS*. 2019;76(22):4511-4524. doi:10.1007/s00018-019-03231-0
243. Moon HW, Han HG, Jeon YJ. Protein Quality Control in the Endoplasmic Reticulum and Cancer. *Int J Mol Sci*. 2018;19(10):E3020. doi:10.3390/ijms19103020
244. Russo A, Russo G, Cuccurese M, Garbi C, Pietropaolo C. The 3'-untranslated region directs ribosomal protein-encoding mRNAs to specific cytoplasmic regions. *Biochim Biophys Acta*. 2006;1763(8):833-843. doi:10.1016/j.bbamcr.2006.05.010
245. Schwarz DS, Blower MD. The endoplasmic reticulum: structure, function and response to cellular signaling. *Cell Mol Life Sci*. 2016;73:79-94. doi:10.1007/s00018-015-2052-6
246. Chino H, Mizushima N. ER-Phagy: Quality Control and Turnover of Endoplasmic Reticulum. *Trends Cell Biol*. 2020;30(5):384-398. doi:10.1016/j.tcb.2020.02.001
247. Pecoraro A, Pagano M, Russo G, Russo A. Role of Autophagy in Cancer Cell Response to Nucleolar and Endoplasmic Reticulum Stress. *Int J Mol Sci*. 2020;21(19):7334. doi:10.3390/ijms21197334
248. Stolz A, Grumati P. The various shades of ER-phagy. *FEBS J*. 2019;286(23):4642-4649. doi:10.1111/febs.15031
249. Wilkinson S. ER-phagy: shaping up and destressing the endoplasmic reticulum. *FEBS J*. 2019;286(14):2645-2663. doi:10.1111/febs.14932
250. Fregno I, Fasana E, Bergmann TJ, et al. ER-to-lysosome-associated degradation of proteasome-resistant ATZ polymers occurs via receptor-mediated vesicular transport. *EMBO J*. 2018;37(17). doi:10.15252/embj.201899259
251. Grumati P, Dikic I, Stolz A. ER-phagy at a glance. *J Cell Sci*. 2018;131(17):jcs217364. doi:10.1242/jcs.217364

252. Dikic I. Open questions: why should we care about ER-phagy and ER remodelling? *BMC Biol.* 2018;16:131. doi:10.1186/s12915-018-0603-7
253. Yang M, Luo S, Wang X, et al. ER-Phagy: A New Regulator of ER Homeostasis. *Front Cell Dev Biol.* 2021;9:684526. doi:10.3389/fcell.2021.684526
254. Oyadomari S, Mori M. Roles of CHOP/GADD153 in endoplasmic reticulum stress. *Cell Death Differ.* 2004;11(4):381-389. doi:10.1038/sj.cdd.4401373
255. Hetz C, Chevet E, Oakes SA. Proteostasis control by the unfolded protein response. *Nat Cell Biol.* 2015;17(7):829-838. doi:10.1038/ncb3184
256. Matsumoto M, Minami M, Takeda K, Sakao Y, Akira S. Ectopic expression of CHOP (GADD153) induces apoptosis in M1 myeloblastic leukemia cells. *FEBS Lett.* 1996;395(2-3):143-147. doi:10.1016/0014-5793(96)01016-2
257. Nam DH, Han JH, Lee TJ, et al. CHOP deficiency prevents methylglyoxal-induced myocyte apoptosis and cardiac dysfunction. *J Mol Cell Cardiol.* 2015;85:168-177. doi:10.1016/j.yjmcc.2015.05.016
258. Wang XZ, Lawson B, Brewer JW, et al. Signals from the stressed endoplasmic reticulum induce C/EBP-homologous protein (CHOP/GADD153). *Mol Cell Biol.* 1996;16(8):4273-4280.
259. Rao J, Zhang C, Wang P, et al. C/EBP homologous protein (CHOP) contributes to hepatocyte death via the promotion of ERO1 α signalling in acute liver failure. *Biochem J.* 2015;466(2):369-378. doi:10.1042/BJ20140412
260. Tabas I, Ron D. Integrating the mechanisms of apoptosis induced by endoplasmic reticulum stress. *Nat Cell Biol.* 2011;13(3):184-190. doi:10.1038/ncb0311-184
261. Shimodaira Y, Takahashi S, Kinouchi Y, et al. Modulation of endoplasmic reticulum (ER) stress-induced autophagy by C/EBP homologous protein (CHOP) and inositol-requiring enzyme 1 α (IRE1 α) in human colon cancer cells.

- Biochem Biophys Res Commun.* 2014;445(2):524-533.
doi:10.1016/j.bbrc.2014.02.054
262. Ke PY, Chen SSL. Autophagy: A novel guardian of HCV against innate immune response. *Autophagy.* 2011;7(5):533-535. doi:10.4161/auto.7.5.14732
263. B'chir W, Chaveroux C, Carraro V, et al. Dual role for CHOP in the crosstalk between autophagy and apoptosis to determine cell fate in response to amino acid deprivation. *Cell Signal.* 2014;26(7):1385-1391. doi:10.1016/j.cellsig.2014.03.009
264. Bootman MD, Chehab T, Bultynck G, Parys JB, Rietdorf K. The regulation of autophagy by calcium signals: Do we have a consensus? *Cell Calcium.* 2018;70:32-46. doi:10.1016/j.ceca.2017.08.005
265. Smaili SS, Pereira GJS, Costa MM, et al. The role of calcium stores in apoptosis and autophagy. *Curr Mol Med.* 2013;13(2):252-265. doi:10.2174/156652413804810772
266. Yang J, Zhao Z, Gu M, Feng X, Xu H. Release and uptake mechanisms of vesicular Ca²⁺ stores. *Protein Cell.* 2019;10(1):8-19. doi:10.1007/s13238-018-0523-x
267. Høyer-Hansen M, Bastholm L, Szyniarowski P, et al. Control of macroautophagy by calcium, calmodulin-dependent kinase kinase-beta, and Bcl-2. *Mol Cell.* 2007;25(2):193-205. doi:10.1016/j.molcel.2006.12.009
268. Demarchi F, Bertoli C, Copetti T, et al. Calpain is required for macroautophagy in mammalian cells. *J Cell Biol.* 2006;175(4):595-605. doi:10.1083/jcb.200601024
269. Kania E, Pająk B, Orzechowski A. Calcium Homeostasis and ER Stress in Control of Autophagy in Cancer Cells. *BioMed Res Int.* 2015;2015:e352794. doi:10.1155/2015/352794
270. Zhang null, Chung null, Oldenburg null. A Simple Statistical Parameter for Use in Evaluation and Validation of High Throughput Screening Assays. *J Biomol Screen.* 1999;4(2):67-73. doi:10.1177/108705719900400206

271. Durant JL, Leland BA, Henry DR, Nourse JG. Reoptimization of MDL Keys for Use in Drug Discovery. *J Chem Inf Comput Sci*. 2002;42(6):1273-1280. doi:10.1021/ci010132r
272. Kuwahara H, Gao X. Analysis of the effects of related fingerprints on molecular similarity using an eigenvalue entropy approach. *J Cheminformatics*. 2021;13(1):27. doi:10.1186/s13321-021-00506-2
273. Livak KJ, Schmittgen TD. Analysis of relative gene expression data using real-time quantitative PCR and the 2⁻(Delta Delta C(T)) Method. *Methods San Diego Calif*. 2001;25(4):402-408. doi:10.1006/meth.2001.1262
274. Ma KY, Fokkens MR, Reggiori F, Mari M, Verbeek DS. Parkinson's disease-associated VPS35 mutant reduces mitochondrial membrane potential and impairs PINK1/Parkin-mediated mitophagy. *Transl Neurodegener*. 2021;10(1):19. doi:10.1186/s40035-021-00243-4
275. Postnikova E, Cong Y, DeWald LE, et al. Testing therapeutics in cell-based assays: Factors that influence the apparent potency of drugs. *PLoS ONE*. 2018;13(3):e0194880. doi:10.1371/journal.pone.0194880
276. Markossian S, Grossman A, Brimacombe K, et al., eds. *Assay Guidance Manual*. Eli Lilly & Company and the National Center for Advancing Translational Sciences; 2004. Accessed February 12, 2022. <http://www.ncbi.nlm.nih.gov/books/NBK53196/>
277. Lee KI, Kim MJ, Koh H, et al. The anti-hypertensive drug reserpine induces neuronal cell death through inhibition of autophagic flux. *Biochem Biophys Res Commun*. 2015;462(4):402-408. doi:10.1016/j.bbrc.2015.04.145
278. Ristic B, Bosnjak M, Arsikin K, et al. Idarubicin induces mTOR-dependent cytotoxic autophagy in leukemic cells. *Exp Cell Res*. 2014;326(1):90-102. doi:10.1016/j.yexcr.2014.05.021
279. Hosokawa S, Koseki H, Nagashima M, et al. Title efficacy of phosphodiesterase 5 inhibitor on distant burn-induced muscle autophagy, microcirculation, and survival rate. *Am J Physiol-Endocrinol Metab*. 2013;304(9):E922-E933. doi:10.1152/ajpendo.00078.2013

280. Booth L, Roberts JL, Poklepovic A, Gordon S, Dent P. PDE5 inhibitors enhance the lethality of pemetrexed through inhibition of multiple chaperone proteins and via the actions of cyclic GMP and nitric oxide. *Oncotarget*. 2016;8(1):1449-1468. doi:10.18632/oncotarget.13640
281. Ikeda T, Ishii KA, Saito Y, et al. Inhibition of autophagy enhances sunitinib-induced cytotoxicity in rat pheochromocytoma PC12 cells. *J Pharmacol Sci*. 2013;121(1):67-73. doi:10.1254/jphs.12158fp
282. Lin CI, Whang EE, Lorch JH, Ruan DT. Autophagic activation potentiates the antiproliferative effects of tyrosine kinase inhibitors in medullary thyroid cancer. *Surgery*. 2012;152(6):1142-1149. doi:10.1016/j.surg.2012.08.016
283. Santoni M, Amantini C, Morelli MB, et al. Pazopanib and sunitinib trigger autophagic and non-autophagic death of bladder tumour cells. *Br J Cancer*. 2013;109(4):1040-1050. doi:10.1038/bjc.2013.420
284. Lopergolo A, Nicolini V, Favini E, et al. Synergistic Cooperation Between Sunitinib and Cisplatin Promotes Apoptotic Cell Death in Human Medullary Thyroid Cancer. *J Clin Endocrinol Metab*. 2014;99(2):498-509. doi:10.1210/jc.2013-2574
285. Elgendy M, Abdel-Aziz AK, Renne SL, et al. Dual modulation of MCL-1 and mTOR determines the response to sunitinib. *J Clin Invest*. 2017;127(1):153-168. doi:10.1172/JCI84386
286. Abdel-Aziz AK, Abdel-Naim AB, Shouman S, Minucci S, Elgendy M. From Resistance to Sensitivity: Insights and Implications of Biphasic Modulation of Autophagy by Sunitinib. *Front Pharmacol*. 2017;8:718. doi:10.3389/fphar.2017.00718
287. Tanida I, Ueno T, Kominami E. LC3 and Autophagy. In: Deretic V, ed. *Autophagosome and Phagosome*. Methods in Molecular Biology™. Humana Press; 2008:77-88. doi:10.1007/978-1-59745-157-4_4
288. Yoshii SR, Mizushima N. Monitoring and Measuring Autophagy. *Int J Mol Sci*. 2017;18(9):1865. doi:10.3390/ijms18091865

289. Baron U, Bujard H. Tet repressor-based system for regulated gene expression in eukaryotic cells: Principles and advances. In: *Methods in Enzymology*. Vol 327. Elsevier; 2000:401-421. doi:10.1016/S0076-6879(00)27292-3
290. Pugsley HR. Assessing Autophagic Flux by Measuring LC3, p62, and LAMP1 Co-localization Using Multispectral Imaging Flow Cytometry. *J Vis Exp JoVE*. 2017;(125):55637. doi:10.3791/55637
291. Pierzyńska-Mach A, Janowski PA, Dobrucki JW. Evaluation of acridine orange, LysoTracker Red, and quinacrine as fluorescent probes for long-term tracking of acidic vesicles. *Cytometry A*. 2014;85(8):729-737. doi:10.1002/cyto.a.22495
292. Bahar E, Kim H, Yoon H. ER Stress-Mediated Signaling: Action Potential and Ca²⁺ as Key Players. *Int J Mol Sci*. 2016;17(9):1558. doi:10.3390/ijms17091558
293. Boolell M, Allen MJ, Ballard SA, et al. Sildenafil: an orally active type 5 cyclic GMP-specific phosphodiesterase inhibitor for the treatment of penile erectile dysfunction. *Int J Impot Res*. 1996;8(2):47-52.
294. Ashburn TT, Thor KB. Drug repositioning: identifying and developing new uses for existing drugs. *Nat Rev Drug Discov*. 2004;3(8):673-683. doi:10.1038/nrd1468
295. Pushpakom S, Iorio F, Eyers PA, et al. Drug repurposing: progress, challenges and recommendations. *Nat Rev Drug Discov*. 2019;18(1):41-58. doi:10.1038/nrd.2018.168
296. Lisurek M, Rupp B, Wichard J, et al. Design of chemical libraries with potentially bioactive molecules applying a maximum common substructure concept. *Mol Divers*. 2010;14(2):401-408. doi:10.1007/s11030-009-9187-z
297. Barth S, Glick D, Macleod KF. Autophagy: assays and artifacts. *J Pathol*. 2010;221(2):117-124. doi:10.1002/path.2694
298. Shang L, Chen S, Du F, Li S, Zhao L, Wang X. Nutrient starvation elicits an acute autophagic response mediated by Ulk1 dephosphorylation and its

- subsequent dissociation from AMPK. *Proc Natl Acad Sci U S A*. 2011;108(12):4788-4793. doi:10.1073/pnas.1100844108
299. Korolchuk VI, Saiki S, Lichtenberg M, et al. Lysosomal positioning coordinates cellular nutrient responses. *Nat Cell Biol*. 2011;13(4):453-460. doi:10.1038/ncb2204
300. Wei Y, An Z, Zou Z, et al. The stress-responsive kinases MAPKAPK2/MAPKAPK3 activate starvation-induced autophagy through Beclin 1 phosphorylation. *eLife*. doi:10.7554/eLife.05289
301. Chen L, Ma K, Han J, Chen Q, Zhu Y. Monitoring Mitophagy in Mammalian Cells. *Methods Enzymol*. 2017;588:187-208. doi:10.1016/bs.mie.2016.10.038
302. Sun L, Meng Z, Zhu Y, et al. TM9SF4 is a novel factor promoting autophagic flux under amino acid starvation. *Cell Death Differ*. 2018;25(2):368-379. doi:10.1038/cdd.2017.166
303. Lauzier A, Normandeau-Guimond J, Vaillancourt-Lavigne V, et al. Colorectal cancer cells respond differentially to autophagy inhibition in vivo. *Sci Rep*. 2019;9(1):11316. doi:10.1038/s41598-019-47659-7
304. Vats S, Manjithaya R. A reversible autophagy inhibitor blocks autophagosome–lysosome fusion by preventing Stx17 loading onto autophagosomes. *Mol Biol Cell*. 2019;30(17):2283-2295. doi:10.1091/mbc.E18-08-0482
305. Liu Z, Wang Y, Zhao S, Zhang J, Wu Y, Zeng S. Imidazole inhibits autophagy flux by blocking autophagic degradation and triggers apoptosis via increasing FoxO3a-Bim expression. *Int J Oncol*. 2015;46(2):721-731. doi:10.3892/ijo.2014.2771
306. Tang ZH, Guo X, Cao WX, Chen X, Lu JJ. Fangchinoline accumulates autophagosomes by inhibiting autophagic degradation and promoting TFEB nuclear translocation. *RSC Adv*. 2017;7(67):42597-42605. doi:10.1039/C7RA02738A

307. Zhang L, Qiang P, Yu J, et al. Identification of compound CA-5f as a novel late-stage autophagy inhibitor with potent anti-tumor effect against non-small cell lung cancer. *Autophagy*. 2018;15(3):391-406. doi:10.1080/15548627.2018.1511503
308. Paha J, Kanjanasirirat P, Munyoo B, et al. A novel potent autophagy inhibitor ECDD-S27 targets vacuolar ATPase and inhibits cancer cell survival. *Sci Rep*. 2019;9:9177. doi:10.1038/s41598-019-45641-x
309. Lemieux B, Percival MD, Falgoutyret JP. Quantitation of the lysosomotropic character of cationic amphiphilic drugs using the fluorescent basic amine Red DND-99. *Anal Biochem*. 2004;327(2):247-251. doi:10.1016/j.ab.2004.01.010
310. Fedele AO, Proud CG. Chloroquine and bafilomycin A mimic lysosomal storage disorders and impair mTORC1 signalling. *Biosci Rep*. 2020;40(4):BSR20200905. doi:10.1042/BSR20200905
311. Laiouar S, Berns N, Brech A, Riechmann V. RabX1 Organizes a Late Endosomal Compartment that Forms Tubular Connections to Lysosomes Consistent with a “Kiss and Run” Mechanism. *Curr Biol*. 2020;30(7):1177-1188.e5. doi:10.1016/j.cub.2020.01.048
312. Duvvuri M, Gong Y, Chatterji D, Krise JP. Weak base permeability characteristics influence the intracellular sequestration site in the multidrug-resistant human leukemic cell line HL-60. *J Biol Chem*. 2004;279(31):32367-32372. doi:10.1074/jbc.M400735200
313. Albrecht LV, Tejada-Muñoz N, De Robertis EM. Protocol for Probing Regulated Lysosomal Activity and Function in Living Cells. *STAR Protoc*. 2020;1(3):100132. doi:10.1016/j.xpro.2020.100132
314. Kawai A, Uchiyama H, Takano S, Nakamura N, Ohkuma S. Autophagosome-lysosome fusion depends on the pH in acidic compartments in CHO cells. *Autophagy*. 2007;3(2):154-157. doi:10.4161/auto.3634
315. Yadati T, Houben T, Bitorina A, Shiri-Sverdlov R. The Ins and Outs of Cathepsins: Physiological Function and Role in Disease Management. *Cells*. 2020;9(7):1679. doi:10.3390/cells9071679

316. Jung M, Lee J, Seo HY, Lim JS, Kim EK. Cathepsin Inhibition-Induced Lysosomal Dysfunction Enhances Pancreatic Beta-Cell Apoptosis in High Glucose. *PLoS ONE*. 2015;10(1):e0116972. doi:10.1371/journal.pone.0116972
317. Cermak S, Kosicek M, Mladenovic-Djordjevic A, Smiljanic K, Kanazir S, Hecimovic S. Loss of Cathepsin B and L Leads to Lysosomal Dysfunction, NPC-Like Cholesterol Sequestration and Accumulation of the Key Alzheimer's Proteins. *PLoS ONE*. 2016;11(11):e0167428. doi:10.1371/journal.pone.0167428
318. Mizunoe Y, Kobayashi M, Tagawa R, Nakagawa Y, Shimano H, Higami Y. Association between Lysosomal Dysfunction and Obesity-Related Pathology: A Key Knowledge to Prevent Metabolic Syndrome. *Int J Mol Sci*. 2019;20(15):3688. doi:10.3390/ijms20153688
319. Kaminsky V, Zhivotovsky B. Proteases in autophagy. *Biochim Biophys Acta BBA - Proteins Proteomics*. 2012;1824(1):44-50. doi:10.1016/j.bbapap.2011.05.013
320. Bonam SR, Wang F, Muller S. Lysosomes as a therapeutic target. *Nat Rev Drug Discov*. 2019;18(12):923-948. doi:10.1038/s41573-019-0036-1
321. Dennemärker J, Lohmüller T, Müller S, et al. Impaired turnover of autophagolysosomes in cathepsin L deficiency. *Biol Chem*. 2010;391(8):913-922. doi:10.1515/BC.2010.097
322. Man SM, Kanneganti TD. Regulation of lysosomal dynamics and autophagy by CTSB/cathepsin B. *Autophagy*. 2016;12(12):2504-2505. doi:10.1080/15548627.2016.1239679
323. Lo YC, Torres JZ. *Chemical Similarity Networks for Drug Discovery*. IntechOpen; 2016. doi:10.5772/65106
324. Chicote J, Yuste VJ, Boix J, Ribas J. Cell Death Triggered by the Autophagy Inhibitory Drug 3-Methyladenine in Growing Conditions Proceeds With DNA Damage. *Front Pharmacol*. 2020;11:1632. doi:10.3389/fphar.2020.580343

325. Labi V, Erlacher M. How cell death shapes cancer. *Cell Death Dis.* 2015;6(3):e1675-e1675. doi:10.1038/cddis.2015.20
326. Towers CG, Wodetzki D, Thorburn A. Autophagy and cancer: Modulation of cell death pathways and cancer cell adaptations. *J Cell Biol.* 2019;219(1):e201909033. doi:10.1083/jcb.201909033
327. McKenzie BA, Fernandes JP, Doan MAL, Schmitt LM, Branton WG, Power C. Activation of the executioner caspases-3 and -7 promotes microglial pyroptosis in models of multiple sclerosis. *J Neuroinflammation.* 2020;17:253. doi:10.1186/s12974-020-01902-5
328. Shim MK, Yoon HY, Lee S, et al. Caspase-3/-7-Specific Metabolic Precursor for Bioorthogonal Tracking of Tumor Apoptosis. *Sci Rep.* 2017;7:16635. doi:10.1038/s41598-017-16653-2
329. Zhu Y, Zhao L, Liu L, et al. Beclin 1 cleavage by caspase-3 inactivates autophagy and promotes apoptosis. *Protein Cell.* 2010;1(5):468-477. doi:10.1007/s13238-010-0048-4
330. Cho DH, Jo YK, Hwang JJ, Lee YM, Roh SA, Kim JC. Caspase-mediated cleavage of ATG6/Beclin-1 links apoptosis to autophagy in HeLa cells. *Cancer Lett.* 2009;274(1):95-100. doi:10.1016/j.canlet.2008.09.004
331. Wirawan E, Vande Walle L, Kersse K, et al. Caspase-mediated cleavage of Beclin-1 inactivates Beclin-1-induced autophagy and enhances apoptosis by promoting the release of proapoptotic factors from mitochondria. *Cell Death Dis.* 2010;1(1):e18-e18. doi:10.1038/cddis.2009.16
332. Wu H, Li W, Wang T, et al. α -Tomatine, a novel early-stage autophagy inhibitor, inhibits autophagy to enhance apoptosis via Beclin-1 in Skov3 cells. *Fitoterapia.* 2021;152:104911. doi:10.1016/j.fitote.2021.104911
333. Firat E, Weyerbrock A, Gaedicke S, Grosu AL, Niedermann G. Chloroquine or Chloroquine-PI3K/Akt Pathway Inhibitor Combinations Strongly Promote γ -Irradiation-Induced Cell Death in Primary Stem-Like Glioma Cells. *PLOS ONE.* 2012;7(10):e47357. doi:10.1371/journal.pone.0047357

334. Ye H, Chen M, Cao F, Huang H, Zhan R, Zheng X. Chloroquine, an autophagy inhibitor, potentiates the radiosensitivity of glioma initiating cells by inhibiting autophagy and activating apoptosis. *BMC Neurol.* 2016;16:178. doi:10.1186/s12883-016-0700-6
335. Sun K, Guo X I, Zhao Q d, et al. Paradoxical role of autophagy in the dysplastic and tumor-forming stages of hepatocarcinoma development in rats. *Cell Death Dis.* 2013;4(2):e501. doi:10.1038/cddis.2013.35
336. Kimmelman AC, White E. Autophagy and Tumor Metabolism. *Cell Metab.* 2017;25(5):1037-1043. doi:10.1016/j.cmet.2017.04.004
337. Pirazzoli V, Nebhan C, Song X, et al. Acquired resistance of EGFR-mutant lung adenocarcinomas to afatinib plus cetuximab is associated with activation of mTORC1. *Cell Rep.* 2014;7(4):999-1008. doi:10.1016/j.celrep.2014.04.014
338. Kawabata S, Mercado-Matos JR, Hollander MC, et al. Rapamycin prevents the development and progression of mutant epidermal growth factor receptor lung tumors with the acquired resistance mutation T790M. *Cell Rep.* 2014;7(6):1824-1832. doi:10.1016/j.celrep.2014.05.039
339. Elkabets M, Vora S, Juric D, et al. mTORC1 inhibition is required for sensitivity to PI3K p110 α inhibitors in PIK3CA-mutant breast cancer. *Sci Transl Med.* 2013;5(196):196ra99. doi:10.1126/scitranslmed.3005747
340. Corcoran RB, Rothenberg SM, Hata AN, et al. TORC1 suppression predicts responsiveness to RAF and MEK inhibition in BRAF-mutant melanoma. *Sci Transl Med.* 2013;5(196):196ra98. doi:10.1126/scitranslmed.3005753
341. Ma Y, Vassetzky Y, Dokudovskaya S. mTORC1 pathway in DNA damage response. *Biochim Biophys Acta BBA - Mol Cell Res.* 2018;1865(9):1293-1311. doi:10.1016/j.bbamcr.2018.06.011
342. Qin X, Jiang B, Zhang Y. 4E-BP1, a multifactor regulated multifunctional protein. *Cell Cycle.* 2016;15(6):781-786. doi:10.1080/15384101.2016.1151581
343. Choo AY, Yoon SO, Kim SG, Roux PP, Blenis J. Rapamycin differentially inhibits S6Ks and 4E-BP1 to mediate cell-type-specific repression of mRNA

translation. *Proc Natl Acad Sci.* 2008;105(45):17414-17419. doi:10.1073/pnas.0809136105

344. Ferraresi A, Titone R, Follo C, et al. The protein restriction mimetic Resveratrol is an autophagy inducer stronger than amino acid starvation in ovarian cancer cells. *Mol Carcinog.* 2017;56(12):2681-2691. doi:10.1002/mc.22711

345. Yik-Sham Chung C, Shin HR, Berdan CA, et al. Covalent Targeting of the Vacuolar H⁺-ATPase Activates Autophagy Via mTORC1 Inhibition. *Nat Chem Biol.* 2019;15(8):776-785. doi:10.1038/s41589-019-0308-4

346. Menon MB, Dhamija S. Beclin 1 Phosphorylation – at the Center of Autophagy Regulation. *Front Cell Dev Biol.* 2018;6:137. doi:10.3389/fcell.2018.00137

347. Ranieri R, Ciaglia E, Amodio G, et al. N6-isopentenyladenosine dual targeting of AMPK and Rab7 prenylation inhibits melanoma growth through the impairment of autophagic flux. *Cell Death Differ.* 2018;25(2):353-367. doi:10.1038/cdd.2017.165

348. Guerra F, Bucci C. Multiple Roles of the Small GTPase Rab7. *Cells.* 2016;5(3):34. doi:10.3390/cells5030034

349. Kuchitsu Y, Fukuda M. Revisiting Rab7 Functions in Mammalian Autophagy: Rab7 Knockout Studies. *Cells.* 2018;7(11):215. doi:10.3390/cells7110215

350. Wek RC, Staschke KA. How do tumours adapt to nutrient stress? *EMBO J.* 2010;29(12):1946-1947. doi:10.1038/emboj.2010.110

351. Matsui T, Jiang P, Nakano S, Sakamaki Y, Yamamoto H, Mizushima N. Autophagosomal YKT6 is required for fusion with lysosomes independently of syntaxin 17. *J Cell Biol.* 2018;217(8):2633-2645. doi:10.1083/jcb.201712058

352. Islam MA, Sooro MA, Zhang P. Autophagic Regulation of p62 is Critical for Cancer Therapy. *Int J Mol Sci.* 2018;19(5):E1405. doi:10.3390/ijms19051405

353. Taniguchi K, Yamachika S, He F, Karin M. p62/SQSTM1-Dr. Jekyll and Mr. Hyde that prevents oxidative stress but promotes liver cancer. *FEBS Lett.* 2016;590(15):2375-2397. doi:10.1002/1873-3468.12301
354. Takamura A, Komatsu M, Hara T, et al. Autophagy-deficient mice develop multiple liver tumors. *Genes Dev.* 2011;25(8):795-800. doi:10.1101/gad.2016211
355. Menon S, Yecies JL, Zhang HH, et al. Chronic activation of mTOR complex 1 is sufficient to cause hepatocellular carcinoma in mice. *Sci Signal.* 2012;5(217):ra24. doi:10.1126/scisignal.2002739
356. Umemura A, He F, Taniguchi K, et al. p62, Upregulated during Preneoplasia, Induces Hepatocellular Carcinogenesis by Maintaining Survival of Stressed HCC-Initiating Cells. *Cancer Cell.* 2016;29(6):935-948. doi:10.1016/j.ccell.2016.04.006
357. Puertollano R, Ferguson SM, Brugarolas J, Ballabio A. The complex relationship between TFEB transcription factor phosphorylation and subcellular localization. *EMBO J.* 2018;37(11):e98804. doi:10.15252/embj.201798804
358. Komatsu M, Kageyama S, Ichimura Y. p62/SQSTM1/A170: physiology and pathology. *Pharmacol Res.* 2012;66(6):457-462. doi:10.1016/j.phrs.2012.07.004
359. Moscat J, Diaz-Meco MT. Feedback on fat: p62-mTORC1-autophagy connections. *Cell.* 2011;147(4):724-727. doi:10.1016/j.cell.2011.10.021
360. Liu WJ, Ye L, Huang WF, et al. p62 links the autophagy pathway and the ubiquitin–proteasome system upon ubiquitinated protein degradation. *Cell Mol Biol Lett.* 2016;21(1):29. doi:10.1186/s11658-016-0031-z
361. Wu Y, Huang P, Dong XP. Lysosomal Calcium Channels in Autophagy and Cancer. *Cancers.* 2021;13(6):1299. doi:10.3390/cancers13061299
362. Kimura T, Takabatake Y, Takahashi A, Isaka Y. Chloroquine in cancer therapy: a double-edged sword of autophagy. *Cancer Res.* 2013;73(1):3-7. doi:10.1158/0008-5472.CAN-12-2464

363. Rashid HO, Yadav RK, Kim HR, Chae HJ. ER stress: Autophagy induction, inhibition and selection. *Autophagy*. 2015;11(11):1956-1977. doi:10.1080/15548627.2015.1091141
364. Osowski CM, Urano F. Measuring ER stress and the unfolded protein response using mammalian tissue culture system. *Methods Enzymol*. 2011;490:71-92. doi:10.1016/B978-0-12-385114-7.00004-0
365. Lei Y, Wang S, Ren B, et al. CHOP favors endoplasmic reticulum stress-induced apoptosis in hepatocellular carcinoma cells via inhibition of autophagy. *PLoS ONE*. 2017;12(8):e0183680. doi:10.1371/journal.pone.0183680
366. Masud Alam Md, Kariya R, Kawaguchi A, Matsuda K, Kudo E, Okada S. Inhibition of autophagy by chloroquine induces apoptosis in primary effusion lymphoma in vitro and in vivo through induction of endoplasmic reticulum stress. *Apoptosis*. 2016;21(10):1191-1201. doi:10.1007/s10495-016-1277-7
367. Jia B, Xue Y, Yan X, et al. Autophagy inhibitor chloroquine induces apoptosis of cholangiocarcinoma cells via endoplasmic reticulum stress. *Oncol Lett*. 2018;16(3):3509-3516. doi:10.3892/ol.2018.9131
368. Sehgal P, Szalai P, Olesen C, et al. Inhibition of the sarco/endoplasmic reticulum (ER) Ca²⁺-ATPase by thapsigargin analogs induces cell death via ER Ca²⁺ depletion and the unfolded protein response. *J Biol Chem*. 2017;292(48):19656-19673. doi:10.1074/jbc.M117.796920
369. Raffaello A, Mammucari C, Gherardi G, Rizzuto R. Calcium at the Center of Cell Signaling: Interplay between Endoplasmic Reticulum, Mitochondria, and Lysosomes. *Trends Biochem Sci*. 2016;41(12):1035-1049. doi:10.1016/j.tibs.2016.09.001
370. Jaskulska A, Janecka AE, Gach-Janczak K. Thapsigargin—From Traditional Medicine to Anticancer Drug. *Int J Mol Sci*. 2020;22(1):4. doi:10.3390/ijms22010004
371. Hu H, Tian M, Ding C, Yu S. The C/EBP Homologous Protein (CHOP) Transcription Factor Functions in Endoplasmic Reticulum Stress-Induced Apoptosis and Microbial Infection. *Front Immunol*. 2019;9. Accessed January 13, 2022. <https://www.frontiersin.org/article/10.3389/fimmu.2018.03083>

372. Shin YJ, Han SH, Kim DS, et al. Autophagy induction and CHOP under-expression promotes survival of fibroblasts from rheumatoid arthritis patients under endoplasmic reticulum stress. *Arthritis Res Ther.* 2010;12(1):R19. doi:10.1186/ar2921
373. Deldicque L, Bertrand L, Patton A, Francaux M, Baar K. ER Stress Induces Anabolic Resistance in Muscle Cells through PKB-Induced Blockade of mTORC1. *PLOS ONE.* 2011;6(6):e20993. doi:10.1371/journal.pone.0020993
374. Denmeade SR, Isaacs JT. The SERCA pump as a therapeutic target: making a “smart bomb” for prostate cancer. *Cancer Biol Ther.* 2005;4(1):14-22. doi:10.4161/cbt.4.1.1505
375. Denmeade SR, Jakobsen CM, Janssen S, et al. Prostate-specific antigen-activated thapsigargin prodrug as targeted therapy for prostate cancer. *J Natl Cancer Inst.* 2003;95(13):990-1000. doi:10.1093/jnci/95.13.990
376. Hou H, Sun H, Lu P, et al. Tunicamycin potentiates cisplatin anticancer efficacy through the DPAGT1/Akt/ABCG2 pathway in mouse Xenograft models of human hepatocellular carcinoma. *Mol Cancer Ther.* 2013;12(12):2874-2884. doi:10.1158/1535-7163.MCT-13-0201
377. Carracedo A, Gironella M, Lorente M, et al. Cannabinoids induce apoptosis of pancreatic tumor cells via endoplasmic reticulum stress-related genes. *Cancer Res.* 2006;66(13):6748-6755. doi:10.1158/0008-5472.CAN-06-0169
378. Landowski TH, Megli CJ, Nullmeyer KD, Lynch RM, Dorr RT. Mitochondrial-mediated dysregulation of Ca²⁺ is a critical determinant of Velcade (PS-341/bortezomib) cytotoxicity in myeloma cell lines. *Cancer Res.* 2005;65(9):3828-3836. doi:10.1158/0008-5472.CAN-04-3684
379. Cubillos-Ruiz JR, Bettigole SE, Glimcher LH. Tumorigenic and Immunosuppressive Effects of Endoplasmic Reticulum Stress in Cancer. *Cell.* 2017;168(4):692-706. doi:10.1016/j.cell.2016.12.004
380. Vu HT, Kobayashi M, Hegazy AM, et al. Autophagy inhibition synergizes with calcium mobilization to achieve efficient therapy of malignant gliomas. *Cancer Sci.* 2018;109(8):2497-2508. doi:10.1111/cas.13695

381. Madreiter-Sokolowski CT, Gottschalk B, Parichatikanond W, et al. Resveratrol Specifically Kills Cancer Cells by a Devastating Increase in the Ca²⁺ Coupling Between the Greatly Tethered Endoplasmic Reticulum and Mitochondria. *Cell Physiol Biochem Int J Exp Cell Physiol Biochem Pharmacol.* 2016;39(4):1404-1420. doi:10.1159/000447844
382. Xie Q, Su J, Jiao B, et al. ABT737 reverses cisplatin resistance by regulating ER-mitochondria Ca²⁺ signal transduction in human ovarian cancer cells. *Int J Oncol.* 2016;49(6):2507-2519. doi:10.3892/ijo.2016.3733

FUNDING

This project has received a Marie Skłodowska-Curie ETN grant under the European Union's Horizon 2020 Research and Innovation Programme (Grant Agreement No 765912 DRIVE).

